

Synthesis of fluorine-18 labelled radiotracers and their pre-clinical and clinical characterization

Dissertation for the degree of Ph.D.

Waqas Rafique



Faculty of Mathematics and Natural Sciences

Department of Chemistry

University of Oslo

2018

© **Waqas Rafique, 2018**

*Series of dissertations submitted to the
Faculty of Mathematics and Natural Sciences, University of Oslo
No. 2013*

ISSN 1501-7710

All rights reserved. No part of this publication may be
reproduced or transmitted, in any form or by any means, without permission.

Cover: Hanne Baadsgaard Utigard.
Print production: Representralen, University of Oslo.

*To two most precious women in the world,
my Mother & my Wife*

Acknowledgement

The research work presented in the thesis was performed at the Nuclear Chemistry group, the Department of Chemistry, University of Oslo, and at the Institute of Basic Medical Sciences, the Department of Medicine, University of Oslo. A part of the work was performed at the Radboud Translational Medicine, Nijmegen, Netherlands; at the Positronpharma, Santiago, Chile; at the Uruguayan Centre of Molecular Imaging (CUDIM), Montevideo, Uruguay; and at the Department of Nuclear Medicine, Friedrich Alexander University, Erlangen, Germany.

Since the process of writing the thesis has come to an end, and the destination seems within reach, I would like to thank all who have been instrumental in supporting me to reach the goal.

Foremost, I am grateful to my main supervisor Dr. Patrick Johannes Riss, for showing confidence in me and providing me opportunity for Ph.D. He has not been just a supervisor, rather a teacher, an advisor, and a counselor to me. His keen interest in discussing the challenges and providing a practical solution to them is truly acknowledged. Though we met couple of unpleasant situations, but I believe his criticism encouraged me to come up with better solutions, and made me independent enough to perform as a good researcher. I am also thankful to him for reviewing the manuscripts and assisting with publication of the articles. It was impossible for me to accomplish this without his support and encouragement.

I am thankful to my co-supervisor, Dr. Jon Petter, for his encouraging and administrative support. Though we did not have many discussions on research projects, but our meetings to ensure smooth running of my Ph.D. is appreciated. I am also thankful to him for radiation protection course, training and meetings. I remember, the first day when I came University, I found him setting office desk for me. That was really gratifying. I always admire his humbleness and efforts to make things efficient and progressive. He really has been an asset for all the students and employees working at the Nuclear Chemistry group.

I would like to thank Dr. Vasko Kramer for organizing the clinical studies. It was not an easy task to cope with multiple institutes while keeping all on track, but he managed it in a proficient way. I am thankful to him for arranging a trip to Chile, and providing me opportunity to work in clinical environment. Thanks for showing me the Santiago city, and accompanying me during my stay in Chile. I am also grateful to Horacio Amaral, Andrea Ballocci Coudeu and to the Positronpharma staff for the good time I had during my stay there.

The people working at the Nuclear Chemistry section deserve a special mentioning. I am thankful to Jimmy Jakobsson and Santosh Reddy Alluri for scientific discussions and valuable input. You people were so cooperative that I did not feel my journey tiring at all. The time we spend together was lovely and would be missed, especially the “Indian jokes” from Alluri 😊. Thomas Rühl: I am thankful to him for showing me the manual radiolabelling set-up, and helping with the semi-preparative HPLC. Mona Milde: I am thankful to her for lipophilicity

measurements of my compounds. Bent Wilhelm Schoultz, Brian Jeffrey Reed and Mikel Gonzalez Esparza: I am thankful to them for training me on Scintomics module, and helping me with automation of radiosynthesis procedures. From collaborators, I am thankful to Tania Pardo for determining the binding affinities of tau-ligands, and to Olaf Prante and Julian Ott for performing the *ex-vivo* and *in-vivo* imaging studies of opioid radiotracers.

Additional acknowledgement belongs to people from hydrometallurgy group for their support, and both scientific and formal discussions. Special thanks to Hans Vigeland Lerum and Zeljka Raskovic-Lovre for assisting me with LSC measurements, and encouraging me under stressful conditions. I am also thankful to all the people from Chemistry department who helped me out in several situations. Special thanks to Dirk Peterson for helping with 2D NMR experiments and Osamu Sekiguchi for doing the MS analysis.

Finally and most importantly, I am thankful to my family members from Pakistan, especially my mother, sisters, and elder brother for their encouragement, affection and countless prayers. All their contributions for bringing me to this height are gratifying, and literally, I have no word to express it. Last but not least, I would like to thank my wife, Kiran for her continuous support, encouragement and unwavering love. Her patience on my occasional indecent moods is itself a testament for her devotion and love. Thank you for standing with me in all situations. I would also like to mention my kids Muhammad Saim and Birrah at this grateful moment. I am sorry kids! I could not spend much time with you since last couple of months, but it would be obliged as now we are going to have a lot of fun☺

Waqas Rafique

Oslo, April 2018

Table of Contents

<i>Acknowledgement</i>	III
<i>Abstract</i>	VII
<i>Graphical Abstract</i>	VIII
<i>Abbreviations</i>	X
<i>List of publications</i>	XII
Chapter 1 – Introduction	1
1.1 Positron Emission Tomography	1
1.2 PET in molecular imaging	1
1.3 Positron emitting radionuclides	3
1.4 Production of PET radionuclides	4
1.5 Cyclotron	5
1.6 Working of a Cyclotron	6
1.7 Introduction of ^{18}F into organic compounds	7
1.7.1 Electrophilic radiofluorination	8
1.7.2 Nucleophilic radiofluorination	9
1.7.2.1 Nucleophilic radiofluorination of aliphatic compounds	9
1.7.2.2 Nucleophilic radiofluorination of aromatic compounds	11
1.8 ^{18}F -Trifluoromethylation	12
1.8.1 ^{18}F -Labelling of aliphatic compounds via trifluoromethylation	12
1.8.2 ^{18}F -Labelling of aromatic compounds via trifluoromethylation	13
1.9 Some limitations of ^{18}F chemistry	14
1.10 Radiolabelling of compounds with ^{11}C	14
1.11 Characterization of radiotracers	16
Chapter 2 – Biology of the target systems	18
2.1 Biology involved in tau aggregation	18
2.1.1 Formation of neurofibrillary tangles	18
2.2 Biology of opioids receptors	19
Chapter 3 – Aim of the Thesis	21

Chapter 4 – Summary of Results and Discussion	22
Chapter 5 – Conclusion and future prospects	27
Chapter 6 – References	28
Appendix	36
Molecular structure of synthesized compounds	38
Articles/ Publications	40

Abstract

Positron Emission Tomography (PET) is an outstanding invention of modern age. It helps in understanding the molecular interactions in living subjects through use of radioactive probes. For the first time mechanistic insights into diverse physiological processes are possible for researchers and clinicians. The pre-clinical and clinical use of a radiotracer labelled with short-lived radionuclides critically depends on its production just in time through use of rapid radiosynthesis procedures. The current thesis work is a progression towards the development of better radiolabelling approaches, applicable to available radiosynthesis hardware for robust outcomes, and provides novel radiotracers.

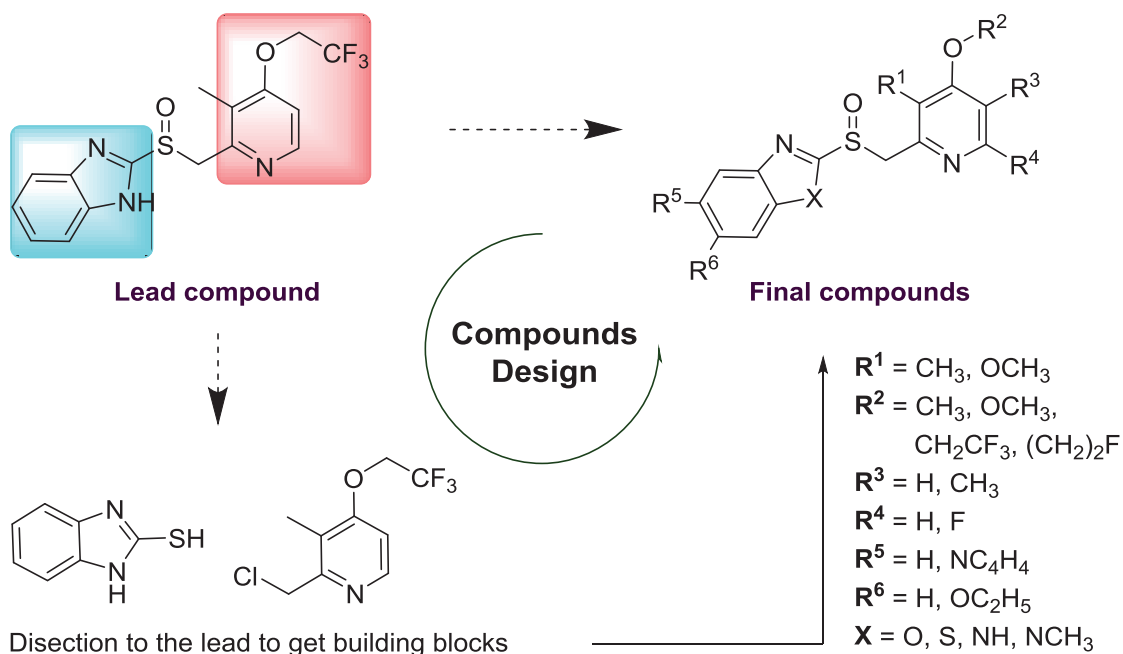
We first focused in developing reliable radiolabelling approaches for straightforward access of ^{18}F -labelled trifluoromethyl ($[^{18}\text{F}]\text{CF}_3$) groups on both aliphatic and aromatic scaffolds. Based on difluorovinyl electrophiles, aliphatic ^{18}F -trifluoroethyl bearing radiotracers were obtained through direct nucleophilic radiofluorination. The method was implemented in the radiosynthesis of lansoprazole ($[^{18}\text{F}]\text{LNS}$) to perform *first-in-man studies* in healthy individuals and clinical trials in Alzheimer patients. In addition, 20 new compounds were synthesized based on known pharmaceuticals with inherent binding affinity for neurofibrillary tangles (NFTs). The compounds were designed in perspective to label with ^{11}C or preferably with ^{18}F . The potency of synthesized analogues towards recombinant human tau protein (htau-441), amyloid beta (amyl- β) and α -synuclein (α -syn) was determined. Three highly selective compounds were identified that may be radiolabelled with ^{11}C or ^{18}F for *in vivo* imaging with PET.

For ^{18}F -trifluoromethylation of aromatic compounds, a single vial radiolabelling method was developed which provides access to a range of arene substrates in up to 90 % RCY within 30 minutes from end of bombardment (EOB). In order to translate the method towards application, a mu-specific opioid agonist AH7921 was selected to derive the PET radiotracer. Almost 20 new compounds were designed having F or CF_3 at various possible positions to develop ^{18}F -radiotracers. The affinity and selectivity of synthesized compounds towards mu (MOR), kappa (KOR), and delta (DOR) opioid receptors was determined. Three MOR selective compounds were identified, and radiolabelled with ^{18}F for *in vivo* characterization in rats. The new radiotracer candidates have high potential to provide the MOR evaluation within 60 minutes post injection (p.i.).

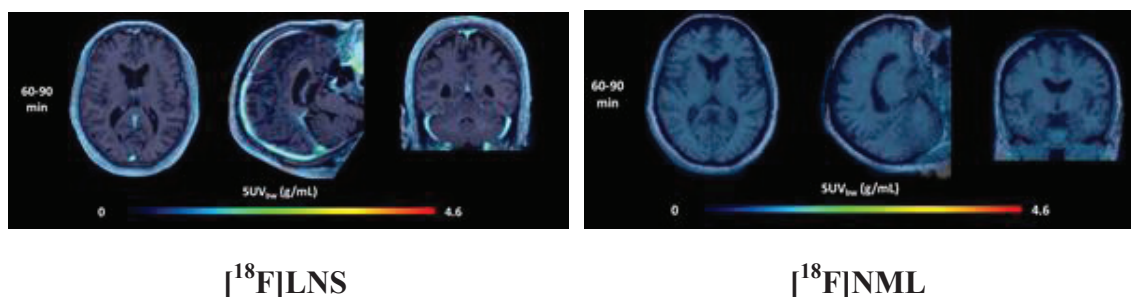
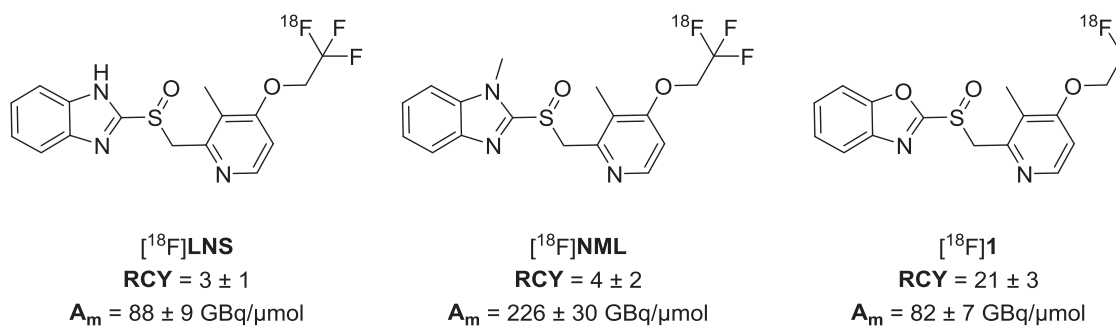
Graphical Abstract – 1

Synthesis of aliphatic trifluoromethyl compounds and radiolabeling of selective candidates.

Compounds Design



In vitro and *in vivo* evaluation

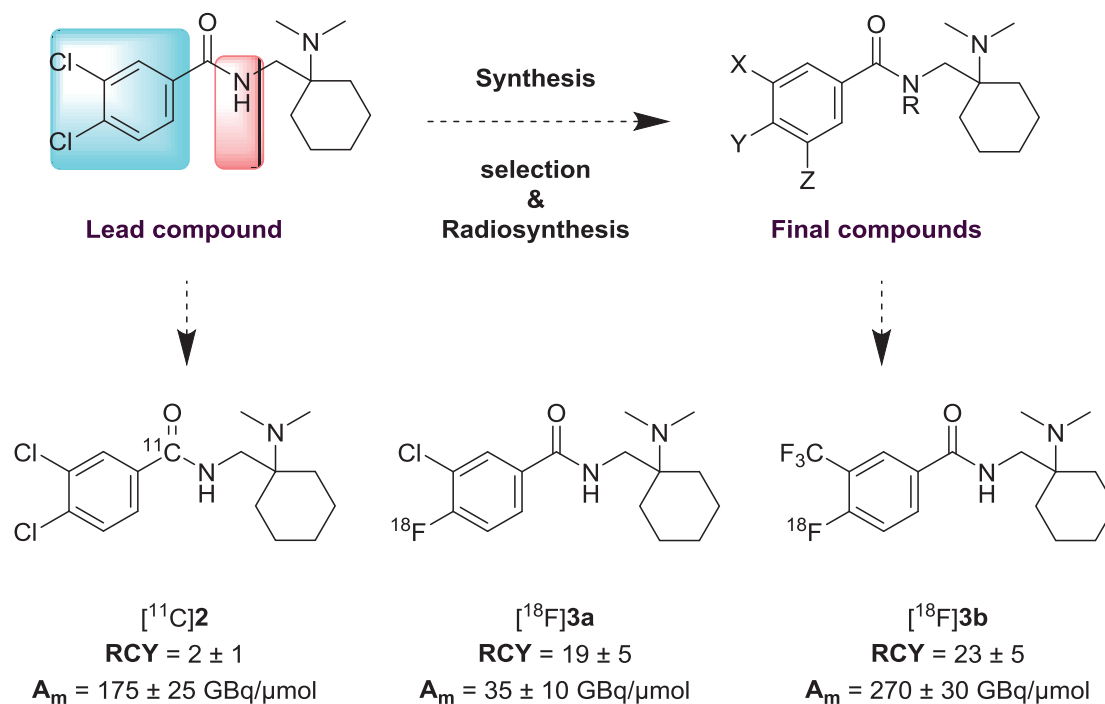


* RCY = non-decay corrected radiochemical yield; A_m = molar activity of radiotracers; PET/MRI fusion images obtained from clinical studies with both [¹⁸F]LNS and [¹⁸F]NML in transversal (left), sagittal (middle) and coronal (right) view. *In vivo* evaluation of [¹⁸F]1 in rats is under process.

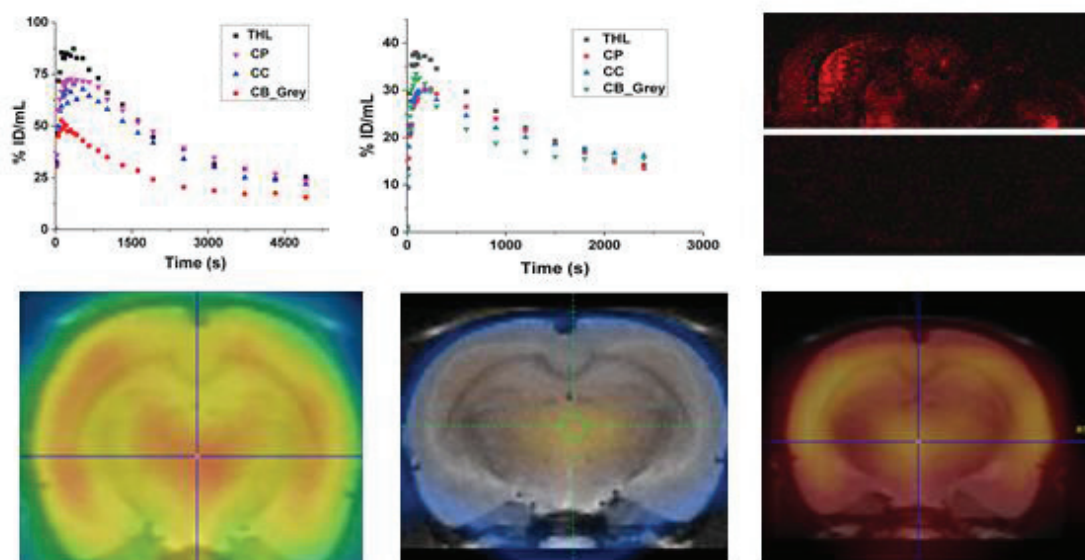
Graphical Abstract – 2

Synthesis of aromatic trifluoromethyl compounds and radiolabeling of selective candidates

Compounds Design



In vitro and *in vivo* evaluation



In vivo evaluation of [¹¹C]2; time-activity curves (TACs) for different brain regions (top left) and PET image showing radiotracer distribution in coronal view (bottom left). *In vivo* evaluation of [¹⁸F]3a; TACs from different brain regions (middle top), PET image showing radiotracer distribution in coronal view (middle bottom); *in vitro* autoradiography image showing direct comparison of [³H]DAMGO binding in absence, and in presence of 1 μM 3b (top right) and *in vivo* distribution of [¹⁸F]3b in coronal view (bottom right)

Abbreviations

A_m	Molar activity
PET	Positron emission tomography
LNS	2-(((3-methyl-4-(2,2,2-trifluoroethoxy)pyridin-2-yl)methyl)sulfinyl)-1H-benzoimidazole (lansoprazole)
NML	1-methyl-2-(((3-methyl-4-(2,2,2-trifluoroethoxy)pyridin-2-yl)methyl)sulfinyl)-1H-benzoimidazole (N-methyl lansoprazole)
RCY	Radiochemical yield
AD	Alzheimer disease
NFTs	Neurofibrillary tangles
Tau	Tubule associate unit
Amyl- β	Amyloids beta
α -syn	α -synuclein
AH7921	3,4-dichloro-N-((1-(dimethylamino) cyclohexyl)methyl)-benzamide
$\text{CH}_3 / \text{CF}_3$	Methyl/ trifluoromethyl
OR	Opioid receptors
CT	Computed tomography
MRI	Magnetic resonance imaging
SPECT	Single photon emission computed tomography
$\beta^+ / e^- / d$	Positron / electron / deuteron
$p / n / \nu$	Proton / neutron / neutrino
$\alpha / \beta / \gamma$	alpha / beta / gamma
k/MeV	killo/mega electron volt
$t_{1/2}$	Half-life
$\text{H}^- / {}^2\text{H}^-$	Hydride ion / deuteride ion
$\text{H}^+ / {}^4\text{He}^{++}$	Proton / helium atom
RF	Radiofrequency
$[{}^{18}\text{F}]\text{F}^-$	$[{}^{18}\text{F}]\text{fluoride ion}$
c.a / n.c.a	carrier added / non-carrier added

crypt-222	4,7,13,16,21,24-hexaoxa-1,10-diazabicyclo[8.8.8]hexacosane
QMA	Quaternary methyl ammonium anionic exchanger
Bq / Ci	Becquerel / Curie
S _N 2 / S _N Ar	Bimolecular nucleophilic substitution / Aromatic nucleophilic substitution reactions
DMF / DMSO	Dimethyl formamide / dimethyl sulfoxide
CF ₂ X	Difluoromethyl halide
[¹⁸ F]CF ₃ H	[¹⁸ F]trifluoromethane
PHF	Paired helical filaments
BBB	Blood-brain barrier
AST	1-[(4-fluorophenyl)methyl]-N-[1-[2-(4-methoxyphenyl)ethyl]-4-piperidyl]benzoimidazol-2-amine (Astemizole)
P-gP	Permeability glycoprotein
MOR / KOR / DOR	Mu / Kappa / delta-(opioid receptors)
EOB	End of bombardment
SUV	Standard uptake value
% ID	Percentage injected dose
htau-441	Recombinant human tau proteins
K _d / K _i	Equilibrium dissociation / inhibition constants
[³ H]DAMGO	Tyr-D-Ala-Gly-N([³ H]Me)Phe-Gly-ol
EC ₅₀ / IC ₅₀	Effective concentration / inhibitory concentration at half-maximum
DIPEA	N,N-Diisopropylethylamine
CHF ₂ I	Difluoroiodomethane
GMP	Good manufacturing practice

List of Publications

- I.** Direct nucleophilic radiosynthesis of [^{18}F]trifluoroethyl tosylate. *(published)*
Riss PJ, **Rafique W**, Aigbirhio FI. In: Scott PJ. Radiochemical synthesis: Further Radiopharmaceuticals for Positron Emission Tomography and New Strategies for Their Production. Vol. 2. Hoboken, New Jersey: John Wiley & Sons; 2015.
- II.** Image guided development of heterocyclic sulfoxides as ligands for tau neurofibrillary tangles: From first-in-man to second generation ligands. *(published)*
Rafique W, Kramer V, Pardo T, Smits R, Spilhaug MM, Hoeppeing A, Savio E, Engler H, Kuljs R, Amaral H, Riss PJ. ACS Omega. 2018;3(7):7567-79.
- III.** Cu(I)-mediated ^{18}F -trifluoromethylation of arenes: Rapid synthesis of ^{18}F -labeled trifluoromethyl arenes. *(published)*
Rühl T, **Rafique W**, Lien VT, Riss PJ. Chem Comm. 2014;50(45):6056-59.
- IV.** Reaching out for Sensitive Evaluation of the Mu Opioid Receptor *in vivo*: Positron Emission Tomography Imaging of the Agonist [^{11}C]AH7921 *(published)*
Rafique W, Khanapur S, Spilhaug MM, Riss PJ. ACS chem neurosci. 2017;8(9):1847-52.
- V.** Fully automated radiosynthesis of three mu-selective opioid receptor agonists for *in vivo* imaging with Positron Emission Tomography *(manuscript)*
Rafique W, Riss PJ.
- VI.** Discovery of an ^{18}F -labelled selective μ -opioid receptor agonist for small animal PET: Radiosynthesis, *in-vitro* and *in-vivo* characterisation of 3-chloro-4- ^{18}F fluoro-N-(1-(dimethylamino)cyclohexyl)methyl benzamide *(manuscript)*
Ott J, **Rafique W**, Maschauer S, Hartvig K, Spilhaug MM, Jakobsson JE, Hübner H, Gmeiner P, Prante O, Riss PJ.

VII. Radiosynthesis and characterization of 3-trifluoromethyl-4-[¹⁸F]fluoro-N-(1-(dimethylamino)cyclohexyl)methyl benzamide as an ¹⁸F-labelled mu-selective opioid receptor agonist. *(manuscript)*

Rafique W, Ott JJ, Maschauer S, Hartvig K, Jakobsson JE, Spilhaug MM, Hübner H, Gmeiner P, Prante O, Riss PJ.

Chapter 1 – Introduction

The current era is the age of science and technology, as we, mankind as a whole, are facing massive challenges due to demographic and social developments. A responsible solution will require us to live, think, and act scientifically. Science has captured the human mind by providing leisure, comfort and enhancing the standards of living that cannot be achieved without it. There is now improved understanding for once fatal diseases, and failing or worn-out organs may be replaced reducing the toll of human lives compared to past.¹ Exploratory surgeries have been replaced by advanced medical techniques including imaging with ultrasound, X-ray machines, Angiography, Computed Tomography (CT) and Magnetic Resonance Imaging (MRI). When combined with Positron Emission Tomography (PET), these diagnostic modalities not only provide non-invasive information about anatomy, but also the physiology and metabolic changes happening during course of the disease.²

1.1 Positron Emission Tomography

PET is among the most sensitive *in vivo* imaging techniques available to clinicians so far. When compared with existing nuclear medicine imaging modalities like scintillation cameras and/or single photon emission computed tomography (SPECT), PET stands out as a powerful next generation evolution. It helps clinicians to understand the mechanistic background of various diseases down to molecular level.²⁻³

PET is a multidisciplinary imaging technique connecting chemists, physicists, engineers and nuclear physicians to make biochemical reactions visible from the outside. The true power of PET is seen in possibility to label small organic molecules with positron emitting nuclides such as carbon-11 (^{11}C), oxygen-15 (^{15}O), nitrogen-13 (^{13}N) and fluorine-18 (^{18}F), without interfering with their biological properties. This enables PET to afford a range of molecular imaging probes for *in vivo* assessments.

1.2 PET in molecular imaging

The use of radioactive elements in biological investigations was started in 1923, when *George de Hevesy* studied the distribution of naturally existing lead-212 (^{212}Pb) in horse-bean plants, and the distribution of bismuth-210 (^{210}Bi) in rabbits.⁴ The concept received widespread

attention when dynamicity of the principle was proven in a study of phosphorus metabolism in rats using artificially produced phosphorus-32 (^{32}P) in 1935.⁵ The first PET imaging was performed in 1951 when an increase in the uptake of ^{64}Cu -labelled phthalocyanin dye was observed in damaged brain areas compared to normal tissues.⁶

The first modern PET machine was made by Robertson in 1973, but issues with image reconstruction and complications in attenuation correction were apparent, until Phelps and Hoffman with assistance of EG&G ORTEC engineers introduced the first commercial PET tomograph.⁷⁻⁹ Since then, PET has been employed in imaging of several static and dynamic processes such as blood perfusion, renal function, cellular metabolism and *in vivo* mapping of receptor-ligand interactions.^{2,10}

The basic concept behind PET imaging is the *tracer principle*, where the labelled analogue of a molecule of interest is injected in trace quantities, i.e. low-to-sub nanomolar amounts, and followed by mapping the radiation emitted. As a PET nuclide or a positron emitting radiopharmaceutical is introduced into the body, the emitted positron (β^+) travels to some distance depending upon the energy of the β^+ (shown in Table 1.1). While passing through the tissues, the β^+ interacts with atoms of the matter, and loses some of its energy. When the β^+ comes to near rest, it meets with an electron (e^-) and annihilates almost instantaneously in a matter-antimatter reaction. The combined masses of the positron and electron is converted into energy, which is released in the form of two photons of 511 keV travelling in opposite direction.¹⁰

An array of detectors arranged in a circular shape detects these coincident photons. In PET, solid scintillation detectors are used because of good stopping power, better detection efficiency, and efficient light output compared to gas or liquid scintillation detectors.¹¹ When an annihilated photon hits with the detector, it results in emission of a flash of light in visible range ($\lambda = 400 - 500 \text{ nm}$). The emitted light is converted to the electrical signal, amplified through photomultiplier tubes, and processed using the internal electronic circuitry of PET scanner. Since the photons originate from the same point, the spatial information is derived by co-incident detection of annihilated photons to define the sight of incidence.¹¹⁻¹² The recorded information is processed independently, or reconstructed into a series of images to get an accurate three dimensional image of radioactivity within the body.

The schematic diagram and processing of a PET scanner is shown in Figure 1.1.

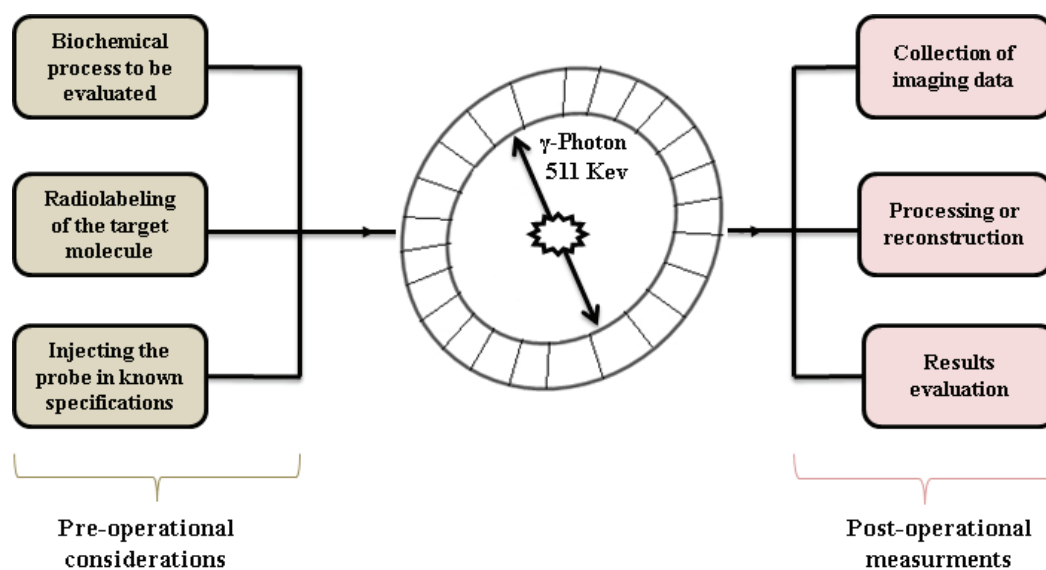


Figure – 1.1: Schematic diagram of a PET imaging system

1.3 Positron emitting radionuclides

In order to get information through a PET scanner, the labelled compound must be carrying a positron emitting radionuclide. While looking at the chart of nuclides, a number of positron emitters having high proton number, and low neutron-to-proton (n/p) ratio can be identified at lower left region of the stability belt. In order to gain stability, the positron emitters change a proton (p) to neutron (n) through emission of a positron (β^+), and an electron neutrino (ν_e) via a process called positron emission and/or electron capture.¹⁰ The general equation for β^+ emission of a proton-rich nuclide X is depicted in Equation 1.1.



Since the new element, Y will have the atomic number one less than the parent nuclide, one orbital electron is also lost to balance the charge during the process.² Hence, the parent nuclide should be at least two electron masses heavier than the daughter nuclide for positron emission to happen. Some prominent positron emitting radionuclides that are/have been used in biological investigations are ${}^{11}\text{C}$, ${}^{13}\text{N}$, ${}^{15}\text{O}$, ${}^{18}\text{F}$, Gallium-68 (${}^{68}\text{Ga}$), and Rubidium-82 (${}^{82}\text{Rb}$).¹³⁻¹⁴ The production route and decay properties of some commonly used PET radionuclides are given in Table 1.1.

Table – 1.1: The production route and properties of some commonly used PET nuclides.¹⁰⁻¹⁴

Radionuclide	Production route	$t_{1/2}$ in minutes (min)	E_{\max} (MeV)	Mode of decay (%)	R_{mean} (mm)
^{18}F	$^{18}\text{O}(\text{p},\text{n})^{18}\text{F}$	109.8	0.63	β^+ (97) EC(3)	0.6
^{11}C	$^{10}\text{B}(\text{d},\text{n})^{11}\text{C}$ $^{14}\text{N}(\text{p},\alpha)^{11}\text{C}$	20.4	0.96	β^+ (100)	1.1
^{13}N	$^{12}\text{C}(\text{d},\text{n})^{13}\text{N}$ $^{16}\text{O}(\text{p},\alpha)^{13}\text{N}$	9.96	1.19	β^+ (100)	1.5
^{15}O	$^{14}\text{N}(\text{d},\text{n})^{15}\text{O}$ $^{15}\text{N}(\text{p},\text{n})^{15}\text{O}$	2.03	1.73	β^+ (100)	2.5
^{68}Ga	$^{68}\text{Ge} - ^{68}\text{Ga}$	68.3	1.89	β^+ (89) EC(11)	2.9
^{82}Rb	$^{82}\text{Sr} - ^{82}\text{Rb}$	1.25	3.40	β^+ (95) EC(5)	5.9

E_{\max} = Maximum energy of positron in MeV, R_{mean} = Mean range in water (mm).

A number of factors have to be considered to prefer one radionuclide over the other. For example production route, physical half-life ($t_{1/2}$), positron range, probability of β^+ emission, energy of emitted positron, and methods for radiolabelling of suitable compounds. ^{11}C and ^{18}F are the nuclides of choice in most applications. ^{18}F has the advantage of a longer half-life ($t_{1/2}=110$ min) which allows to perform multistep synthesis, shorter β^+ range in tissues ($R_{\text{mean}}=0.6$ mm) permitting to get high resolution images, and convenient schemes for introduction of ^{18}F into organic molecules.

1.4 Production of PET radionuclides

Cyclotrons are commonly employed for production of PET nuclides, except those that are obtained through radionuclide generators. Generators are made based on mother-daughter (decay-growth) relationship and provide the most economic route to get radionuclides even to locations far away from the manufacturing sites. Various PET radionuclide generators, for example ($^{68}\text{Ge} - ^{68}\text{Ga}$),¹⁵ ($^{82}\text{Sr} - ^{82}\text{Rb}$),¹⁶ ($^{90}\text{Sr} - ^{90}\text{Y}$),¹⁷ and ($^{62}\text{Zn} - ^{62}\text{Cu}$)¹⁸ have been developed and used commercially. However, possibilities of radionuclide contaminations

from parent radionuclide itself or during its production by fission, and difficulties in finding an ideal parent-daughter relationship are limitation in getting PET radionuclides through generators.

Reactors are another option, but most of the PET nuclides follow (p,n), (p, α), (d,n), (d, α) and (d,2n) nuclear reactions, very few PET radionuclides are produced through reactors undergoing fission (n,f) or neutron capture (n, γ) reactions.¹⁰ Some PET radionuclides, e.g. isotopes of copper (⁶⁰Cu, ⁶¹Cu), bromine (⁷⁶Br, ⁷⁷Br) and iodine (¹²⁴I, ¹²⁵I) are obtained as fission by-products of heavy elements, but continuous supply of neutrons may cause fission among the product radionuclides.¹³ In addition, chances of radionuclide contaminations from fission by-products are additional challenges seen in reactors.

1.5 Cyclotron

Linear accelerators were the prime source for production of radionuclides until *Ernest. O. Lawrence* proposed a way to accelerate the particles in a continuous beam in 1929.¹⁹ Since then, cyclotrons have gained an indispensable place in the production of PET nuclides. In cyclotron, both negatively charged ions, e.g. hydride (H⁻) and deuteride (²H⁻) and positively charged ions e.g. proton (H⁺) and deuteron (d) can be accelerated to very high speed under the influence of an alternating electric, and a perpendicular magnetic field.¹⁰⁻¹¹ The H⁻ ions are accelerated in modern cyclotrons because of good extraction efficiency, limited beam losses, and inactivation of the cyclotron housing, permitting easy maintenance and less radiation dose to workers.²⁰ Additionally, in negative ion cyclotrons the beam may be split through carbon-stripping foils for simultaneous irradiation of two or more target systems.

When a high-energy projectile generated by cyclotron collides with the nucleus of the target atom, an unstable compound nucleus is formed, which on emission of a n, p or α -particle (depending upon the nature of the projectile and the target nucleus) produces the desired radionuclide. The production route of the three most commonly used PET radionuclides, i.e. ¹⁸F, ¹¹C, ¹³N is shown in Figure 1.2.

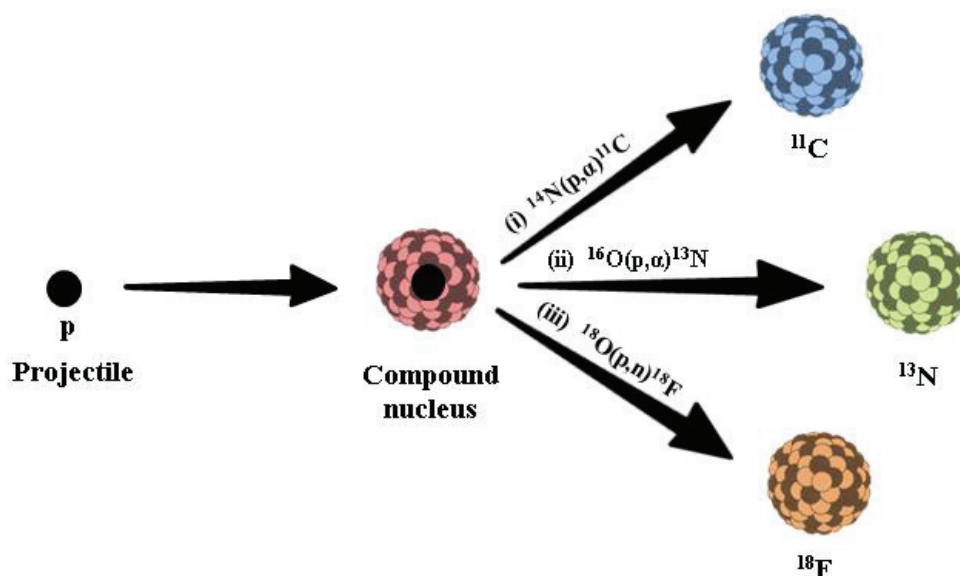


Figure – 1.2: Graphical presentation of three commonly used PET radionuclides produced through cyclotron. P = proton.

1.6 Principle of a Cyclotron

A cyclotron consists of two big D-shaped copper electrodes called *dees* (except few that have four as quarter of a pie) placed between the poles of a big electromagnet. The dees are connected to an alternating high-voltage radiofrequency (RF) generator, which is synchronized so that the polarity of each dee is changed after a specific time interval.¹⁰ An ion source, located in the centre, or outside the field creates the charge particles (H^+ or H^-) under the influence of a high-voltage electric current. Once the ions are produced, they are pulled out of the ion source chamber through a slit, and are confined in the centre between the dees.¹¹ The acceleration of the particles start due to attraction of the ions towards the oppositely charged dee as is described for H^- ions below.

As the H^- ions reach the centre between the dees, they are repelled by the negatively charged dee and/or attracted towards the positive one. On reaching to the positively charged dee, the H^- ions experience a constant electric field, but the magnetic field existing perpendicular drive the H^- ions to take a circular path. Hence, the H^- ions makes a rotation and reach to the exit of the positively charged dee. Since, the polarity between the dees is changed, the H^- ions are then repelled by the negatively charged dee, and attracted towards the positive one.^{7,10} This continues and the velocity and radius of the H^- ions keep on increasing at each rotation. When the H^- particles attain a certain energy/speed and reach the periphery of the system, the H^-

beam is extracted by stripping the electrons off through a thin carbon window of 2 – 5 μm thickness, and the proton beam is deflected towards the target nucleus.¹⁰

The internal assembly of a cyclotron is shown in Figure 1.3.

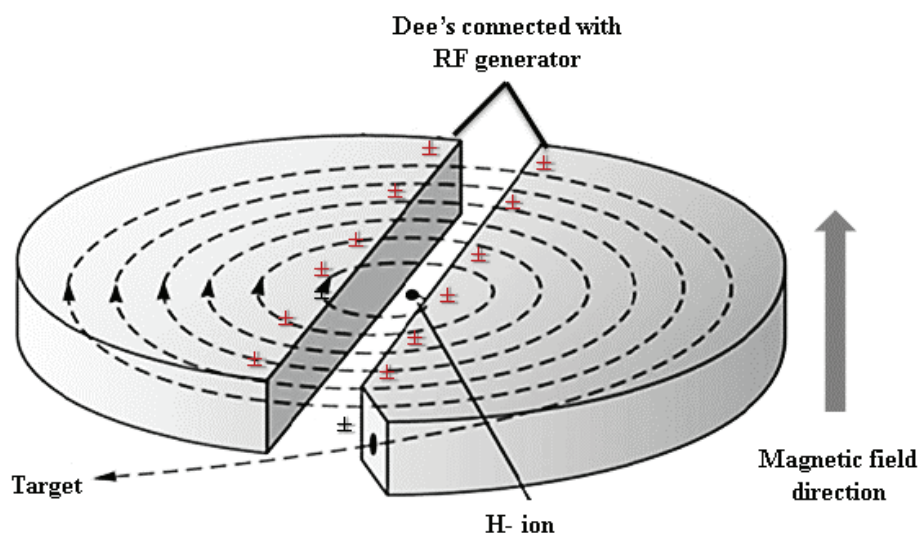


Figure – 1.3: Internal assembly of a cyclotron highlighting the acceleration of the H^- ions. (Taken from ref. 10)

Today, almost 85% of positron emitters used in research and clinical field are produced by cyclotrons, and a major portion of these is covered by ^{11}C and ^{18}F .

1.7 Introduction of ^{18}F into organic compounds

Despite a small number of naturally existing fluorinated compounds, fluorine incorporation into biological active small molecule drug scaffolds to access ^{18}F -labelled analogues is getting considerable attention. This is because of the outstanding features of ^{18}F as positron emitter, the extraordinary stability of the carbon-fluorine (C–F) bond, and steric and electronic similarities of C–F with carbon-hydrogen (C–H) and carbon-hydroxyl (C–OH) bonds.²¹

Several ^{18}F -radiolabelling approaches have been devised so far. The simplest of these is the direct approach where ^{18}F is introduced into the target molecules by substitution of a leaving group (one-step reaction), or the indirect approach wherein a ^{18}F -labelled intermediate is synthesized, and reacted further to get the molecule of interest (two-step method). In general, ^{18}F radiochemistry may be classified into two broad categories depending upon the source of ^{18}F used, and the nature of the labelling reaction as;

- (i) Electrophilic, where carrier-added (c.a.) molecular fluorine (^{18}F – ^{19}F) F_2 is used as ^{18}F source and,
- (ii) Nucleophilic, where [^{18}F]fluoride ion ($[\text{}^{18}\text{F}]\text{F}^-$) is used as nucleophile

Both methods have its own advantages and limitations as are described in detail below.

1.7.1 Electrophilic radiofluorination

Electrophilic radiofluorination is the method of choice where nucleophilic approach may not be employed, for example substrates abundant in negative charge like electron rich arene rings, alkenes and carbanions.³ In this approach, (^{18}F – ^{19}F) F_2 is obtained from cyclotrons using neon-20 (^{20}Ne) or oxygen-18 ($^{18}\text{O}_2$) enriched gas targets via $^{20}\text{Ne}(\text{d},\alpha)^{18}\text{F}$ or $^{18}\text{O}(\text{p},\text{n})^{18}\text{F}$ nuclear reactions, respectively.²²⁻²³ The produced ^{18}F is adsorbed on to the walls of the target material, and need to be released with the help of fluorine-19 (^{19}F) resulting in carrier-added ^{18}F . This explains why the specific activity (A_s = activity per mass of compound) or better molar activity (A_m) of compounds obtained through electrophilic radiofluorination is exceptionally low.

Molar activity is the ratio between the activity (in Bq) to amount of substance (in mol), and is given in GBq/ μmol . It is an important parameter in tracer principle as injected mass at, or beyond the saturation level may affect the purpose of the study. Additionally, the molar activity of radiotracers should be high enough to map low-density receptor regions, which further limits the use of electrophilic radiofluorination or other c.a. radiolabelling approaches, particularly in small animals.

Another issue experienced in electrophilic radiofluorination is the high reactivity of (^{18}F – ^{19}F) F_2 . This lessens the control over the reaction and leads to side products, which in turn drops the radiochemical yield (RCY) and selectivity of desired products.²⁴ Various modifications have been adopted to convert (^{18}F – ^{19}F) F_2 to less reactive fluorinating agents, such as trifluoromethyl hypo[^{18}F]fluorite ($\text{CF}_3\text{O}[\text{}^{18}\text{F}]\text{F}$),²⁴ xenon [^{18}F]difluoride ($\text{Xe}[\text{}^{18}\text{F}]\text{F}_2$),²⁵ acetyl hypo[^{18}F]fluorite ($\text{CH}_3\text{CO}_2[\text{}^{18}\text{F}]\text{F}$),²⁶ perchloryl[^{18}F]fluoride ($[\text{}^{18}\text{F}]\text{FCIO}_3$),²⁷ 1-[^{18}F]Fluoropyridinium trifluoromethanesulfonate,²⁸ and N-[^{18}F]fluoro-N-alkyl sulfonamides²⁹ but no real improvement was achieved.

1.7.2 Nucleophilic radiofluorination

Nucleophilic is the preferred way of ^{18}F -fluorination and >90 % of ^{18}F chemistry is carried through this approach. This is because ^{18}F may be obtained in non-carrier added (n.c.a.) quality, and in high molar activity in the form of a nucleophile as $[\text{}^{18}\text{F}]\text{F}^-$, via the $^{18}\text{O}(\text{p},\text{n})^{18}\text{F}$ nuclear reaction using ^{18}O -enriched H_2O (>99.8 %) liquid target. Since ^{18}F is obtained as anion, it gets hydrated to significant extent because of surrounding water molecules, and behaves as inactive nucleophile unless treated to make it reactive.

A mixture of inorganic base e.g. carbonates or bicarbonates in presence of large size cations i.e. caesium (Cs^+), alkylammonium ion (R_3N^+), or aminopolyethers such as 4,7,13,16,21,24-hexaoxa-1,10-diazabicyclo[8.8.8]hexacosane (crypt-222) in polar aprotic solvents is used to recover $[\text{}^{18}\text{F}]\text{F}^-$ from the aqueous media.³⁰⁻³¹ This is a mandatory application to all ^{18}F production batches, and is widely achieved through Sep-Pak Accell Plus light QMA cartridges followed by azeotropic distillation using acetonitrile under mild flow of an inert gas.³²

Since trace amounts of radioactive fluorine is present in the reaction mixture, removal of water is a crucial part in nucleophilic radiofluorination reactions. For example, a source of 1 GBq of ^{18}F in 200 μL of H_2O will contain 28 ng (1.5 nmol) of $[\text{}^{18}\text{F}]\text{F}^-$, compared to 10 mmol of H_2O molecules, hence presence of traces of water may explicitly render the inertness of $[\text{}^{18}\text{F}]\text{F}^-$. In addition to drying, nature of the precursor and leaving group/s used, type of reaction to be performed (aliphatic or aromatic), and stability of precursors under radiolabelling conditions are additional parameters to be considered for high radiolabelling throughput.

A detailed discussion on these parameters will be followed under individual reaction types. The nucleophilic radiofluorination may further be divided into two broad categories.

1.7.2.1 Nucleophilic radiofluorination of aliphatic compounds: ($\text{S}_\text{N}2$ reactions)

It is the most straightforward way of ^{18}F -fluorinations as reaction may be carried without any need of activating group/s. The only requirement for such reactions is protection of competitive sites that may lead to secondary reactions. For example, groups like hydroxyl ($-\text{OH}$), carbonic acid ($-\text{COOH}$), amine ($-\text{NH}$) and thiol ($-\text{SH}$) may sequester $[\text{}^{18}\text{F}]\text{F}^-$ considerably through hydrogen bonding or protonation, therefore these must be protected before $[\text{}^{18}\text{F}]\text{F}^-$ attack. The choice of protective group/s is made based on its stability to

withstand precursor synthesis, and easy removal under mild conditions such as hydrolysis (acidic or basic) or redox chemistry.³³ Ether and ester protection is widely adopted protective strategy in aliphatic nucleophilic radiofluorination as de-protection may be achieved by simple hydrolysis.

Likewise, leaving group/s should also be cleavable quite fairly under radiolabelling conditions. Bromo (–Br) or Chloro (–Cl) substituents and sulphonic acid esters, like methanesulfonate (mesylate), 4-methylbenzenesulfonate (tosylate), and methyl trifluoromethanesulfonate (triflate) are leaving groups commonly used in ^{18}F -substitution reactions.³⁴ The alternative way to $\text{S}_{\text{N}}2$ ^{18}F -fluorination reactions is the indirect approach where a small sized ^{18}F -labelled motif is made, and carried further to access the molecule of interest. Radiosynthesis of compounds containing fluoroalkyl synthons, e.g. 1-bromo-2- ^{18}F fluoroalkanes, 1-tosyloxy- or 1-mesyloxy-2- ^{18}F fluoroalkanes are the examples obtained through this approach.³⁵⁻³⁶ Some developed radiotracers obtained through direct nucleophilic radiofluorination in one (direct) or two-step reactions (involving de-protection and hydrolysis) are shown in Figure 1.4.³⁷⁻⁴¹

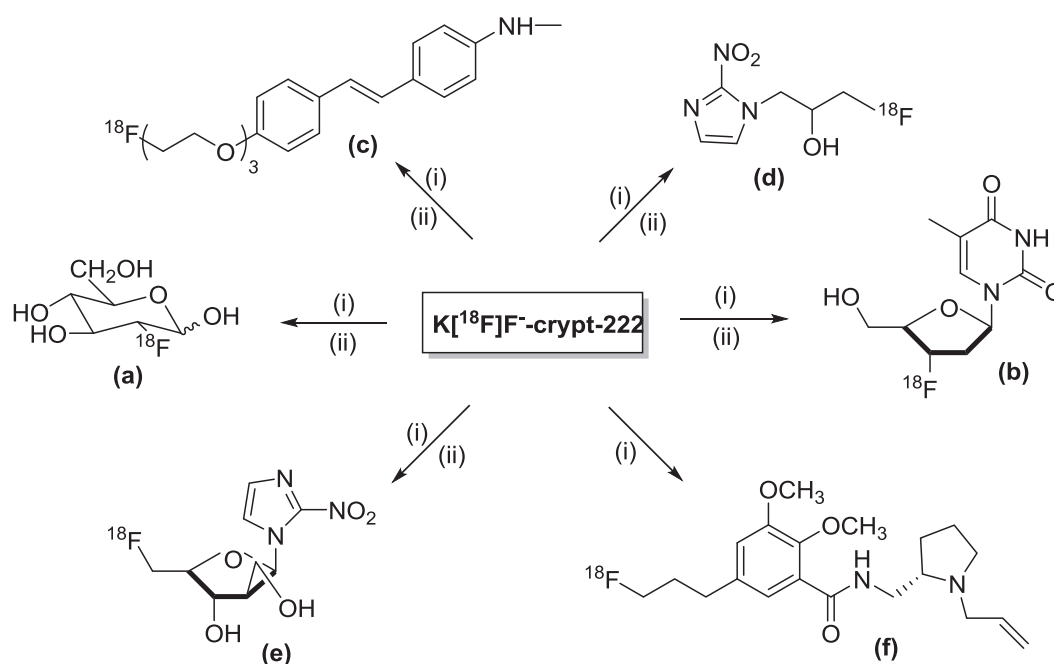


Figure – 1.4: Some clinically used ^{18}F -labelled radiotracers produced by aliphatic nucleophilic radiofluorination through direct (single-step) or indirect (two-step) approach. (i) Nucleophilic radiofluorination, (ii) deprotection.

1.7.2.2 Nucleophilic radiofluorination of aromatic compounds: (S_NAr reactions)

Radiofluorination of sp^2 -hybridized carbon centre has also gained considerable attention because of abundance of fluoroarenes in medicinal products. Like S_N2 , S_NAr radiofluorination is also achieved via a direct or indirect approach, but contrary to S_N2 reactions, substrates used in S_NAr must possess an electron-withdrawing activating group, i.e. nitro ($-NO_2$), cyano ($-CN$), carbonyl ($-C=O$) or trifluoromethyl ($-CF_3$) in *ortho* or *para* position to the leaving group to support the reaction.³⁴ However this must not be taken a reaction limitation as the activating groups may sometimes be transformed to access complex molecules which are difficult to obtain under normal radiolabelling conditions. Furthermore, the use of iodonium salts and iodonium ylides have allowed the ^{18}F -fluorination on a number of non-activated or electron-rich aromatic compounds in high yields and good molar activity.^{3,42}

The nitro group is a versatile nucleofuge used in S_NAr reactions, but sometimes trialkylammonium arenes are preferred because a better HPLC separation may be achieved between radiolabelled product and charged precursor.²⁴ Since S_NAr reactions often proceed at higher temperatures (100 – 170 °C) they require high boiling solvents like dimethyl formamide (DMF) and dimethyl sulfoxide (DMSO) as reaction media. Despite the harsh reaction conditions, S_NAr radiofluorination is employed for direct installation of ^{18}F among a small number of aromatic compounds. Several radiotracers that have been used in clinical investigations prepared through S_NAr radiofluorination are 4-[4-(4-chlorophenyl)-4-hydroxypiperidin-1-yl]-1-(4- ^{18}F fluorophenyl)butan-1-one ([^{18}F]Haloperidol),⁴³ 2-methoxyphenyl-(N-2-pyridinyl)-p-[^{18}F]fluorobenzamidoethyl piperazine ([^{18}F]MPPF),⁴⁴ and 3-[2-[4-(4- ^{18}F fluorobenzoyl)piperidin-1-yl]ethyl]-2-sulfanylidene-1H-quinazolin-4-one ([^{18}F]altanserin)⁴⁵. The radiosynthesis of [^{18}F]altanserin is shown in Figure 1.5.

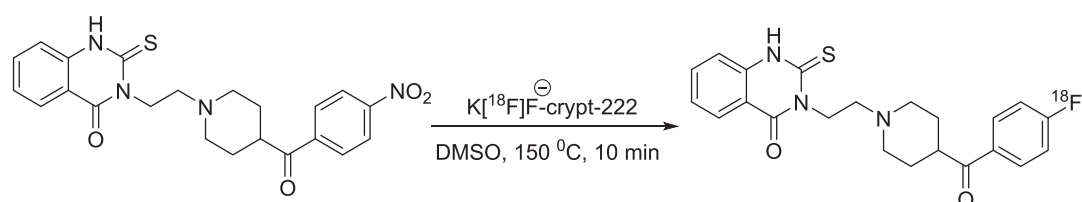


Figure – 1.5: Radioynthesis of altanserin through NO_2 -to- ^{18}F substitution

Direct S_NAr radiofluorination is not always the choice to obtain ^{18}F -labelled compounds, especially when sensitive or thermally labile substrates are involved.⁴⁶ To access these compounds, an indirect approach is adopted as may be seen in the radiosynthesis of N-

succinimidyl-4- ^{18}F fluorobenzoate (^{18}F SFB),⁴⁷ 1-(4- ^{18}F fluoromethylbenzoyl)amino-butane 4-amine (^{18}F FMBA),⁴⁸ N-[2-(4- ^{18}F fluorobenzamido)ethyl]maleimide ^{18}F FBEM,⁴⁹ and N-(4- ^{18}F fluorobenzyl)-2-bromoacetamide ^{18}F FBnBrA.⁵⁰

1.8 ^{18}F -Trifluoromethylation

^{18}F -Trifluoromethylation is an indispensable part of ^{18}F -fluorination reactions. Trifluoromethyl ($-\text{CF}_3$) are abundant fluorine containing groups among several biological active compounds, hence radiolabelling of CF_3 is getting considerable attention. The steric and electronic properties of CF_3 are comparable to $-\text{Cl}$ and methyl ($-\text{CH}_3$) groups, making it an ideal substitute for these in drug design and optimization of lead candidates.⁵¹ In addition, the introduction of CF_3 group to organic molecules increases compounds stability towards metabolising enzymes.

The reaction schemes used for introduction of CF_3 to organic compounds have been applied for ^{18}F -trifluoromethylation too, but later is hindered due to inapplicability of conventional organic approaches to be used under stoichiometric amounts of n.c.a ^{18}F F^- , multistep synthesis which is difficult to adopt under radiochemistry set-up, formation of unstable reactive intermediates complicating the automation during radiosynthesis, and immanent liability of isotopic dilution through degradation of ^{19}F -substrates used as precursors.⁵² Some procedures that have been applied to access ^{18}F -labelled trifluoromethyl compounds for both aliphatic and aromatic scaffolds are described below.

1.8.1 ^{18}F -Labelling of aliphatic compounds via trifluoromethylation

Trifluoromethyl or trifluoroalkyl groups are active motifs in drug design, and are found among a high number of pharmaceuticals. Primarily, the radiosynthesis of aliphatic ^{18}F -labelled trifluoromethyl compounds was achieved through isotope exchange method, however besides low RCYs, the major issue with isotopic exchange method is the poor molar activity of radiolabelled products, as only a fraction of molecules in the reaction mixture would be found containing ^{18}F -label.

Difluoromethyl halide precursors (CF_2X ; where $\text{X} = \text{Cl}, \text{Br}$) have also been used are seen in radiosynthesis of 1H-1-(3- ^{18}F fluoro-2-hydroxypropyl)-2-nitroimidazole ^{18}F FMISO, and 2,2,2- ^{18}F trifluoroethyl trifluoromethanesulfonate.⁵³⁻⁵⁴ Since low RCYs, harsh reaction conditions and troubles to synthesize CF_2X precursors were evident, oxidative

fluorodesulfurization scheme was introduced. The procedure undergoes desulfurization of esters or di-ester precursors to get ^{18}F -labelled building blocks, which on further reaction yield the respective ^{18}F -labelled nitroimidazoles.⁵⁵ The molar activity of radiolabelled products was comparatively better but still not useful.

A real progress towards aliphatic ^{18}F -trifluoromethylation was made when radiolabelling of ^{18}F -labelled motifs was achieved using difluorovinyl precursor/s.⁵⁶ The substrate undergoes direct nucleophilic attack of $[\text{}^{18}\text{F}]\text{F}^-$ on a difluorovinyl carbon to give 1,1,1- $[\text{}^{18}\text{F}]$ trifluoroalkanes in good RCY (up to 70%) and superior molar activity ($A_m = 100 - 150$ GBq/ μmol).

1.8.2 ^{18}F -Labelling of aromatic compounds via trifluoromethylation

Arenes containing CF_3 group/s are essential building blocks for a variety of agrochemicals and drug molecules. A radiolabelling method that could substantially provide ^{18}F -labelled analogues of these compounds in good molar activity is highly desired. The procedures used in aliphatic ^{18}F -trifluoromethylation have also been applied in radiosynthesis of aromatic compounds. This includes both direct ^{19}F -to- ^{18}F exchange, (isotopic exchange method), and X substitution of CF_2X substrates, but low RCY and poor molar activity was a pertinent challenge. A major improvement in ^{18}F -trifluoromethylation of aromatic compounds was observed when recently developed procedures involving *in-situ* synthesis of $[\text{}^{18}\text{F}]$ trifluoromethane ($[\text{}^{18}\text{F}]\text{CF}_3\text{H}$), and Cu(I) coupled fluorocarbene ($\text{Cu}[\text{}^{18}\text{F}]\text{CF}_3$) were implemented.⁵⁷⁻⁵⁸ The RCY has improved up to 90 %, but molar activity was still 10 – 100 times lower than what is practically achievable through a nucleophilic radiofluorination methods using n.c.a $[\text{}^{18}\text{F}]\text{F}^-$.⁵²

A slight improvement in molar activity was observed when some optimization in radiosynthesis of $[\text{}^{18}\text{F}]\text{CF}_3\text{H}$ was achieved, and 4-nitro-1- $([\text{}^{18}\text{F}])$ trifluoromethylbenzene was obtained in molar activity of 22 – 32 GBq/ μmol .⁵⁹ Though the molar activity was improved, but the method is challenging to adopt because of two-steps approach, as only few automated synthesizers have an in-build two reaction vial set-up for such synthesis. Furthermore $[\text{}^{18}\text{F}]\text{CF}_3\text{H}$, is a gas at room temperature, and trapping or distillation of this at -80 °C under radiolabelling conditions further limits the method applicability. Nonetheless, $[\text{}^{18}\text{F}]\text{CF}_3\text{H}$ and $\text{Cu}[\text{}^{18}\text{F}]\text{CF}_3$ have provided access to a broad range of substrates in short reaction times, and high RCY. The overall progression about development of ^{18}F -labelled arenes via trifluoromethylation is surmised in Figure 1.6.

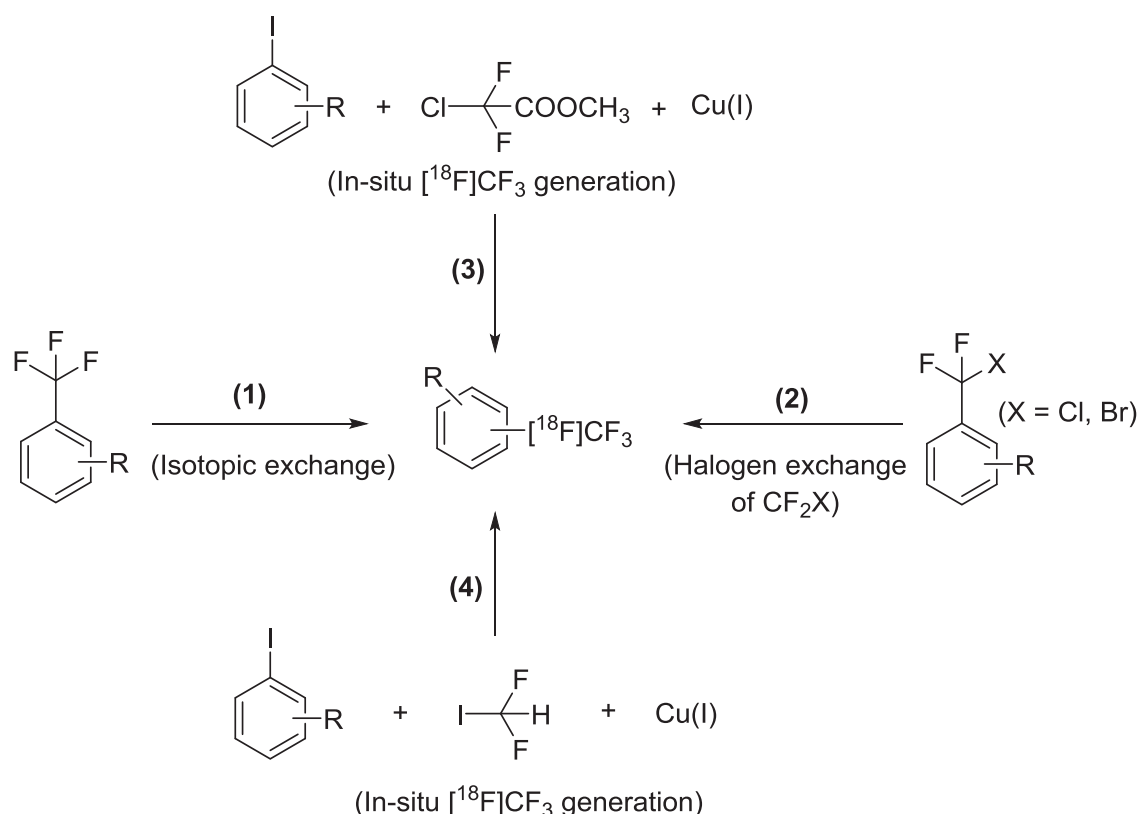


Figure – 1.6: Different schemes employed for ^{18}F -trifluoromethylation of arenes. Isotopic exchange method (1), halogen substitution of difluoroalkyl halide substrates (2), through *in-situ* synthesis of $\text{Cu}^{18}\text{F-CF}_3$ and $^{18}\text{F-CF}_3\text{H}$ (3 and 4)

1.9 Some limitations of ^{18}F chemistry

Several factors influence the production of $^{18}\text{F-F}^-$. For example beam current, irradiation time, targetry including composition and purity of the target material, and ^{19}F contamination of the radionuclide, either from the production system or through the transfer lines affect the quality of $^{18}\text{F-F}^-$ for radiotracer applications.⁶⁰⁻⁶¹ The low concentration of $^{18}\text{F-F}^-$ in nanomolar quantities during radioactive experiments can be problematic because trace amounts of cationic impurities or proton source may reduce the availability of $^{18}\text{F-F}^-$ for nucleophilic attack.⁶¹⁻⁶² This is why some reactions are difficult to reproduce under radiolabelling conditions, but work in normal organic synthesis.

1.10 Radiolabelling of compounds with ^{11}C

Considering that carbon is an essential component of all organic molecules, carbon-11 (^{11}C) is another attractive candidate from the PET radionuclide series. Radiolabelling of biologically active compounds with ^{11}C may provide PET radiotracers that would have exactly the same

pharmacological profile as their non-radioactive analogues. Positron range of ^{11}C in tissues ($R_{\text{mean}} = 1.1$ mm) and energy ($E_{\text{max}} = 0.96$ MeV) is appropriate to get good quality images, but the major concern with ^{11}C -radiotracers is the shorter half-life ($t_{1/2} = 20.4$ min), which limits their applications.¹⁰⁻¹¹

^{11}C is produced by cyclotron irradiation using the $^{14}\text{N}(p,\alpha)^{11}\text{C}$ nuclear reaction. It is obtained as ^{11}C -labelled carbon dioxide ($[^{11}\text{C}]\text{CO}_2$) or ^{11}C -labelled methane ($[^{11}\text{C}]\text{CH}_4$) in the presence of small amounts of Oxygen (< 1%) or hydrogen (~ 5%) respectively.⁶³⁻⁶⁴ $[^{11}\text{C}]\text{CO}_2$ is reactive enough and may be used directly, while $[^{11}\text{C}]\text{CH}_4$ is converted to more reactive and easy to control secondary precursors, for example, iodo $[^{11}\text{C}]$ methane ($[^{11}\text{C}]\text{CH}_3\text{I}$),⁶⁵ $[^{11}\text{C}]$ methyl trifluoromethanesulfonate ($[^{11}\text{C}]\text{CH}_3\text{OTf}$),⁶⁶ $[^{11}\text{C}]$ methyl magnesium iodide ($[^{11}\text{C}]\text{CH}_3\text{MgI}$),⁶⁷ nitro $[^{11}\text{C}]$ methane ($[^{11}\text{C}]\text{CH}_3\text{NO}_2$),⁶⁸ hydrogen $[^{11}\text{C}]$ cyanide $[^{11}\text{C}]\text{HCN}$,⁶⁹ $[^{11}\text{C}]$ carbonyl dichloride ($[^{11}\text{C}]\text{COCl}_2$),⁷⁰ and other useful reagents shown in Figure 1.7.

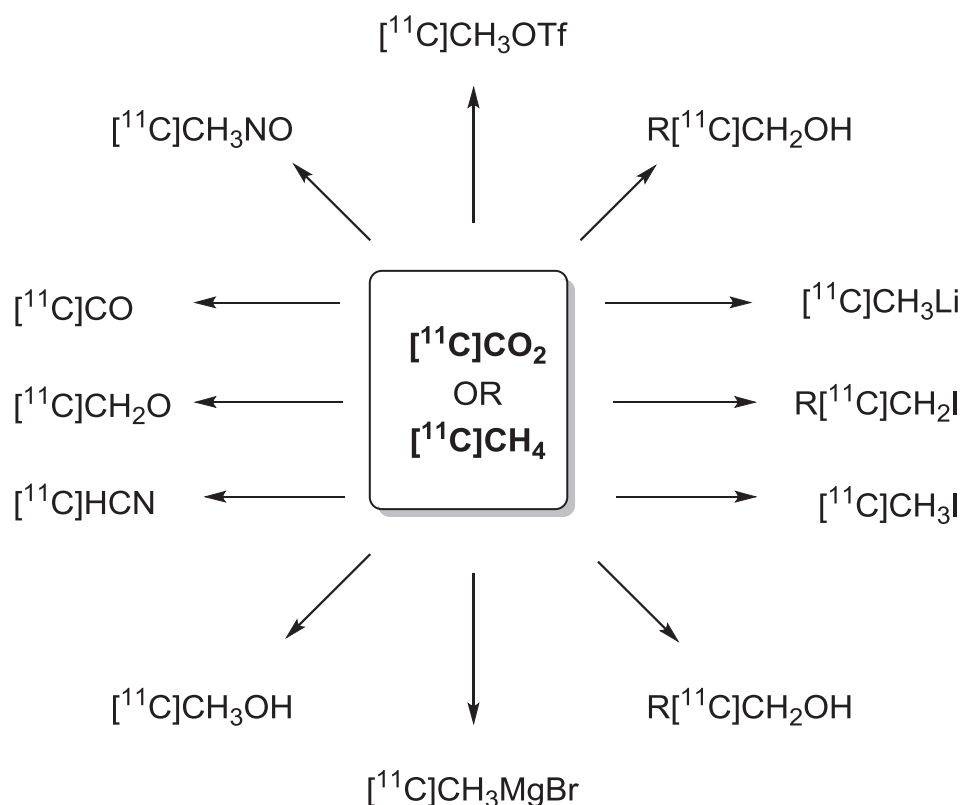


Figure – 1.7: The scope of secondary precursors available from $[^{11}\text{C}]\text{CO}_2$ and $[^{11}\text{C}]\text{CH}_4$.

^{11}C -methylation is the most frequently employed method to get ^{11}C -labelled radiotracers. ^{11}C -methylation of organic compounds is achieved through $[^{11}\text{C}]\text{CH}_3\text{I}$ or $[^{11}\text{C}]\text{CH}_3\text{OTf}$, because of their pronounced reactivity, convenient access in both solution or gas form, and possibility

to introduce the ^{11}C at later stages of radiosynthesis. The method employs $-\text{N}$, $-\text{O}$ or $-\text{S}$ alkylation with $[^{11}\text{C}]\text{CH}_3\text{I}$ or other alkylating agents, i.e. iodo $[^{11}\text{C}]\text{ethane}$ or iodo $[^{11}\text{C}]\text{propane}$,⁷¹ as may be seen among a number of radiotracers used in pre-clinical and clinical applications including $[^{11}\text{C}]\text{methyl-1-(2-phenylethyl)-4-[phenyl(propanoyl)amino]piperidine-4-carboxylate}$ ($[^{11}\text{C}]\text{carfentanil}$),⁷² $3,5\text{-dichloro-N-}[[\text{(2S)-1-ethylpyrrolidin-2-yl]methyl] \text{-2-hydroxy-6-} [^{11}\text{C}]\text{methoxybenzamide}$ ($[^{11}\text{C}]\text{raclopride}$),⁷³ and $2\text{-}(4\text{-} [^{11}\text{C}]\text{methylaminophenyl})\text{-6-hydroxybenzothiazole}$ ($[^{11}\text{C}]\text{Pittsburgh Compound-B}$).⁷⁴

^{11}C -carboxylation is a powerful but underused method to access ^{11}C -radiotracers. In ^{11}C -carboxylation reactions, $[^{11}\text{C}]\text{CO}_2$ obtained from cyclotron is converted to ^{11}C -labelled carboxylic acids ($\text{R}[^{11}\text{C}]\text{COOH}$). The radiolabel is situated in the ^{11}C -carboxyl group. Most applications of the reaction involve organolithium or Grignard reagents.⁷⁵ The reaction is attractive considering the short half-life of ^{11}C . Normally more than half of the starting activity is lost during the production of secondary labelling reagents from $[^{11}\text{C}]\text{CO}_2$. Hence, direct approaches involving straightforward incorporation of ^{11}C with $[^{11}\text{C}]\text{CO}_2$ are more appropriate.⁷⁶⁻⁷⁷

1.11 Characterization of radiotracers

The main objective behind the development of PET radiotracers is their use in investigation of biological processes or mechanism of diseases. Rodents, specifically rats are normally used as biological models to study the suitability of new candidates for translation to man. *In vivo* imaging in rats is a frequently applied tool to characterize the effectiveness of developed radiotracers in living subjects. All newly developed radioligands are carried through a thorough pre-clinical evaluation including *in vivo*, *ex vivo* and *in vitro* characterization before proceeding to clinical trials.

The *in vivo* PET imaging provides information about the binding and kinetic distribution of radiotracers. It is performed both under baseline conditions, where the pure radioligand is injected and the time dependent concentration per volume is recorded. Typical units include percent injected dose per mL (%ID/mL), activity concentration in tissues (Bq/mL) or standard-uptake value (SUV). In order to confirm the specific binding, a blocked study is performed where a non-radioactive blocking agent (specific to the target) in saturating amounts is injected prior to the radiotracer. An anatomical MRI template is used to define the region of interest (ROI) and activity concentration curves as function of time (time-activity curves; TAC) are derived for both baseline and blocked studies.

Some PET studies require blood sampling to analyse the true (non-metabolized) concentration of radiotracer, especially when a radioactive metabolite interferes with the specific signal. For these studies, the arterial blood is taken at various time-points to evaluate the fraction of intact radiotracer, which is then used to correct the plasma input function for specified models. *Ex vivo* studies may also be performed to analyse the metabolites, but provides a single point value as the analysis is made after sacrificing the animals. Additionally, the brain may be sliced and binding of the radiotracer may be defined through autoradiography imaging.

In vitro autoradiography is another technique used to analyse binding (both specific and non-specific) of candidate radioligands. The desired compound should be labelled with a low-energy nuclide e.g. tritium (^3H) or iodine-125 (^{125}I). The non-radioactive reference compounds are used at decreasing concentrations to determine the percent inhibition in binding using a target selective ^3H or ^{125}I -labelled radioligands.

Chapter 2 – Biology of the target systems

Two biological target systems were selected to apply the new methods in the synthesis of radiotracers. The radioligands obtained through aliphatic ^{18}F -trifluoromethylation were used for detection of neurofibrillary tangles (NFTs) in Alzheimer's disease (AD). The compounds radiolabelled through the aromatic ^{18}F -trifluoromethylation method were applied for the quantification of mu-opioid receptors (MOR).

2.1 Biology involved in aggregation of tau-proteins

Neurodegeneration is a group of diseases identified by structural deformities, and mitochondrial damage of the neurons.⁷⁸ It results in accumulation of toxic proteins both inside (intra-) and outside (extra-cellular) of the neurons, named tau-proteins, amyloid beta (amy β), α -synuclein (α -syn), prion, huntingtin and ataxins.⁷⁹ AD is a neurodegenerative disease affecting more than 7 million people in Europe alone.⁸⁰ Besides other ramifications, the existence of paired helical filaments (PHFs) resulting in aggregation of intra-neuronal masses called neurofibrillary tangles (NFTs) is a known manifestation to the disease.⁸¹⁻⁸²

2.1.2 Formation of neurofibrillary tangles

NFTs are abnormal aggregates of disrupted tau-protein fragments. Tau is a microtubules associated protein which helps in stabilizing microtubules for regular transportation of cellular components.⁸³ Due to hyperphosphorylation, microtubules disintegrate resulting in dispersion of several tau-filaments. These dispersed filaments stick to one another to form the paired helical filaments (PHFs), which on higher aggregation form the tangles.⁸⁴⁻⁸⁵ As a result, the internal transport between the neurons is disrupted and inter-neuronal connection is destroyed.

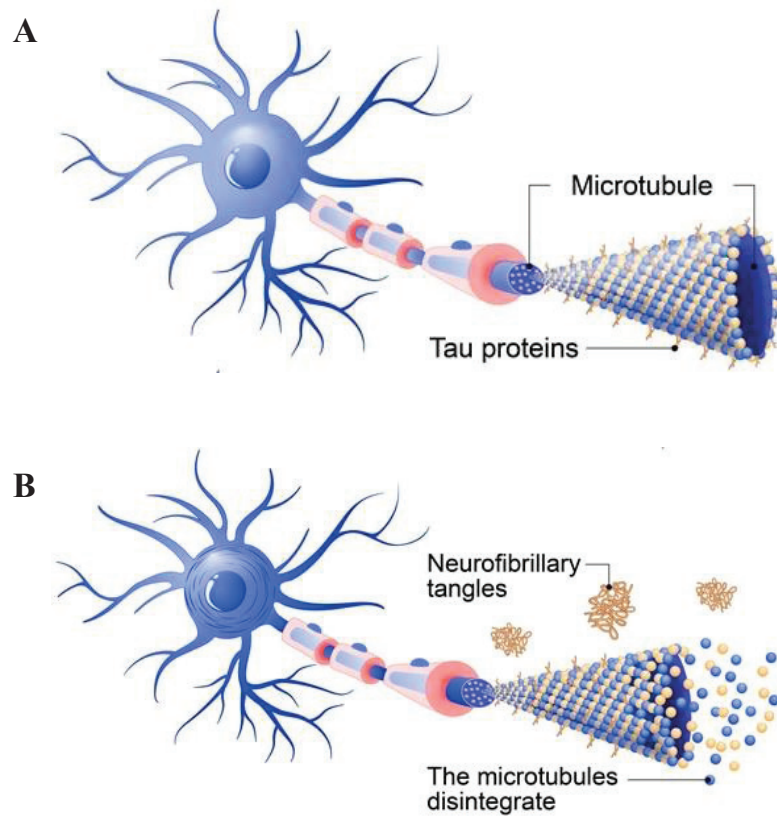


Figure – 2.1: A healthy neuron with intact microtubules (A), a damaged neuron showing disintegration of microtubules and formation of NFTs (B) (The figure was taken from shutterstock.com)

Since the existence of NFTs is a known neuropathological hallmark in AD, which could be made visible with PET, diagnostic radiotracers with low nanomolar affinity and appropriate selectivity are under development. Some radiotracers have been used in clinical trials but confound with low radiotracer uptake, non-specific binding, and cross-affinity to other target proteins.⁸⁶⁻⁹⁰

2.2 Biology of opioids receptors

Opioid receptors (OR) are G-protein coupled receptors, which are distributed throughout the brain and peripheral regions of the body. Out of the known subtypes of ORs, mu (MOR), kappa (KOR) and delta (DOR) opioid receptors are of major importance due to their involvement in a variety of diseases and behaviours.⁹¹⁻⁹³

Despite the confined locality and 50 – 70% homology, distribution of ORs has been defined to much extent. It is known that MOR are highly expressed in thalamus, striatum, cortex, and foci of the brain-stem, while KOR are located within the base of anterior forebrain, olfactory

tubercle and nucleus accumbens, whereas DOR in cerebellum, olfactory bulbs, neocortex and basolateral nuclei of the amygdala.⁹⁴⁻⁹⁵

Several ¹¹C or ¹⁸F-labelled radioligands have been developed and used clinically, but are hindered due to antagonist nature, high binding affinity and poor selectivity resulting in lack of discrimination between receptors.⁹⁶⁻¹⁰⁰ Additionally, tightly bound radiotracers provide delayed equilibration of binding *in vivo*. Hence, sub-type selective low-to-moderate affinity radioligands are needed.

Chapter 3 – Aim of the Thesis

^{18}F -Trifluoromethylation has gained considerable attention due to existence of trifluoromethyl ($-\text{CF}_3$) groups among a wide range of pharmaceuticals and drug molecules. Substantial progress regarding introduction of CF_3 to organic compounds have been achieved, but translation of these methodologies to radiochemistry is challenging.

The first objective was to develop the procedures that may lead to introduction of $[\text{}^{18}\text{F}]\text{CF}_3$ into both aliphatic and aromatic substrates.

The second objective was to prove the applicability of established procedures. To achieve this, lansoprazole (LNS), a known drug with inherent selectivity for NFTs, and a derivative of AH7921, a μ -selective opioid agonist were radiolabelled successfully.

The third objective was to discover new radiotracer candidates that have an equal or better affinity/selectivity profile compared to lead compounds, LNS and AH7921, and may be radiolabelled with ^{11}C or preferably with ^{18}F . For this, more than 20 new compounds were designed for each target system, and few candidates were radiolabelled from each series for *in vivo* characterization with PET.

Chapter 4 – Summary of Results and Discussion

In **Paper-1** of the thesis, a monograph, radiosynthesis of 2,2,2-[^{18}F]trifluoroethyl tosylate is described. The compound was obtained using 2,2-difluorovinyl precursor in single step within 40 minutes from end of bombardment (EOB) in 70 % RCY, and with molar activity of 150 GBq/ μmol , which is so far the best molar activity reported for aliphatic ^{18}F -trifluoromethylation reactions. Furthermore, the method does not demand troublesome synthesis of CF_2X precursors, instead it proceeds through direct nucleophilic attack of [^{18}F]F $^-$ on difluorovinyl carbon via formation of an anionic intermediate as shown in Figure 4.1.

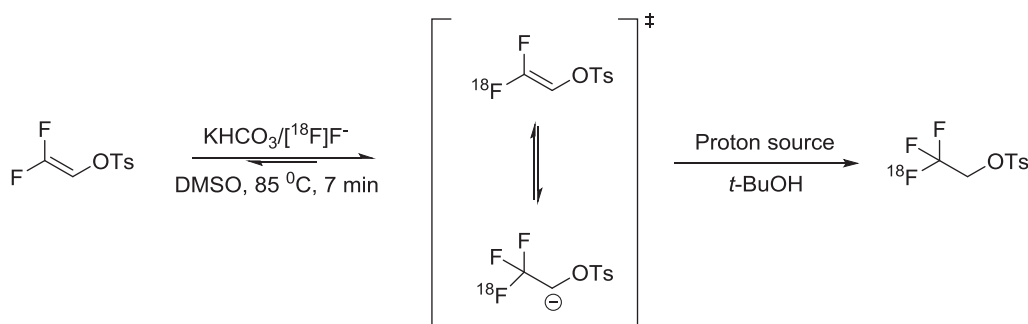


Figure – 4.1: The proposed mechanism for ^{18}F -trifluoromethylation of aliphatic substrates using a difluorovinyl precursor.

Since the intermediate anion undergoes addition-elimination, the reaction may lead to a mixture of by-products with possibly an increase in cold mass, therefore a proton source ($t\text{-BuOH}$) was used to trap the intermediate anion and to shift the reaction outcome towards the desired product.

As an application to the method, 2-(((3-methyl-4-(2,2,2-trifluoroethoxy)pyridin-2-yl)methyl)sulfinyl)-1H-benzimidazole, a known drug named lansoprazole (LNS) was radiolabelled. There were two reasons to select LNS; **a)** the compound has an in-built CF_3 group and may be labelled using developed ^{18}F -trifluoromethylation method, **b)** LNS has shown marked affinity for tau aggregates *in vitro*.¹⁰¹⁻⁰² Hence radiolabelling of LNS will document the applicability of our method on one side, whereas on other, it will allow to perform the clinical studies for detection of tau in AD patients.

Since LNS is a registered medicinal product, performing clinical studies with [^{18}F]LNS is fairly straightforward. Hence, clinical studies with [^{18}F]LNS in human volunteers were performed to confirm if it crosses the blood-brain barrier (BBB) in healthy subjects. In the next phase, retention of the radiotracer in the brain of AD positive patients was tested. To accomplish this, fully automated GMP compliant radiosynthesis of [^{18}F]LNS and 2-(((4-(2,2-difluoro-2- ^{18}F ethoxy)-3-methylpyridin-2-yl)methyl)sulfinyl)-1-methyl-1H-benzoimidazole ([^{18}F]NML) were performed on IBA Synthera module (IBA radioPharma solutions, Belgium). A total of seven participants, 4 healthy volunteers (mean age 60.2 ± 6.0 years) and three AD positive patients (mean age 72.0 ± 6.0 years) clinically diagnosed with mild-to-moderate AD were included in the study.

The clinical studies performed with [^{18}F]NML show good brain penetration and promising grey matter binding, whereas with [^{18}F]LNS insufficient brain penetration was observed (Paper 2: Fig 1). A SUV of 2 g/mL (6.6 kBq/mL) peaked at 10 – 20 seconds was observed with [^{18}F]LNS, which was reduced to SUV of 0.5 g/mL (2.4 kBq/mL) within 5 minutes. The activity remained constant after 5 minutes throughout the scan, and no significant difference in [^{18}F]LNS uptake between healthy controls and AD patient was observed.

Through clinical studies it was confirmed that [^{18}F]LNS does not show reasonable brain penetration, but [^{18}F]NML does. Based on clinical results, a set of 22 new compounds was synthesized using a retrosynthesis approach. The new compounds were designed so that they may be labelled with ^{11}C or with ^{18}F for *in vivo* studies with PET. The affinity of the compounds was determined using recombinant human tau proteins (htau-441) with the help of ^3H -labelled astemizole, AST (^3H AST) autoradiography. Selectivity of the compounds against amy β and α -syn was determined using thioflavine-T fluorescence assay. Three most potent compounds with good selectivity profile were selected and 2-(((4-(2- ^{18}F fluoroethoxy)-3-methylpyridin-2-yl)methyl-sulfinyl)benzoxazole, [^{18}F]1 was radiolabelled for *in vivo* characterization with PET. The synthesis of compounds, their structure activity relationship, binding profile towards tau, amy β and α -syn, and radiosynthesis of [^{18}F]1 is described in **Manuscript-II** of the thesis.

In **Paper-III**, a radiolabeling method for direct installation of [^{18}F]CF $_3$ into a range of aromatic substrates is described. ^{18}F -trifluoromethylation of arenes have not been achieved with such a simple procedure before. The developed method allows widespread access to [^{18}F]CF $_3$ arenes using standardised radiosynthesis instrumentation, and does not involve

delicate reactive intermediates. The proposed mechanism for ^{18}F -trifluoromethylation of aromatic compounds is shown in Figure 4.2.

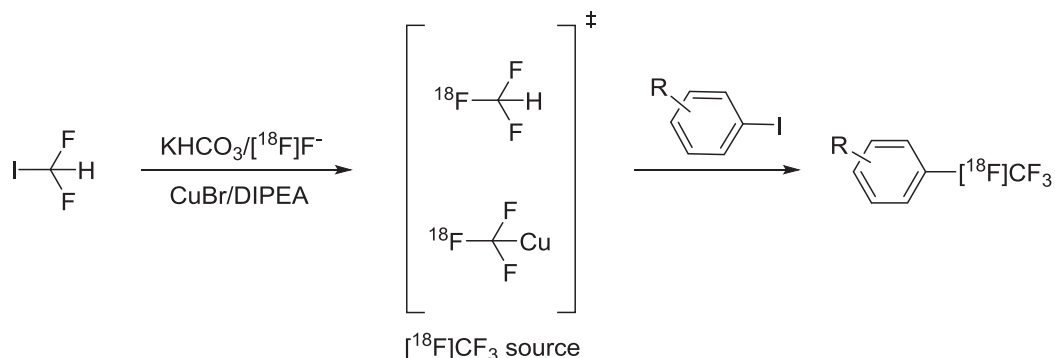


Figure – 4.2: Scheme for ^{18}F -trifluoromethylation of aromatic compounds.

As an application of the method, a μ -selective opioid agonist, 3,4-dichloro-*N*-((1-(dimethylamino)cyclohexyl)methyl)benzamide, (AH7921, **2**) was selected. The compound **2** is an interesting candidate because of attractive combination of physical and chemical properties. **2** is an opioid agonist, and has analgesic properties comparable to morphine.¹⁰³ In addition, the compound has $-\text{Cl}$ substituents, at meta and para to a benzamide moiety, which provides suitable sites for ^{18}F -trifluoromethylation because of isosteric equivalence of $-\text{Cl}$ to $-\text{CF}_3$.

Despite a good affinity of 1.8 nM for MOR, no *in vivo* binding information was available for compound **2**. Hence, radiolabelling of **2** was performed using ^{11}C -labelled 3,4-dichloro benzoylchloride, which on coupling with 1-(aminomethyl)-*N,N*-dimethylcyclohexylamine provide $[^{11}\text{C}]\mathbf{2}$ in an overall non-decay corrected RCY of 1 – 2 %. The $[^{11}\text{C}]\mathbf{2}$ was characterized in rats with PET and autoradiography using agonist, Tyr-D-Ala-Gly-N($[^3\text{H}]\text{Me}$)Phe-Gly-ol ($[^3\text{H}]\text{DAMGO}$) and antagonists (4R,4aS,7aR,12bS)-4a,9-dihydroxy-3-prop-2-enyl-2,4,5,6,7a,13-hexahydro- $[^3\text{H}]-4,12$ -methanobenzofuro[3,2-*e*]isoquinoline-7-one ($[^3\text{H}]\text{naloxone}$) radioligands. Both PET and autoradiography experiments confirmed good radiotracer uptake, and moderate binding affinity to regions rich in MOR. The radiosynthesis, and *in vitro* and *in vivo* characterization of $[^{11}\text{C}]\mathbf{2}$ in rat is explained in **Paper-IV** of the thesis.

After confirming the μ -selective binding of **2**, a new set of compounds was synthesized based on slight modification to **2**. Considering activated benzoyl moiety for direct nucleophilic radiofluorination with $[^{18}\text{F}]\text{F}^-$, and isosteric equivalence of $-\text{Cl}$ to $-\text{CF}_3$, 20 new compounds were designed carrying F or CF_3 at various possible positions for ^{18}F -radiolabelling. The agonist potency of the compounds for MOR, KOR, and DOR was

determined. Despite small modifications, almost all compounds retain affinity towards MOR and have an attractive combination of affinity and selectivity. Three new compounds were selected from the series, and ^{18}F -radiolabelling was achieved for *in vivo* quantification of MOR in rats. The structures and radiosynthesis of selected candidates is shown in Figure 4.3.

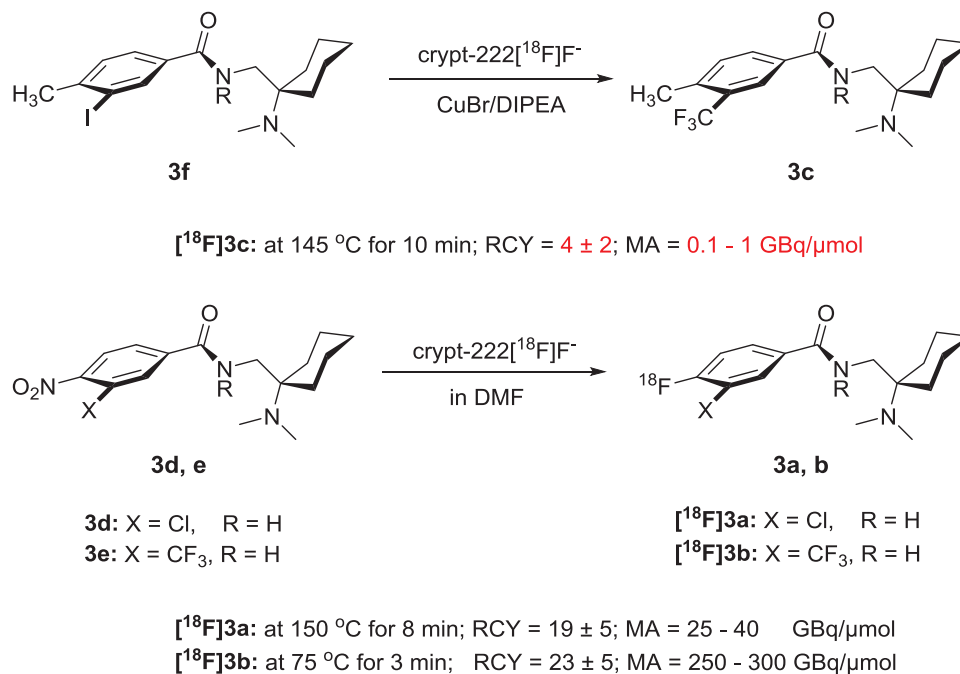


Figure – 4.3: Schemes for radiosynthesis of [^{18}F]3c, [^{18}F]3a, and [^{18}F]3b

The compound *N*-((1-(dimethylamino)cyclohexyl)methyl)-4-methyl-3-(trifluoromethyl)benzamide, **3c** was the most interesting candidate with an affinity of 1 nM for MOR, compared to 45 nM and 88 nM for KOR and DOR respectively. In addition, the compound has CF₃ group and may be labelled using the developed [^{18}F]CF₃ radiolabelling methods of arenes. Eventually, the iodo precursor, *N*-((1-(dimethylamino)cyclohexyl)methyl)-3-iodo-4-methylbenzamide, **3f** was synthesized, and radiolabelling of [^{18}F]3c was performed using procedure described in paper-III of the thesis.

The [^{18}F]3c was obtained in 71 % yield, but with molar activity of 0.01 GBq/ μmol . Since the quality of radiotracer was not sufficient to perform PET studies in small animals, a series of experiments were performed where the amount of CHF₂I was reduced to find a compromise between the RCY and molar activity using 4-iodobenzonitrile as substrate (Paper 5: Figure 2). After optimizing the amount of CHF₂I and applying the same reaction conditions to radiosynthesis of **3c**, [^{18}F]3c was obtained in 34 % RCY in molar activity of 0.02 – 0.05 GBq/ μmol . With some further tuning, [^{18}F]3c was obtained in 4 ± 2 % RCY when 3 μmol of CHF₂I was used, in molar activity of 0.1 – 0.3 GBq/ μmol (n = 2). Only traces of

product was obtained when less than 3 μmol CHF_2I was used. Even using high activity batches of ^{18}F (up to 10 GBq), $[^{18}\text{F}]\mathbf{3c}$ was obtained in molar activity of 0.1 – 1 GBq/ μmol . The optimization of CHF_2I used for reaction, and radiosynthesis of $[^{18}\text{F}]\mathbf{3c}$ is described in **Manuscript-V** of the thesis.

As the minimum requirements for rodent PET studies were not reached, and the efforts to improve the molar activity of $[^{18}\text{F}]\mathbf{3c}$ did not lead to success, it was not possible to use $[^{18}\text{F}]\mathbf{3c}$ for *in vivo* characterization under these circumstances. Since a couple of interesting compounds in good-to-moderate affinity were found which may be labelled in high molar activity via direct nucleophilic radiofluorination using $[^{18}\text{F}]\text{F}^-$. Hence radiosynthesis of 3-chloro-N-((1-(dimethylamino)cyclohexyl)methyl)-4- $[^{18}\text{F}]\text{fluorobenzamide}$ ($[^{18}\text{F}]\mathbf{3a}$) and N-((1-(dimethylamino)cyclohexyl)methyl)-4- $[^{18}\text{F}]\text{fluoro-3-(trifluoromethyl)benzamide}$ ($[^{18}\text{F}]\mathbf{3b}$) was performed. Both candidates have good-to-moderate affinity for MOR (EC_{50} ($\mathbf{3a}$) = 24.8 nM; EC_{50} ($\mathbf{3b}$) = 8.6 nM) and would result in fast radiotracer binding equilibrium *in vivo*.

Radiosynthesis of $[^{18}\text{F}]\mathbf{3a}$ was studied first. Precursor *3-chloro-N-((1-(dimethylamino)cyclohexyl)methyl)-4-nitrobenzamide* ($\mathbf{3d}$) was synthesized and NO_2 -to- ^{18}F substitution was achieved in 78 % RCY after optimisation of reaction parameters (Paper 5: Figure 3). The $[^{18}\text{F}]\mathbf{3a}$ was obtained in 19 ± 5 % non-decay corrected RCY in final formulation with molar activity of 25 – 40 GBq/ μmol . The radiosynthesis, *in vivo* and *in vitro* characterization of $[^{18}\text{F}]\mathbf{3a}$ is described in **Manuscript-VI** of the thesis.

When $[^{18}\text{F}]\mathbf{3b}$ was synthesized using the conditions described in radiosynthesis of $[^{18}\text{F}]\mathbf{4a}$, high mass of the reference compound $\mathbf{3b}$ was observed in the reaction mixture. Control experiments were performed and it was found the precursor, N-((1-(dimethylamino)cyclohexyl)methyl)-4-nitro-3-(trifluoromethyl)benzamide ($\mathbf{3e}$) degrades on heating and generates excess ^{19}F , which results in high amounts of non-radioactive product. Hence, the condition were re-optimized to obtain $[^{18}\text{F}]\mathbf{3b}$ in good quality.

It was decided to use lower temperatures combined with shorter reaction time and lower precursor quantity. Radiolabeling was performed at various temperatures gradually decreasing from 150 $^\circ\text{C}$ to 75 $^\circ\text{C}$ where only 0.8 μg (2.3 nmol/mL) of reference compound was obtained in final formulation using 2.5 – 3 mg $\mathbf{3e}$ at 75 $^\circ\text{C}$ for 3 minutes (Paper 5: Fig 4). Eventually, $[^{18}\text{F}]\mathbf{3b}$ was achieved via a fully automated protocol in 23 ± 5 % RCY in molar activity of 250 – 300 GBq/ μmol . The *in vivo* and *in vitro* characterization of $[^{18}\text{F}]\mathbf{3b}$ is provided in **Manuscript-VII** of the thesis.

Chapter 5 – Conclusion and future prospects

The efficient procedures to access [^{18}F]CF₃ labelled compounds for both aliphatic and aromatic substrates were developed. Both methods are applicable to available radiochemistry hardware for robust outcomes, and provide radiolabelled products in good RCY.

The aliphatic radiolabelling method was applied to radiosynthesis of [^{18}F]LNS and [^{18}F]NML, and translated to GMP-production for detection of NFTs in clinical studies. Aromatic [^{18}F]CF₃ labelling was achieved through copper catalyzed coupling of [^{18}F]CF₃Cu using iodoarenes via a single vial one-step method. As proof of principle, the method was applied to radiosynthesis of a derivative of AH7921.

More than 20 new compounds preferably containing F or CF₃ were synthesized for each target system to derive ^{18}F -labelled PET radiotracer/s. The structure-activity relationship of designed compounds provide further insights about binding profile and *in vitro* activation of the target systems. Several interesting candidates from each series were identified and radiolabelled with ^{18}F for *in vivo* characterization with PET.

Based on initial findings, an additional set of compounds was prepared and is under investigation to get a more detailed understanding about *in vivo* pharmacological profile of developed radiotracers candidates. The results would be communicated in continuation to the performed studies when completed.

Chapter 6 – References

1. Walker HK. The origin of history and physical examination. In: clinical methods: the history, physical, and laboratory examinations. 3rd ed. Boston: Butterworths; 1990. p. 5-21.
2. Maisey MN. Positron Emission Tomography in Clinical Medicine. In: Bailey DL, Townsend DW, Valk PE, Maisey MN. Positron emission tomography: basic sciences. London: Springer-Verlag; 2005. p. 1-12.
3. Miller PW, Long NJ, Vilar R, Gee AD. Synthesis of ^{11}C , ^{18}F , ^{15}O , and ^{13}N radiolabels for positron emission tomography. *Angew Chem Int Ed.* 2008;47:8998-9033.
4. Myers WG. Georg Charles De Hevesy: The father of nuclear medicine. *J Nucl Med.* 1979;20(6):590-94.
5. Chiewitz O, Hevesy G. Radioactive indicators in the study of phosphorus metabolism in rats. *Nature.* 1935;136:754-55.
6. Wrenn FR, Good ML, Handler P. The use of positron-emitting radioisotopes for the localization of brain tumours. *Science.* 1951;113(2940):525-27.
7. Tian J. Molecular imaging: fundamentals and applications. Heidelberg, New York, Dordrecht, London: Springer-Verlag; 2013.
8. Nutt R. The history of positron emission tomography. *Mol Imaging Biol.* 2002;4(1):11-26.
9. Ter-Pogossian MM, Phelps ME, Hoffman EJ, Mullani NA. A positron-emission transaxial tomograph for Nuclear Imaging (PETT). *Radiology.* 1975;114:89-98.
10. Saha GB. Fundamentals of nuclear pharmacy. 6th ed. New York, Heidelberg, Dordrecht, London: Springer-Verlag; 2010.
11. Bailey DL, Karp JS, Surti S. Physics and Instrumentation in PET. In: Bailey DL, Townsend DW, Valk PE, Maisey MN. Positron emission tomography: basic sciences. London: Springer-Verlag; 2005. p. 13-40.
12. Saha GB. Basics of pet imaging: physics, chemistry, and regulations. New York: Springer-Verlag; 2005.
13. Saha GB, MacIntyre WJ, Go RT. Cyclotrons and positron emission tomography radiopharmaceuticals for clinical imaging. *Semin Nucl Med.* 1992;22(3):150-61.

14. Browne E, Firestone RB. Table of radioactive isotopes. New York: John Wiley & Sons; 1986.
15. Arino H, Skraba WJ, Kramer HH. A new $^{68}\text{Ge}/^{68}\text{Ga}$ radioisotope generator system. *Int J Appl Radiat Isot.* 1978;29(2):117-20.
16. Grant PM, Erdal BR, O'Brien HA. A $^{82}\text{Sr}-^{82}\text{Rb}$ isotope generator for use in nuclear medicine. *J Nucl Med* 1975;16(4):300-04.
17. Skraba WJ, Arino H, Kramer HH. A new $^{90}\text{Sr}/^{90}\text{Y}$ radioisotope generator. *Int J Appl Radiat Isot.* 1978;29(2):91-96.
18. Robinson GD, Zielinski FW, Lee AW. The zinc-62/copper-62 generator: a convenient source of copper-62 for radiopharmaceuticals. *Int J Appl Radiat Isot.* 1980;31(2):111-16.
19. Lawrence EO. The evolution of the cyclotron. Nobel Lecture; 1951.
20. Jongen Y. High beam intensities for cyclotron-based radioisotope production. International Atomic Energy Agency, Technical Document. 1999;1065:133-38.
21. Riss PJ, Rösch F. A convenient chemo-enzymatic synthesis and ^{18}F -labelling of both enantiomers of trans-1-toluenesulfonyloxymethyl-2-fluoromethyl-cyclopropane. *Org Biomol Chem.* 2008;6:4567-74.
22. Lambrecht RM, Neirinckx R, Wolf AP. Cyclotron isotopes and radiopharmaceuticals: novel anhydrous ^{18}F -fluorinating intermediates. *Int J Appl Radiat Isot.* 1978;29:175-83.
23. Bishop A, Satyamurthy N, Bida G, Hendry G, Phelps M, Barrio JR. Proton irradiation of $[\text{O}]_2$: production of $[\text{F}]_2$ and $[\text{F}]_2 + [\text{F}]\text{OF}_2$. *Nuc Med Biol.* 1996;23:189-99.
24. Banister S, Roeda D, Dolle F, Kassiou M. Fluorine-18 chemistry for pet: a concise introduction. *Curr Radiopharm.* 2010;3:68-80.
25. Chirakal R, Firnau G, Schrobilgen JG, McKay J, Garnett ES. The synthesis of $[\text{F}]_2$ from $[\text{F}]_2$ gas. *Int J Appl Radiat Isot.* 1984;35:401-04.
26. Shiue CY, Salvadori PA, Wolf AP. A new synthesis of 2-deoxy-2- $[\text{F}]_2$ -D-glucose from ^{18}F -labeled acetyl hypofluorite. *J Nucl Med.* 1982;23:899-903.
27. Ehrenkauf RE, MacGregor RR. Synthesis of $[\text{F}]_2$ -perchloryl fluoride and its reactions with functionalized aryl lithiums. *Int J Appl Radiat Isot.* 1983;34:613-15.
28. Oberdorfer F, Hofmann E, Maier-Borst W. Preparation of ^{18}F -labeled N-fluoropyridinium triflate. *J Label Compds Radiopharm.* 1988;25:999-1005.

29. Satyamurthy N, Bida GT, Phelps ME, Barrio JR. Fluorine-18 labeled N-[¹⁸F]fluoro-N-alkylsulfonamides: novel reagents for mild and regioselective radiofluorination. *Appl Radiat Isot.* 1990;41:733-38.
30. Hamacher K, Coenen HH, Stöcklin G. Efficient stereospecific synthesis of no-carrier-added 2-[¹⁸F]-fluoro-2-deoxy-D-glucose using aminopolyether supported nucleophilic substitution. *J Nucl Med.* 1986;27(2):235-38.
31. Coenen HH. Fluorine-18 labeling methods: features and possibilities of basic reactions. *ernst schering res found workshop.* 2007;62:15-50.
32. Schlyer DJ, Bastos MA, Alexoff D, Wolf AP. Separation of [¹⁸F]fluoride from [¹⁸O]water using anion exchange resin. *Int J Rad Appl Instrum.* 1990;41(6):531-33.
33. Wuts GM, Greene TW. *Greene's protective groups in organic synthesis.* 4th ed. Hoboken, New Jersey: John Wiley & Sons; 2007.
34. Kilbourn MR. *Fluorine-18 labeling of radiopharmaceuticals.* Washington: National academy press; 1990.
35. Block D, Coenen HH, Stöcklin G. The n.c.a. nucleophilic ¹⁸F-fluorination of 1,N-disubstituted alkanes as fluoroalkylation agents. *J Label Compds Radiopharm.* 1987;24(9):1029-42.
36. Zhang MR, Suzuki K. [¹⁸F]Fluoroalkyl agents: synthesis, reactivity and application for development of pet ligands in molecular imaging. *Curr Top Med Chem.* 2007;7:1817-28.
37. Shields AF, Grierson JR, Dohmen BM, Machulla HJ, Stayanoff JC, Lawhorn-Crews JJ, et. al. Imaging proliferation *in vivo* with [¹⁸F]FLT and positron emission tomography. *Nat Med.* 1998;4:1334-36.
38. Villemagne VL, Ong K, Mulligan RS, Holl G, Pejoska S, Jones G, et. al. Amyloid imaging with ¹⁸F-Florbetaben in alzheimer disease and other dementias. *J Nucl Med.* 2011;52(8):1210-17.
39. Tang G, Wang M, Tang X, Gan M, Luo L. Fully automated one-pot synthesis of [¹⁸F]fluoromisonidazole. *Nucl Med Biol.* 2005;32(5):553-58.
40. Reischl G, Ehrlichmann W, Bieg C, Solbach C, Kumar P, Wiebe LI, et. al. Preparation of the hypoxia imaging PET tracer [¹⁸F]FAZA: reaction parameters and automation. *Appl Radiat Isot.* 2005;62:897-901.
41. Mukherjee J, Yang ZY, Das MK, Brown T. Fluorinated benzamide neuroleptics: development of N-[(1-allyl-2-pyrrolidiny)methyl]-5-(3-[¹⁸F]fluoropropyl)-2,3-

- dimethoxybenzamide as an improved dopamine D-2 receptor tracer. *Nucl Med Biol.* 1995;22(3):283-96.
42. Jakobsson JE, Grønnevik G, Riss PJ. Organocatalyst-assisted Ar-¹⁸F bond formation: a universal procedure for direct aromatic radiofluorination. *Chem Comm.* 2017;53(96):12906-09.
 43. Kilbourn MR, Welch MJ, Dence CS, Tewson TJ, Saji H, Maeda M. Carrier-added and no-carrier-added syntheses of [¹⁸F]spiroperidol and [¹⁸F]haloperidol. *Int J Appl Radiat Isot.* 1984;35(7):591-98.
 44. Shiue CY, Shiue GG, Mozley PD, Kung MP, Zhuang ZP, Kim HJ, et. al. p-[¹⁸F]-MPPF: a potential radioligand for pet studies of 5-HT1A receptors in humans. *Synapse.* 1997;25(2):147-54.
 45. Lemaire C, Cantineau R, Guillaume M, Plenevaux A, Christiaens L. Fluorine-18 altanserin: a radioligand for the study of serotonin receptors with pet: radiolabeling and *in vivo* biologic behavior in rats. *J Nucl Med.* 1991;32:2266-72.
 46. Okarv SM. Recent progress in fluorine-18 labelled peptide radiopharmaceuticals. *Eur J Nucl Med.* 2001;28(7):929-38.
 47. Vaidyanathan G, Zalutsky MR. Synthesis of N-succinimidyl 4-[¹⁸F]fluorobenzoate: an agent for labeling proteins and peptides with ¹⁸F. *Nat Protoc.* 2006;1(4):1655-61.
 48. Shai Y, Kirk KL, Channing MA, Dunn BB, Lesniak MA, Eastman RC, et. al. ¹⁸F-labeled insulin: a prosthetic group methodology for incorporation of a positron emitter into peptides and proteins. *Biochemistry.* 1989;28(11):4801-06.
 49. Cai W, Zhang X, Wu Y, Chen X. A thiol-reactive ¹⁸F-labeling agent, N-[2-(4-¹⁸F-fluorobenzamido)ethyl]maleimide and synthesis of rgd peptide-based tracer for pet Imaging of $\alpha_v\beta_3$ integrin expression. *J Nucl Med.* 2006;47(7):1172-80.
 50. Kuhnast B, Dollé F, Terrazzino S, Rousseau B, Loc'h C, Vaufrey F, et. al. General method to label antisense oligonucleotides with radioactive halogens for pharmacological and imaging studies. *Bioconjug Chem.* 2000;11:627-36.
 51. Yale HL. The trifluoromethyl group in medical chemistry. *J Med Chem.* 1958;1(2):121-33.
 52. Lien VT, Riss PJ. Radiosynthesis of [¹⁸F]trifluoroalkyl groups: scope and limitations. *BioMed Res Int.* 2014;380124:1-10.
 53. Suehiro M, Yang G, Torchon G, Ackerstaff E, Humm J, Koutcher J, Ouerfelli O. Radiosynthesis of the tumor hypoxia marker [¹⁸F]TFMISO via O-[¹⁸F] trifluoroethylation reveals a striking difference between trifluoroethyl tosylate and

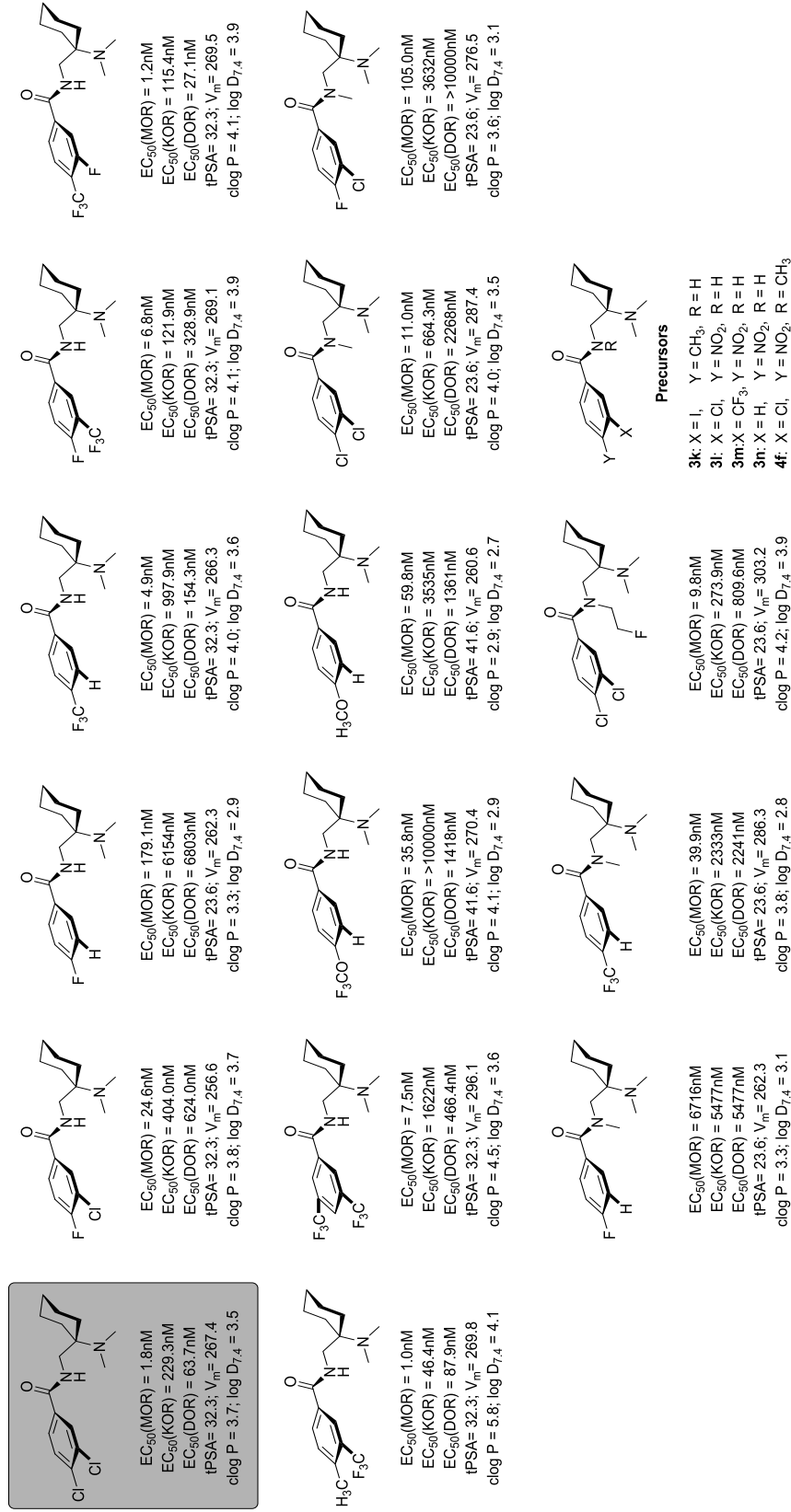
- iodide in regiochemical reactivity toward oxygen nucleophiles. *Bioorg Med Chem.* 2011;19(7): 2287-97.
54. Johnström P, Stone-Elander S. The ^{18}F -labelled alkylating agent 2,2,2-trifluoroethyl triflate: Synthesis and specific activity. *J Label Compds Radiopharm.* 1995;36(6):537-47.
 55. Josse O, Labar D, Georges B, Grégoire V, Marchand-Brynaert J. Synthesis of [^{18}F]-labeled EF3 [2-(2-nitroimidazol-1-yl)-N-(3,3,3-trifluoropropyl)-acetamide], a marker for PET detection of hypoxia. *Bioorganic Med Chem.* 2001;9(3):665-75.
 56. Riss PJ, Aigbirhio FI. A simple, rapid procedure for nucleophilic radiosynthesis of aliphatic [^{18}F]trifluoromethyl groups. *Chem Comm.* 2011;47(43):11873-75.
 57. Huiban M, Tredwell M, Mizuta S, Wan Z, Zhang X, Collier TL, et al. A broadly applicable [^{18}F]trifluoromethylation of aryl and heteroaryl iodides for pet imaging. *Nat Chem.* 2013;5(11):941-44.
 58. Van der Born D, Herscheid JK, Orru RV, Vugts DJ. Efficient synthesis of [^{18}F]trifluoromethane and its application in the synthesis of PET tracers. *Chem Commun.* 2013;49(38):4018-20.
 59. Van der Born D, Sewing C, Herscheid JK, Windhorst AD, Orru RV, Vugts DJ. A universal procedure for the [^{18}F]trifluoromethylation of aryl iodides and aryl boronic acids with highly improved specific activity. *Angew Chem.* 2014;126(41):11226-30.
 60. Tewson TJ. Procedures, pitfalls and solutions in the production of [^{18}F]2-deoxy-2-fluoro-d-glucose: a paradigm in the routine synthesis of fluorine-18 radiopharmaceuticals. *Nucl Med Biol.* 1989;16(6):533-51.
 61. Nickles RJ, Gatley SJ, Votaw JR, Kornguth ML. Production of reactive fluorine-18. *Int J Rad Appl Instrum.* 1986;37(8):649-61.
 62. Svadberg A, Clarke A, Dyrstad K, Martinsen I, Hjelstuen OK. A critical study on borosilicate glassware and silica-based QMA's in nucleophilic substitution with [^{18}F]fluoride: influence of aluminum, boron and silicon on the reactivity of [^{18}F]fluoride. *Appl Radiat Isot.* 2011;69(2):289-94.
 63. Qaim SM, Clark JC, Crouzel C, Guillaume M, Helmeke HJ, Nebeling B, et. al. Pet radionuclide production. In: Stöcklin G, Pike VW, Vol. 24: Radiopharmaceuticals for positron emission tomography: methodological aspects. Kluwer Academic Publishers; 1993. p. 1-43.
 64. Vallabhajosula S. *Molecular Imaging: Radiopharmaceuticals for pet and spect.* Berlin Heidelberg: Springer-Verlag; 2009.

65. Marazano C, Maziere M, Berger G, Comar D. Synthesis of methyl iodide- ^{11}C and formaldehyde- ^{11}C . *Int J Appl Radiat Isot.* 1977;28(12):49-52.
66. Jewett DM. A simple synthesis of [^{11}C]methyl triflate. *Appl Radiat Isot.* 1992;43(11):1383-85.
67. Elsinga PH, Keller E, De Groot TJ, Visser GM, Vaalburg W. Synthesis of [^{11}C]methyl magnesium iodide and its application to the introduction of [^{11}C]-N-*tert*-butyl groups and [^{11}C]-*sec*-alcohols. *Appl Radiat Isot.* 1995;46(4):227-31.
68. Schoeps KO, Halldin C, Någren K, Swahn CG, Karlsson P, Hal H, et al. Preparation of [1- ^{11}C]dopamine, [1- ^{11}C]p-tyramine and [1- ^{11}C]m-tyramine: autoradiography and pet examination of [1- ^{11}C]dopamine in primates. *Nucl Med Biol.* 1993;20(5):669-78.
69. Christman DR, Finn RD, Karlstrom KI, Wolf AP. The production of ultra-high activity ^{11}C -labeled hydrogen cyanide, carbon dioxide, carbon monoxide and methane via the $^{14}\text{N}(p,\alpha)^{11}\text{C}$ reaction. *Int J Appl Radiat Isot.* 1975;26(8):435-42.
70. Diksic M, Jolly D, Farrokhzad S. An on-line synthesis of no-carrier-added [^{11}C]phosgene. *Int J Nucl Med Boil.* 1982;9(4):283-85.
71. Antoni G, Långström B. Synthesis of racemic [3- ^{11}C]-labelled alanine, 2-aminobutyric acid, norvaline, norleucine, leucine and phenylalanine and preparation of L-[3- ^{11}C]alanine and L-[3- ^{11}C]phenylalanine. *J Labelled Comp Radiopharm.* 1987;24(2):125-43.
72. Frost JJ, Douglass KH, Mayberg HS, Dannals RF, Links JM, Wilson AA, et al. Multicompartmental analysis of [^{11}C]-carfentanil binding to opiate receptors in humans measured by positron emission tomography. *J Cereb Blood Flow Metab.* 1989;9(3):398-409.
73. Smith GS, Dewey SL, Brodie JD, Logan J, Vitkun SA, Simkowitz P, et al. Serotonergic modulation of dopamine measured with [^{11}C]raclopride and pet in normal human subjects. *Am J Psychiatry.* 1997;154(4):490-96.
74. Klunk WE, Engler H, Nordberg A, Wang Y, Blomqvist G, Holt DP, et al. Imaging brain amyloid in alzheimer's disease with pittsberg compound-B. *Ann Neurol.* 2004;55(3):306-19.
75. Långström B, Itsenko O, Rahman, O. [^{11}C]carbon monoxide, a versatile and useful precursor in labelling chemistry for pet-ligand development. *J Labelled Comp Radiopharm.* 2007;50(10):794-810.
76. Hooker JM, Reibel AT, Hill SM, Schueller MJ, Fowler JS. One-Pot, direct incorporation of [^{11}C]CO₂ into Carbamates. *Angew Chem Int Ed.* 2009;48(19):3482-85.

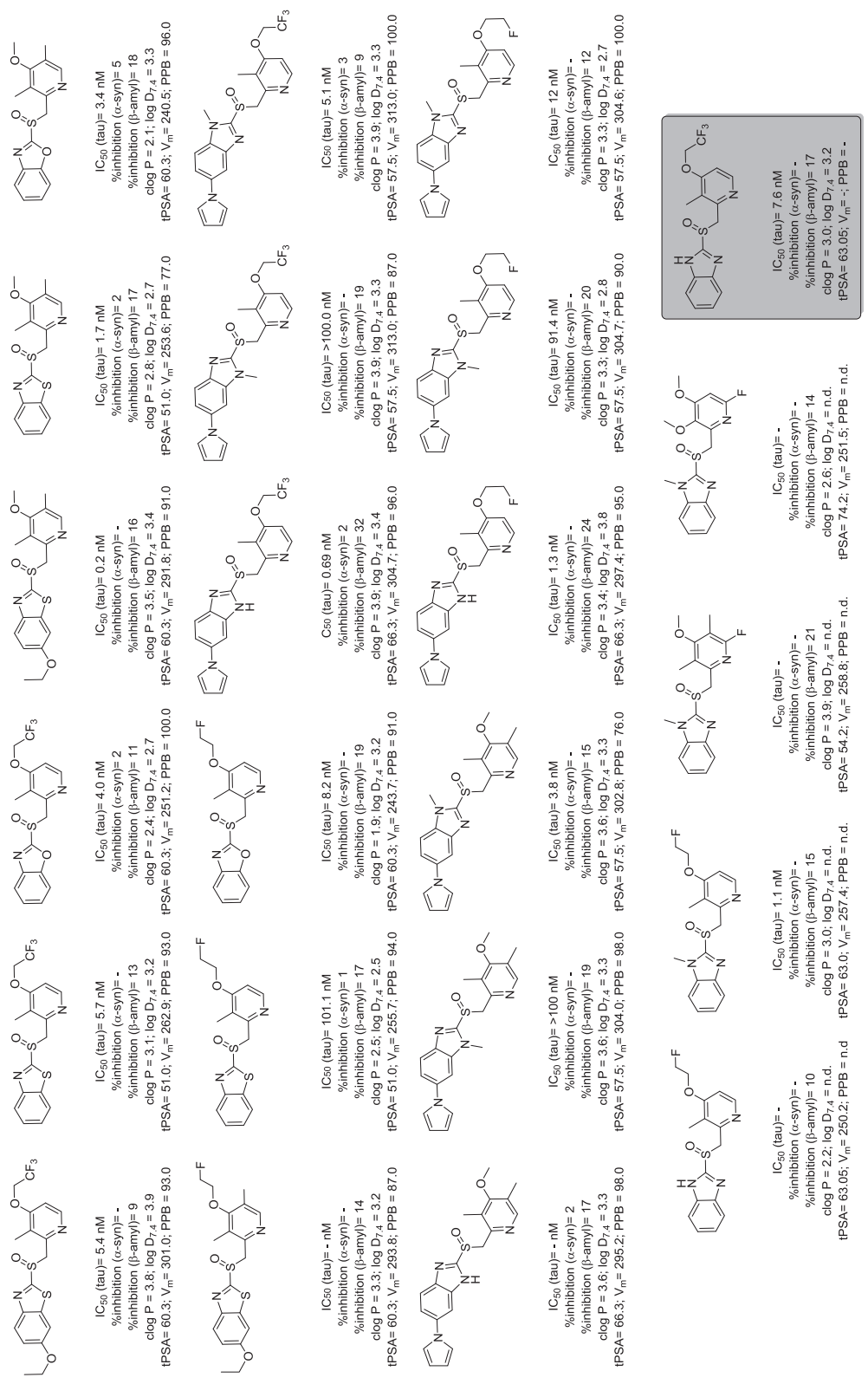
77. Riss PJ, Lu S, Telu S, Aigbirhio FI, Pike VW. CuI-catalyzed ^{11}C carboxylation of boronic acid esters: a rapid and convenient entry to ^{11}C -labeled carboxylic acids, esters, and amides. *Angew Chem Int Ed*. 2012;51(11):2698-702.
78. Alzheimer's Association. Alzheimer's disease facts and figures. *Alzheimer's & dementia*. 2013;9(2):208-45.
79. Soto C. Unfolding the role of protein misfolding in neurodegenerative diseases. *Nat Rev Neurosci*. 2003;4(1):49-60.
80. <http://www.neurodegenerationresearch.eu/about/>
81. Ballatore C, Lee VM, Trojanowski JQ. Tau-mediated neurodegeneration in Alzheimer's disease and related disorders. *Nat Rev Neurosci*. 2007;8(9):663-72.
82. Bossy-Wetzel E, Schwarzenbacher R, Lipton SA. Molecular pathways to neurodegeneration. *Nat Med*. 2004;10:2-9.
83. <https://www.nia.nih.gov/alzheimers/publication/part-2-what-happens-brain-ad/hallmarks-ad>
84. Spillantini MG, Goedert M. Tau protein pathology in neurodegenerative diseases. *Trends neurosci*. 1998;21(10):428-33.
85. Lee H, Perry G, Moreira PI, Garrett MR, Liu Q, Zhu X, et al. Tau phosphorylation in Alzheimer's disease: pathogen or protector? *Trends Mol Med*. 2005;11(4):164-69.
86. Villemagne VL, Furumoto S, Fodero-Tavoletti M, Harada R, Mulligan RS, Kudo Y, et al. The challenges of tau imaging. *Future Neurol*. 2012;7(4):409-21.
87. Villemagne VL, Okamura N. In vivo tau imaging: obstacles and progress. *Alzheimers Dement*. 2014;10(3):254-64.
88. Vermeiren C, Mercier J, Viot D, Mairet-Coello G, Hannestad J, Courade JP, et al. T807, a reported selective tau tracer, binds with nanomolar affinity to monoamine oxidase-A. *Alzheimers Dement*. 2015;11(7):283.
89. Dani M, Brooks DJ, Edison P. Tau imaging in neurodegenerative diseases. *Eur J Nucl Med Mol Imaging*. 2016 ;43(6):1139-50.
90. Saint-Aubert L, Lemoine L, Chiotis K, Leuzy A, Rodriguez-Vieitez E, Nordberg A. Tau PET imaging: present and future directions. *Mol Neurodegener*. 2017;12(1):1-21.
91. Pert CB, Snyder SH. Opiate receptor: demonstration in nervous tissue. *Science*. 1973;179(4077):1011-14.
92. Dhawan BN, Cesselin F, Raghbir R, Reisine T, Bradley PB, Portoghese PS, et al. International Union of Pharmacology. XII. Classification of opioid receptors. *Pharmacol Rev*. 1996;48(4):567-92.

93. Minami M, Satoh M. Molecular biology of the opioid receptors: structures, functions and distributions. *Neurosci Res.* 1995;23(2):121-45.
94. Mansour A, Khachaturian H, Lewis ME, Akil H, Watson SJ. Anatomy of CNS opioid receptors. *Trends neurosci.* 1988;11(7):308-14.
95. Pfeiffer A, Pasi A, Mehraein P, Herz A. Opiate receptor binding sites in human brain. *Brain Res.* 1982;248:87-96.
96. Hume SP, Lingford-Hughes AR, Nataf V, Hirani E, Ahmad R, Davies AN, et al. Low sensitivity of the positron emission tomography ligand [¹¹C]diprenorphine to agonist opiates. *J Pharmacol Exp Ther.* 2007;322:661-67.
97. Dannals RF, Ravert HT, Frost JJ, Wilson AA, Burns HD, Wagner HN. Radiosynthesis of an opiate receptor binding radiotracer:[¹¹C]carfentanil. *Int J Appl Radiat Isot.* 1985;36(4):303-06.
98. Marton J, Schoultz BW, Hjørnevik T, Drzezga A, Yousefi BH, Wester HJ, et al. Synthesis and evaluation of a full-agonist orvinol for PET-Imaging of opioid receptors:[¹¹C]PEO. *J Med Chem.* 2009;52(18):5586-89.
99. Schoultz BW, Hjørnevik T, Reed BJ, Marton J, Coello CS, Willoch F, et al. Synthesis and evaluation of three structurally related ¹⁸F-labeled orvinols of different intrinsic activities: 6-O-[¹⁸F]fluoroethyl-diprenorphine ([¹⁸F]FDPN), 6-O-[¹⁸F]fluoroethyl-buprenorphine ([¹⁸F]FBPN), and 6-O-[¹⁸F]fluoroethyl-phenethyl-orvinol ([¹⁸F]FPEO). *J Med Chem.* 2014;57(12):5464-69.
100. Riss PJ, Hong YT, Marton J, Caprioli D, Williamson DJ, Ferrari V. Synthesis and evaluation of ¹⁸F-FE-PEO in rodents: an ¹⁸F-labeled full agonist for opioid receptor imaging. *J Nuc Med.* 2013;54(2):299-305.
101. Rojo LE, Alzate-Morales J, Saavedra IN, Davies P, Maccioni RB. Selective interaction of lansoprazole and astemizole with tau polymers: potential new clinical use in diagnosis of Alzheimer's disease. *J Alzheimers Dis.* 2010;19(2):573-89.
102. Fawaz MV, Brooks AF, Rodnick ME, Carpenter GM, Shao X, Desmond TJ, et al. High affinity radiopharmaceuticals based upon lansoprazole for pet imaging of aggregated tau in alzheimer's disease and progressive supranuclear palsy: synthesis, preclinical evaluation and lead selection. *ACS Chem Neurosci.* 2014;5(20):718-30.
103. Brittain RT, Kellett DN, Neat ML, Stables R. Proceedings: Anti-nociceptive effects in N-substituted cyclohexylmethylbenzamides. *Br J Pharmacol.* 1973;49(1):158-59.

Appendix



Appendix – 1: The compounds synthesized based on slight modifications to the lead compound AH7921 (upper left, highlighted). The agonist potency at human MOR, KOR and DOR receptors, topological polar surface area (tPSA), octanol/water partition coefficient (both calculated (clogP) and measured (log $D_{7,4}$), and molecular volume (V_m) are provided. Almost all compounds have F or CF₃ at various possible positions, and have high potential to develop the ¹⁸F-labelled PET radiotracers.



Appendix – 2: The compounds synthesized based on combination of building blocks obtained through dissection of the lead compound lansoprazole (lower right, highlighted). Affinity of the compounds towards tau, amy1- β and α -syn, lipophilicity (clog P and log $D_{7,4}$), tPSA, V_m , and plasma-protein binding (PPB) are provided. Several compounds have a good combination of affinity and selective, and may be labelled with ^{11}C or ^{18}F for development of tau-selective PET radioligands.

Paper

I

Paper

II

Image-Guided Development of Heterocyclic Sulfoxides as Ligands for Tau Neurofibrillary Tangles: From First-in-Man to Second-Generation Ligands

Waqas Rafique,[†] Vasko Kramer,^{#,‡,∇} Tania Pardo,^{||} René Smits,[⊥] Mona M. Spilhaug,[†] Alexander Hoepping,[⊥] Eduardo Savio,^{||} Henry Engler,^{||} Rodrigo Kuljs,[○] Horacio Amaral,^{#,‡,∇} and Patrick J. Riss^{*,†,‡,§,||,⊥,○}

[†]Realomics SRI, Kjemisk Institutt, Universitetet i Oslo, Sem Sælands vei 26, Kjemibygningen, 0371 Oslo, Norway

[‡]Klinik for Kirurgi og Nevrologi, Oslo Universitets Sykehus HF—Rikshospitalet, Postboks 4950 Nydalen, 0424 Oslo, Norway

[§]Norsk Medisinsk Syklotronsenter AS, Gaustad, Postboks 4950 Nydalen, 0424 Oslo, Norway

^{||}Departamento de Montevideo, Uruguayan Centre of Molecular Imaging (CUDIM), Av. Dr. Américo Ricaldoni 2010, 11600 Montevideo, Uruguay

[⊥]Advanced Biochemical Compounds GmbH, Heinrich-Glaeser-Strasse 10-14, D-01454 Radeberg, Germany

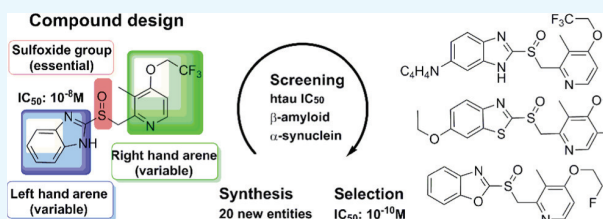
[#]Positronpharma SA, Rancagua 878, 7500921 Providencia, Santiago, Chile

[∇]Center of Nuclear Medicine Positronmed, Julio Prado 714, 7501068 Providencia, Santiago, Chile

[○]Zdrav Mozak Clinical Neuroscience Center, Julio Prado 714, 7501068 Providencia, Santiago, Chile

Supporting Information

ABSTRACT: Positron emission tomography (PET) imaging of misfolded protein aggregates that form in neurodegenerative processes of the brain is key to providing a robust marker for improved diagnosis and evaluation of treatments. We report the development of advanced radiotracer candidates based on the sulfoxide scaffold found in proton pump inhibitors (lansoprazole, prevacid) with inherent affinity to neurofibrillary tangles in Alzheimer's disease and related disorders (e.g., dementia with Lewy bodies and the frontotemporal degeneration syndrome). First-in-man results obtained with [¹⁸F]lansoprazole and *N*-methyl-[¹⁸F]lansoprazole were used to guide the design of a set of 24 novel molecules with suitable properties for neuroimaging with PET. Compounds were synthesized and characterized pharmacologically, and the binding affinity of the compounds to synthetic human tau-441 fibrils was determined. Selectivity of binding was assessed using α -synuclein and β -amyloid fibrils to address the key misfolded proteins of relevance in dementia. To complete the pharmacokinetic profiling in vitro, plasma protein binding and lipophilicity were investigated. Highly potent and selective new radiotracer candidates were identified for further study.



INTRODUCTION

Alzheimer's disease (AD) is a progressive neurodegenerative disease of ageing, characterized by a gradual decline of cognitive and behavioral performances and subsequent deterioration of activities in daily living. Because the diagnosis based solely on clinical manifestations is imprecise and may thus lead to difficulties, means to accurately diagnose the underlying molecular pathology, as well as to monitor the effects of strategies for therapeutic intervention, are required to mitigate the escalating impact of the disease worldwide.^{1–4} Abnormal aggregation of a microtubular protein called tubule-associated unit (tau) is widely felt to be implicated in neurodegenerative diseases, such as AD, frontotemporal degeneration, progressive supranuclear palsy, corticobasal degeneration, and chronic traumatic encephalopathy.^{5–8} Misfolded fragments of tau form aggregates of fibrillar matter

named neurofibrillary tangles (NFTs) inside neurons when a threshold concentration is exceeded. Although monomers are believed to cause damage, the presence of NFTs is a definitive endpoint of progressing disease and can be imaged using positron emission tomography (PET) for diagnosis, treatment development, and evaluation.^{9–12}

Despite the promising results in clinical studies using investigational radioligands for tau imaging, the first generation of radiotracers designed for the detection of NFTs in brain is not yet suitable for routine clinical use. Low specific signal in brain, heterogeneous nonspecific binding, blood–brain barrier penetrating radiometabolites, and cross-affinity to other

Received: May 11, 2018

Accepted: June 15, 2018

Published: July 9, 2018

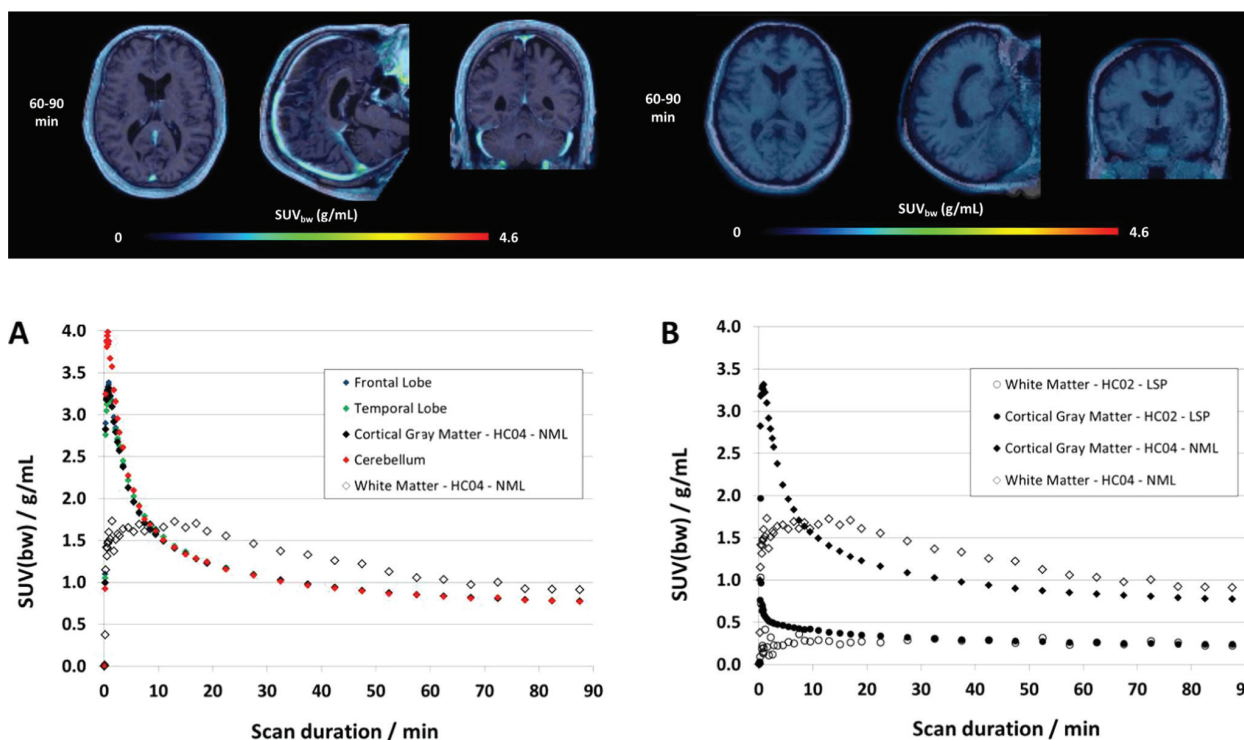


Figure 1. Top: transversal, sagittal, and coronal views of averaged PET/MRI fusion images of $[^{18}\text{F}]\mathbf{1}$ (left) and $[^{18}\text{F}]\mathbf{2}$ (right) 75 min postinjection. Bottom: (A) time–activity curves (TACs) of $[^{18}\text{F}]\mathbf{2}$ in the frontal lobe (blue), temporal lobe (green), cortical gray matter (black), white matter (white), and cerebellum (red); (B) comparison of TACs for $[^{18}\text{F}]\mathbf{1}$ (circles) and $[^{18}\text{F}]\mathbf{2}$ (diamonds) in cortical gray and white matter, respectively.

proteins hamper the current application of the technology.^{13–15} For instance, $[^{18}\text{F}]\text{T807}$ has shown to bind to monoamine oxidase A with high affinity, which might contribute to tracer binding in tau-rich regions outside the striatum.¹⁵ $[^{18}\text{F}]\text{THK-5351}$, another tau tracer currently in clinical trials, shows high affinity for monoamine oxidase B, which is expressed in activated microglia, associated with inflammation and neurodegeneration and which also contributes to nonspecific binding in relevant brain regions. Therefore, further investigation is needed to obtain more specific radiotracers with an improved clinical scope for the detection of NFTs in the brain.

Our objective is to identify new, specific ligands binding to synthetic aggregated paired helical filaments (PHFs) of human tau (hTau).¹⁶ In practice, only lipophilic small molecules ($M < 450$ g/mol) labeled with the short-lived radionuclides ^{11}C ($t_{1/2} = 20$ min) or ^{18}F ($t_{1/2} = 110$ min) provide optimal chemical, physical, and pharmacological properties for design of reversibly binding PET radiotracers. Because of the cost and handling constraints originating from a short half-life, clinical radiotracers should preferably be labeled with ^{18}F .

NFTs are challenging targets for small-molecule ligands. In contrast to functional proteins, they constitute macromolecular assemblies composed of misfolded tau fragments. These fragments are formed in low concentration during the progression of neurodegenerative diseases and do not possess functional binding pockets. Most known ligands are derived from aromatic dyes binding to residual β -sheet folds in the NFT superstructure, which complicates selective detection of NFTs over other misfolded proteins with intrinsic β -sheet structures, e.g., β -amyloid or α -synuclein.^{17–21}

RESULTS AND DISCUSSION

Lead Validation in Clinical Imaging. Proton pump inhibitor lansoprazole (**1**, 2-(((3-methyl-4-(2,2,2-trifluoroethoxy)pyridin-2-yl)methyl)sulfinyl)-1H-benzimidazole) caught our attention when NFT binding and some inherent selectivity over other misfolded protein aggregates were associated with the drug.^{22–25} For lead compounds astemizole and lansoprazole, in vitro affinities of 1.9 ± 0.1 and 2.5 ± 0.4 nM to heparin-induced tau filaments (HITFs) and 2.1 ± 0.1 and 830 ± 180 nM to paired helical tau filaments (PHF-Tau) were determined by radioligand binding assays.²² The selective interaction of **1** with PHF-Tau was further proved by a comparison of immunohistochemical staining of PHF-Tau. Although it was not possible to obtain crystal structures of the native tau protein to obtain information about the binding site of **1**, the authors were able to show a strong interaction of **1** with hexapeptide 386TDHGAE391 located in the center of PHF-Tau. Taking these promising preclinical results into account, **1** as a registered medicinal product is safe and well suited for human application, which allowed for PET studies to deduce the risk of progressing with the compound. Hence, we initiated a first-in-man PET study in a small group of healthy volunteers to obtain information on the kinetic profile of ^{18}F -labeled lansoprazole in the brain. To our dismay, $[^{18}\text{F}]\mathbf{1}$ had a very limited brain uptake because of N–H-acidity ($\text{pK}_a \sim 4$) of the imidazolyl sulfoxide moiety.²⁵ Another hypothetical culprit may be near quantitative plasma protein binding; the irreversible, covalent mechanism of action as a proton pump inhibitor; or active transport via multidrug resistance-proteins.²⁵

Previous experiments in animals suggested that methylation of the nitrogen in the benzimidazole scaffold leads to higher

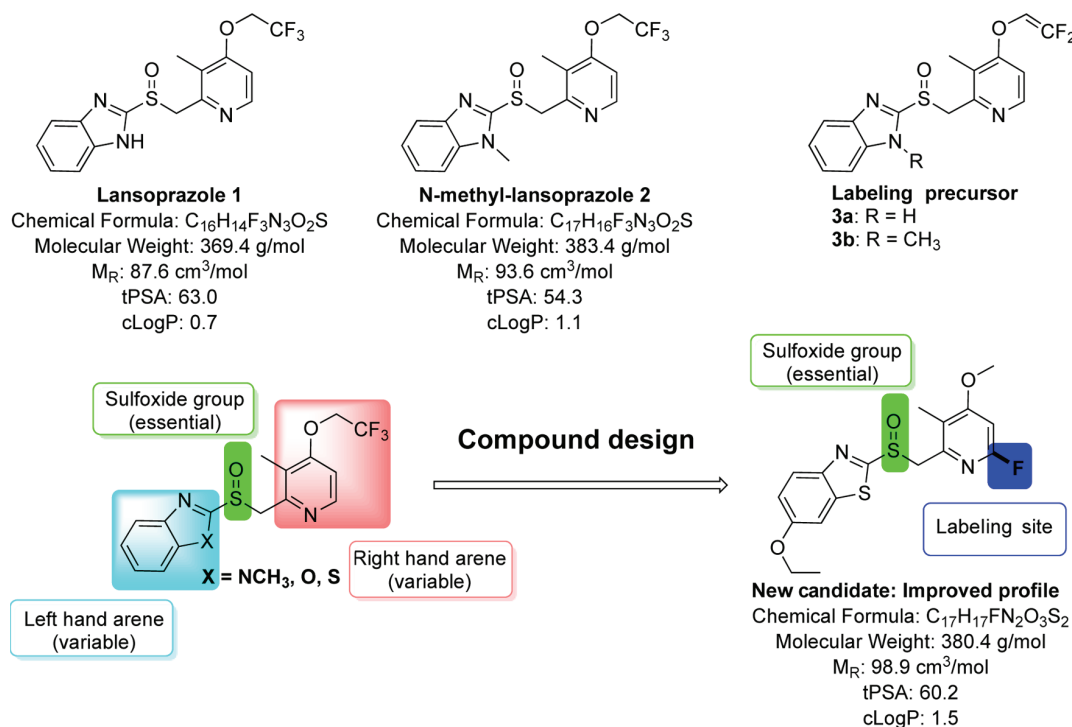


Figure 2. Top: lansoprazole (1) and *N*-methyl-lansoprazole (2) the original leads. Bottom: dissection of lansoprazole into building blocks (blue, green) and generic scheme depicting the design of new analogues.

brain uptake; however, clinical data has not been reported to the best of our knowledge. We therefore progressed with a clinical study to investigate *N*-methyl- $[^{18}F]$ lansoprazole ($[^{18}F]$ 2) in comparison to lead $[^{18}F]$ 1. The study was approved by the regional Ethics Committee (SSM Oriente), and written informed consent was obtained from all subjects. Inclusion criteria for all participants were age of 50–70 years, not having clinical signs of any neurological or psychiatric disorder, and using contraceptives for at least 6 months after last imaging visit in case of possible pregnancy. $[^{18}F]$ 1 was obtained in $1.4 \pm 0.5\%$ radiochemical yield (RCY) with >98% radiochemical purity (RCP) and molar activity (A_m) of 80–98 GBq/ μ mol (2.5 Ci/ μ mol). $[^{18}F]$ 2 was obtained in $2.1 \pm 1.4\%$ RCY with >98% RCP and molar activity of 230–310 GBq/ μ mol (6 Ci/ μ mol). A total of four healthy volunteers (mean age 60.2 ± 6.0 years) were included to study the physiological distribution of $[^{18}F]$ 1 and $[^{18}F]$ 2 in the human brain. All subjects received a single intravenous bolus injection of 300–350 MBq of either $[^{18}F]$ 1 or $[^{18}F]$ 2 with an injected mass in the range of 0.1–1.5 μ g. PET images were corrected for motion, fused to individual T1-weighted magnetic resonance imaging (MRI) or computed tomography scans, and normalized to Montreal Neurological Institute (MNI) space. Standard volume of interest (VOI) maps were outlined from the available brain atlas in MNI space for frontal cortex, temporal cortex, parietal cortex, occipital cortex, whole brain, white matter, and cerebellar cortex as reference regions. Time–activity curves (TACs) were calculated for all brain regions, and brain uptake was calculated in percent injected dose (% i.D.) in the whole brain at different time points.

For the whole brain, peak uptakes of 2.5–3.5% i.D. for $[^{18}F]$ 1 and 5.0–6.0% i.D. for $[^{18}F]$ 2 were observed during the initial perfusion phase 1 min postinjection (p.i.). For $[^{18}F]$ 1, most of

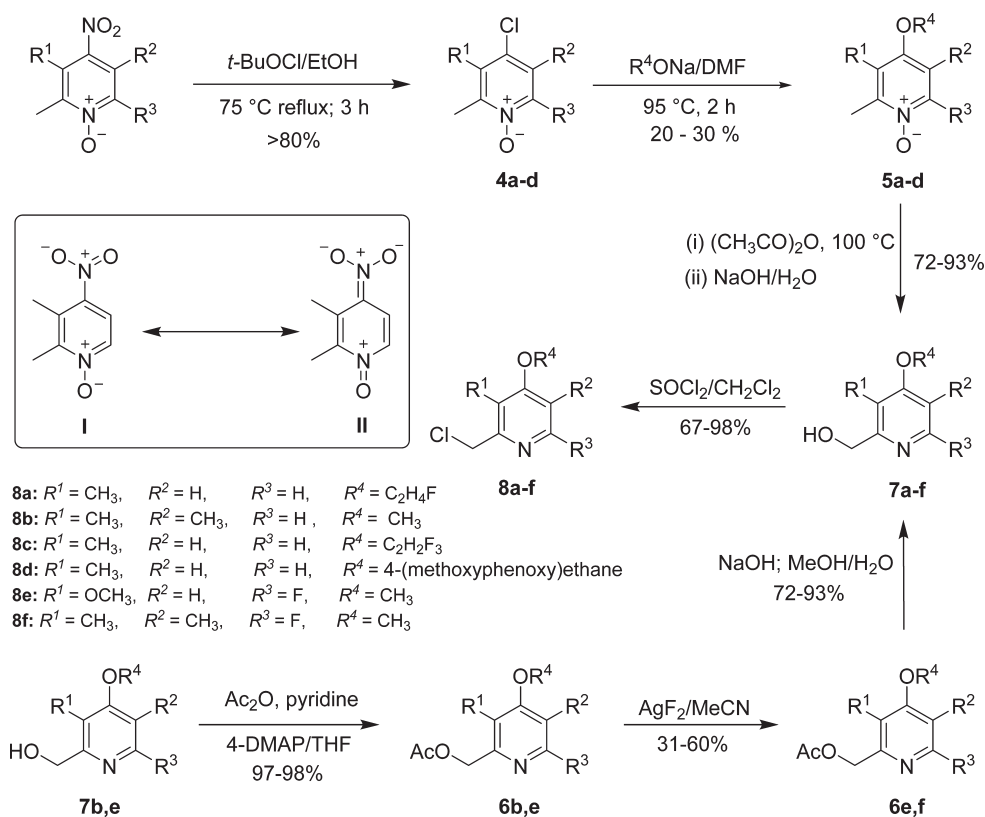
the activity was confined to the venous vascularization, dropping fast to less than 1.0% i.D. at 2 min p.i. and below 0.5% after 90 min. $[^{18}F]$ 2 showed good penetration into brain tissue and fast, homogeneous clearance from the brain. Radioactivity concentrations in brain were about 3.0, 2.0, and 1.3% of the injected dose at 10, 27, and 90 min, respectively. In general, an uptake of 3.0–5.0% i.D. in brain can be considered suitable for the application of a tracer for neuroimaging. The comparative study revealed attractive characteristics for radiotracer development inherent to the scaffold. Fast clearance and no indications on binding to targets in the healthy brain other than in white matter have been observed (Figure 1).

Of particular importance here is the complete absence of specific binding in any brain region including the striatum, indicating that lead $[^{18}F]$ 2 has a negligible affinity toward monoamine oxidase A and B, typically expressed in this region. The phenomenon of white matter binding is in accordance with previously reported results observed for other NFT PET tracers, perhaps related to the high amount of β -sheet-rich myelin tissue in white matter. This is not a desired characteristic for a tau imaging agent but confirms the brain penetration of the tracer and is not an issue for further progression as it is cleared rapidly from the tissue.

On this basis, we decided to develop the lead into a library of new ligands with a chemical and pharmacological profile suitable for PET imaging, in particular by increasing the in vitro affinity toward HITF and the selectivity over α -synuclein and β -amyloid fibrils and by increasing brain permeability.

Compound Design. The scaffold of 1 was used as a template to design molecules with the desired physical, chemical, and pharmacological characteristics. During the design phase, permeative properties derived from in silico

Scheme 1. Illustration of the Synthesis Routes to Pyridines 8a–f



data such as polar surface area (tPSA), partition coefficients ($\log P$, $\log D_{7.4}$), molecular weight, and molecular volume were used for guidance.^{26,27} Figure 2 shows the lead radioligands and the design of new derivatives.

Using retrosynthesis, the lead was segmented into three building blocks: the heteroaryl building block (variable, blue), the central sulfoxide function (green), and the arylmethyl building block (variable, red). New compounds were designed by combining such basic building blocks in silico. The library obtained was filtered for key criteria of relevance for its purpose. For example, the combined mass of all three components should not exceed 450 g/mol and one moiety should allow for direct, nucleophilic radiolabeling using no-carrier-added [¹¹C]CH₃I and/or ¹⁸F-fluoride ion. Particular emphasis was put on mapping the activity and selectivity of new derivatives devoid of the benzimidazol-N–H function. The following selection criteria were applied (in weighted order):

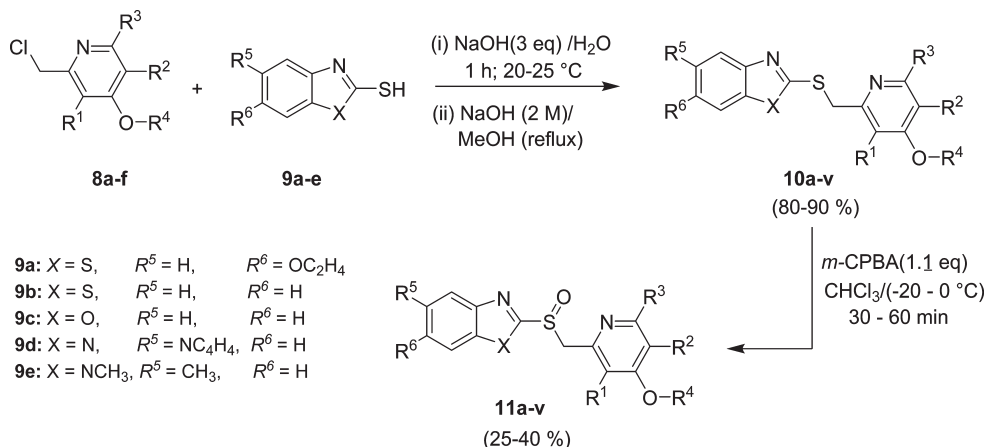
1. Polar surface area <80 Å²
2. Aliphatic, primary C–F bond
3. $\log D_{7.4} > \log P$; 1.5
4. Molecular weight, $M < 450$ g/mol
5. Molecular volume, V_m (candidate) = V_m (lead) \pm 15%
6. Aliphatic, secondary C–F bond or aromatic C–F bond

Synthesis of Compounds. To obtain new derivatives based on these constraints, building blocks were synthesized when necessary or procured when commercially available. Segmentation into such simple building blocks facilitated the synthesis of final compounds in only two synthetic steps. The compound library closely resembled the original template under exclusion of the acidic proton. A number of compounds

accommodate reliable ¹⁸F-labeling protocols and some structural variation.

Despite several attempts, the nitro-function in the starting material proved to be difficult to substitute for alkoxy substituents directly. In addition, some nucleophiles such as sodium *p*-methoxybenzylate and sodium *tert*-butyl-dimethylsilylate underwent oxidation even under Ar or N₂ as observed by NMR. We attributed the issue to an unusually stable isomer,²⁸ formed in an intramolecular attack centered on a hyperconjugated pyridine nitrogen to form (1-oxopyridin-1-ium-4(1*H*)-ylidene)azinate (Scheme 1, II). The intermediate would constitute a stable compound with low electrophilicity on the ipso-carbon of the leaving group, thus preventing the Meisenheimer complex necessary for S_NAr reactions. To circumvent the issue, we introduced a chloro substituent using *tert*-butyl hypochlorite (*t*-BuOCl) to obtain the 4-chloropyridine analogues in 80–95% yield.^{29–31} Substitution of the chloride was still hampered by somewhat low yields and competing formation of oxidation products. An optimization of the reaction conditions led to the omission of excess alcoholic solvent; instead, 3 equiv of 2-fluoroethanol was added dropwise to dimethylformamide containing stoichiometric NaH. The obtained solution was reacted with 4a–d to afford alkyl aryl ether 5a–d in only 25% yield.⁴² Ether 5a–d was converted to pyridine derivative 7a–d using a sequence of transformations. In brief, acylation of the N-oxide, followed by a [3,3]-sigmatropic rearrangement was used to install the benzylic oxy-function. Hydrolysis of the acetyl intermediate with NaOH afforded the product in 72–93% yield over three steps in one pot. Compound 7a–f was treated with thionyl chloride to obtain the pyridine building block 8a–f in 67–98%

Scheme 2. General Scheme for the Synthesis of Final Compounds over Two Steps



yield.^{32,33} Via this route, pyridines were synthesized in an overall yield of about 10% over six steps.

Pyridine fluorination was achieved on intermediates **6b** and **6e** using the method of Fier and Hartwig.³⁴ Because of technical limitations, AgF₂ had to be handled without the precautions indicated by the authors. As a result, best yields were obtained when using fresh AgF₂. Nonetheless, we obtained a 60% yield with fresh AgF₂ in contrast to the original report of 81% isolated fluoropyridine **6e**. An aged sample of silver difluoride in stock gave only 31% **6f**.

Final compounds were obtained under fairly mild conditions as follows. Compounds **9a–e** were treated with aqueous NaOH (3 equiv) and allowed to react with pyridines **8a–f** for 1 h at room temperature (rt). Compounds **10a–v** were isolated in an overall yield of 70–90% and characterized. Isolation is not strictly necessary prior to the final oxidation, which eased scale-up of the reaction. Direct oxidation to furnish radiotracer candidates **11a–v** was achieved with *meta*-chloroperbenzoic acid (*m*-CPBA, 1.1 equiv) in low to moderate yields of 25–40%. We attributed some low yield to overoxidation of the sulfur and nitrogen. However, no further attempts were made to optimize the reaction at this point because sufficient amounts were available for biological studies (Scheme 2).

Characterization. Traditionally, binding of candidate molecules to the target of interest is the first and foremost selection criterion for the development of a PET radiotracer. To visualize a target, a reasonable ratio between the available number of binding sites (B_{avail}) and dissociation constant k_d , also termed binding potential, is crucial. In the case of misfolded protein pathology, the expression patterns differ between diseases, from subject to subject and with the disease stage.^{2–4,35} Therefore, we surmised that an optimal candidate would (1) bind to hTau-441 NFT with equal or better affinity than lead compounds **1** and **2** and (2) have a suitable selectivity for NFT over α -synuclein and β -amyloid and show better brain uptake. We tested all compounds for their binding characteristics to hTau-441, α -synuclein, and β -amyloid fibrils. A number of reference compounds were included to improve our understanding of the structure–activity relationship between imidazolyl-sulfoxides and misfolded protein aggregates. In addition to binding, we had to keep in mind the insufficient brain uptake of the lead structure, which leads us to investigate additional pharmacological parameters such as the

lipophilicity and the protein-bound fraction in plasma of each candidate.

Because the purity of each test compound had to be determined prior to binding studies, we devised a purpose-made high-performance liquid chromatography (HPLC) method derived from OECD guidelines for testing of chemicals.³⁶ The HPLC method was calibrated using 30 reference compounds to allow for simultaneous determination of purity and of the distribution coefficient $\log D_{7.4}$ as a surrogate of lipophilicity (Supporting Information).

To assess the effect of structural modification on plasma protein binding, a plasma dialysis method was developed and validated. Porcine full blood was used because of its similarity to human blood. Samples were obtained, and plasma was separated. Following incubation of compounds **11a–v** as well as internal standards, plasma was subjected to membrane dialysis and the protein-free plasma samples were analyzed by HPLC (Supporting Information). Plasma protein binding remained high for all compounds in both pig and human blood. Notable exceptions include compounds **11e** and **11o**, which show a remarkable drop in activity of 10–20% relative to the rest of the series.

To determine the interaction of the new compounds with different misfolded proteins, we compared their in vitro binding affinity toward synthetic fibrils composed of hTau-441, α -synuclein, and β -amyloid. We decided to work with synthetic fibrils in this stage to avoid issues commonly associated with screening for binding in tissue samples. The main disadvantage of binding assays performed with the human (or animal) tissue specimen is false positive assessment of the binding profile, particularly when working with misfolded protein pathology. This is due to low target expression on one hand and substantial co-localization of functional proteins (e.g., butyryl choline esterase and monoamino oxidase) in both tau and amyloid brain lesions on the other. Reversible binding to these proteins may have mislead researchers in their structural optimization efforts, thus creating a cross-affinity to additional targets as reported previously. Nevertheless, we intend to evaluate the most promising candidates identified in this work by autoradiography (AR) on human tissue at a later time points to verify their affinity toward PHF-Tau.

Binding Affinity to hTau-441. Synthetic fibrils were prepared by aggregation of hTau-441 in the presence of Heparin at 37 °C for 7 days during which the aggregation

process was monitored by light scattering to investigate the size of the aggregate fibrils. At baseline conditions, only one distinct species with a hydrodynamic radius, r_h , of 322 nm was detected. At later time points up to 7 days, this species pertained ($r_h = 322$ nm) alongside some larger aggregates and small fragments. A globular protein of 60 kDa mass has an approximate r_h of 3.4 nm, which increases to about 5.1 nm at 150 kDa, which suggests that distinct aggregates are already present after 1 day of incubation.

In addition, we validated the fibrils and assay conditions for every aggregation batch by verifying maximum binding, displacement, and dissociation constant (k_d) using [^3H]-astemizole as the reference ligand as previously described.²² Therefore, synthetic fibrils were freshly suspended in buffer and incubated with the radioligand in the presence of increasing concentration of 1×10^{-10} – 3×10^{-5} M non-radioactive astemizole and the calculated k_d was compared to literature values for quality control.

Binding affinities of new reference compounds toward hTau-441 fibrils were determined by inhibition of [^3H]-astemizole measured by autoradiography (AR) and at radioligand concentrations that gave the best specific signal. Reference compounds were tested at 10 concentrations spanning 1×10^{-10} – 1×10^{-5} M, and inhibition potency was determined (half-maximal inhibitory concentration (IC_{50})).

Of a total of 24 newly synthesized compounds, we obtained reliable data for 19 compounds in the range of 0.2–100.0 nM (IC_{50}). Derivatives containing the ethoxy-substituted (**11a**, **11d**, and **11g**) and nonsubstituted “azol” structures are almost devoid of any simple trend of potency. It appears that fluorine or fluorinated aliphatic moieties are tolerated to a lesser extent, perhaps reflecting electrostatic or steric effects in the binding environment. As a result, the presence of the 4-methoxypyridine residue is highly beneficial for the overall potency (**11d**–**f**). Again, some trend is observed within the respective benzothiazole series throughout all pyridine moieties (e.g., **11a**, **11d**, and **11g**), of which the more electron-rich methoxy derivative (**11d**) demonstrates the highest potency of this series.

In contrast, introduction of the electron-withdrawing pyrrole substituent affects binding in a different way and the lowest affinity is found for the of the *N*-methyl imidazoles series (**11k**, **11n**, and **11q**). In fact, the rotamers show a remarkable distinction of their respective potencies (see [Supporting Information](#) for structure assignment by NMR). Whereas the corresponding syn-series (**11l**, **11o**, and **11r**) shows low nanomolar inhibition potency, the syn-analogues are between 8- and 20-fold less affine and require such high ligand concentration for displacement of astemizole that we approached the edge of quantification in our assay. Another intriguing observation is the pronounced effect of the imidazole-N–H function within the pyrrole series (**11j** and **11p**). Relative to the other pyrrolyl derivatives, these two molecules are remarkably potent binders of hTau but show only a small increase in inhibition binding to α -synuclein and β -amyloid. These findings indicate that the imidazole proton or its direct vicinity plays a major role in both the binding affinity and selectivity of binding among the three misfolded protein species. Unfortunately, pronounced N–H-acidity in these derivatives renders brain uptake very unlikely.

Interestingly, *N*-methyl derivatives devoid of the pyrrole substituent did not show significant affinity toward hTau-441, except compound **11t**, which binds with very high affinity.

Phenomenologically, this may be attributed to the lack of conformational rigidity because no stable rotamers are present in these structures.

Nonetheless, in the light of these results, we plan to carry forward **11d**, **11i**, **11j**, and **11t** for direct comparison with **1** and other derivatives to further elucidate the mechanism of binding. All compounds except **11i** have a very high affinity around 1.0 nM and are superior to both leads **1** and **2** in this regard.

Binding Affinity to α -Synuclein and β -Amyloid. All compounds were furthermore analyzed for their binding potency toward α -synuclein and β -amyloid fibrils using well-established and validated binding assays with thioflavin-T fluorescence as read-out (for details, see [Supporting Information](#)) to determine whether structural modifications influence the selectivity of the original lead.

Because the compound library was primarily designed to produce hTau-binding compounds, we simplified the assay as much as possible and tested all compounds at three concentrations (10, 100, and 1000 nM) in triplicate for their inhibition of thioflavin binding to the fibrils. To calculate selectivity, we assumed that compounds showing less than 50% inhibition at the highest concentration of 1000 nM would have IC_{50} values >1000 nM, which could be considered as negligible. Should a significant inhibition of binding to α -synuclein or β -amyloid fibrils be observed, we would perform a concentration-dependent inhibition assay to obtain exact IC_{50} values.

For the purpose of assay validation, the aggregation of synthetic fibrils was monitored with thioflavin-T dyes for 7 days as described previously. Total binding of dye to fibrils in the absence of inhibitor was roughly 20-fold higher than nonspecific signal in the presence of a saturating concentration of LDS-798. These parameters translate to a robust assay with a pronounced effect. Studies with the reference compound LDS-798 showed concentration-dependent displacement of dye binding to α -synuclein and β -amyloid. To minimize the nonspecific signal as well as the noise from the fluorescence detection, plates were pre-read before addition of thioflavin-T to determine autofluorescence of the test solutions.

Among the novel radiotracer candidates tested, most compounds have shown very little displacement of the fluorescent dye thioflavin-T from aggregated α -synuclein. On the other hand, some binding to β -amyloid fibrils was apparent for most test compounds at the highest concentration of 1000 nM, for which a variable but low degree of displacement was observed. Values range between 9 and 32% inhibition; however, no pronounced inhibition potency was observed for any of the new entities **11a**–**v** at lower concentrations of 10 and 100 nM. With less than 50% inhibition at 1000 nM, we conclude that the IC_{50} would be >1000 nM and represent a negligible affinity toward both fibrils.

In terms of structural attributes, the binding to β -amyloid fibrils shows some correlation with the individual lipophilicity of compounds within each series. As a general trend (**11a**–**c**, **11d**–**f**, and **11g**–**i**), the lowest potency of inhibition is found in the most lipophilic analogue. A more electron-rich “azol”-heterocycle appears to benefit a lower potency as well. The trend persists within the respective series with a constant pyridine motif (**a**–**c**, **d**–**f**, and **g**–**i**). The 3-methyl-4-trifluoroethoxypyrid-2-yl-methyl residue generally produces the least potent derivative in the series. When introducing an electron-withdrawing pyrrole substituent, the trends are gravely

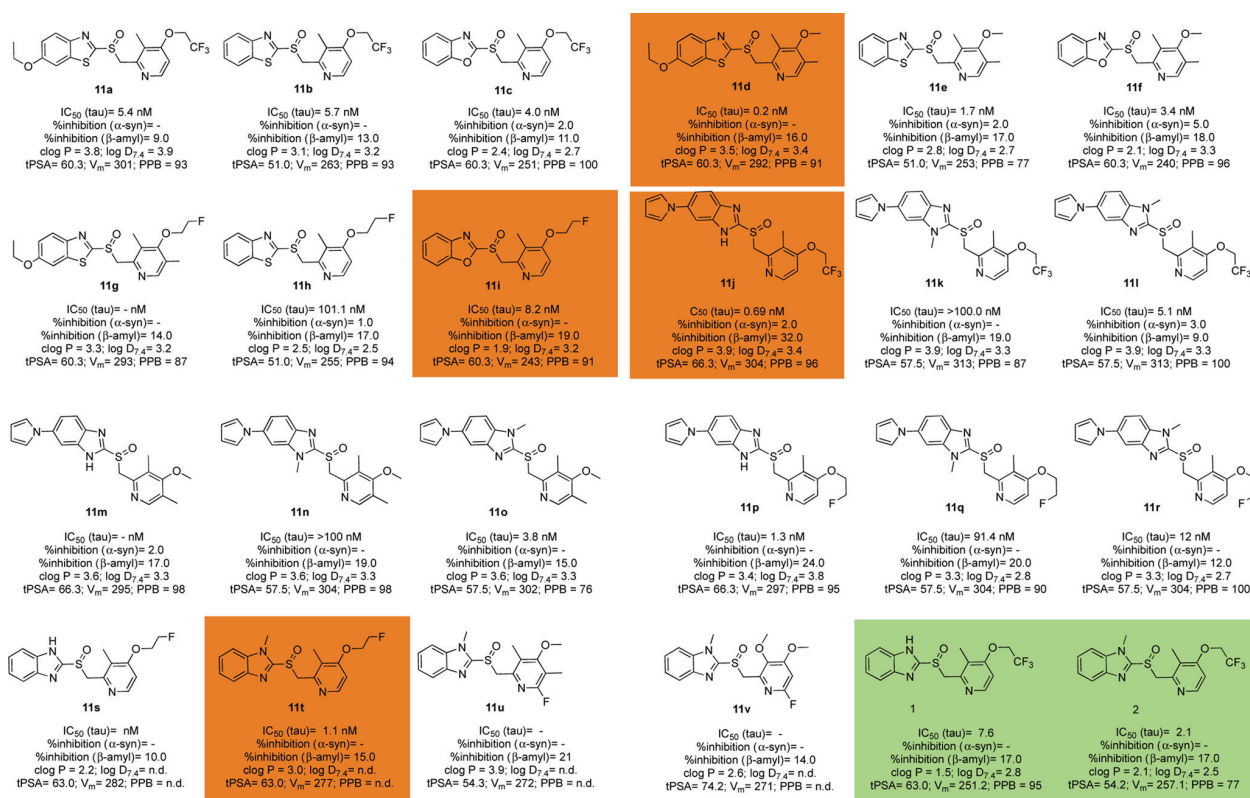


Figure 3. Molecular structures and in silico and in vitro properties of compounds **11a–v**. Reference value from the literature. IC_{50} values are given as the average of 3–9 replicates; see [Supporting Information](#) for details. Replicated twice with a broader range of concentrations. Based on single experiment, clog P = calculated with ChemDraw Ultra V13. Log $D_{7.4}$: decadic logarithm of the distribution coefficient between aqueous and lipid phases at pH 7.4. tPSA = topographic polar surface area, V_m = molecular volume in $\text{\AA}^3/\text{mol}$. PPB = protein-bound fraction in percent of total concentration. n.d. = not determined. The best candidates are highlighted in orange, and lead structures **1** and **2** are highlighted in green.

affected. Interestingly, the syn-rotamer (**11l**, **11o**, and **11r**) of all *N*-methyl pyrrolobenzimidazoles is significantly less potent than the anti-rotamer (**11k**, **11n**, and **11q**), whereas the desmethyl analogues (**11j**, **11m**, and **11p**) show the most pronounced displacement, indicating some importance of the imidazole-*N*-H for β -amyloid fibril binding.

LDS-798 and **1** displaced the dye from β -amyloid at 1000 nM very well, which is in line with an expected strong interaction with fibrils. When tested, **1** did not show competitive inhibition of thioflavin-T binding, which is in line with (a lack of) corresponding literature evidence. We presume that astemizole binds in a different part of the misfolded protein, unlike thioflavin S and T, which are known to interact with β -sheet folds.

The results obtained from α -synuclein and β -amyloid binding studies indicate a low tendency of most novel candidates to bind misfolded proteins other than NFTs. These results bode for selective interaction with the target of interest, which is crucial in the development of selective PET radiotracers for NFT imaging.

We selected compounds **11i** and **11t** for further progression and **11d** and **11j** as backup as these provide the most attractive or outstanding combination of properties (Figure 3, highlighted in orange). As part of future studies, these compounds will be labeled with ^{18}F and/or ^{11}C for μPET imaging studies in healthy mice and animal models of AD to prove their capacity for brain penetration and target interaction. In addition, autoradiography on healthy human tissue and

samples of patients with different tauopathies as well as radioligand binding assays using brain homogenates will be performed in the near future.

CONCLUSIONS

Herein, we report the lead validation of [^{18}F]lansoprazole by human PET imaging to support chemical synthesis of a small library of lansoprazole analogues designed with the aim of identifying potential radiotracer candidates for PET imaging. Compounds were designed with the aid of calculated properties, and following synthesis were successively characterized in vitro with emphasis on pharmacological criteria of relevance for brain imaging studies. Binding affinities were measured against synthetic hTau-441, β -amyloid, and α -synuclein fibrils. Lipophilicity and plasma protein binding were investigated experimentally using HPLC and membrane dialysis protocols. The data was used to gather a preliminary understanding of the structure–activity relationship for heteroarylmethyl-sulfoxides with respect to protein binding to successively optimize the lead. On the basis of the dataset, candidates **11i** and **11t** were selected for radiolabeling to allow for further progression into the preclinical imaging stage to assess the performance of new compounds as NFT imaging agents in human tissue sections and animal models. Derivatives **11d** and **11j** will be investigated in vitro and in silico to assess the importance of their structural features for binding.

EXPERIMENTAL SECTION

Materials and Methods. All chemicals, reagents, and solvents used in the experimental work were of highest commercially available quality and applied without further purification. Materials used herein were purchased from Sigma-Aldrich (Sigma-Aldrich AS, Norway), VWR (VWR International, Norway), Acros Organics (Now VWR International), Strem, ABCR, Combi-Blocks, and Fisher Scientific (Fisher Scientific AS, Oslo, Norway) unless specified here. 5-(1*H*-Pyrrol-1-yl)-2-mercaptobenzimidazole was obtained from Carbosynth (Carbosynth Limited, Berkshire, U.K.). The [¹⁸F]fluoride ion for radioactive work was obtained from Norwegian Medical Cyclotron Centre AS (Gaustad, Oslo, Norway). Solid phase extraction cartridges, Sep-Pak Accell plus light QMA cartridges, and Sep-Pak C18 plus light cartridges were purchased from Waters (Waters International, Norway).

Characterization of synthesized compounds was performed using an AVIII HD 400 nuclear magnetic resonance spectrometer (Bruker ASX Nordic, Oslo, Norway). Chloroform-*d* (CDCl₃; $\delta = 7.226$ ppm) was used as the reference standard. Chemical shifts (δ) for ¹H (400 MHz), ¹³C (100 MHz), and ¹⁹F (377 MHz) NMR are reported in parts per million (ppm). High-resolution mass spectrometry was conducted on a micromass Q-ToF-2 mass analyzer (Waters International, Oslo, Norway) and maXis II ETD (Bruker ASX Nordic, Oslo, Norway) using electron spray ionization in positive mode (ESI+). High-performance liquid chromatography (HPLC) was performed on an analytical HPLC system (Agilent technologies, California) equipped with a quaternary pump, diode array detector (DAD), and sodium iodide detector (NaI crystal; 2 × 2) using GABI-star software (Raytest, Straubenhardt, Germany) for UV and radioactive quantifications.

Chemical purity and lipophilicity (log *D*_{7.4}) of the final compounds was determined on a Shimadzu iProminence HPLC system (Shimadzu Europa GmbH, Duisburg, Germany) using a Chromolith RP-18e column (100 × 4.6 mm²; Merck KGaA, Darmstadt, Germany) as a stationary phase and mixtures of methanol–50 mM 3-morpholinopropane-1-sulfonic acid (MOPS) buffer, 1:1, or methanol–50 mM phosphate-buffered saline buffer, 70:30, as mobile phases with a flow rate of 2 mL/min. Complementary confirmation of the chemical purity of synthesized compounds was obtained using a pentafluorophenyl-functionalized reversed-phase column as a stationary phase (Luna PFP(2), 5 μ m; 100 Å; 150 × 4.6 mm² column; Phenomenex, Norway) and a mixture of MeCN–H₂O, 30:70, at a flow rate of 2 mL/min as a mobile phase or using a Thermo Scientific device (Thermo Scientific UltiMate 3000 HPLC, Chromeleon) consisting of a quaternary pump, diode array detector (220 nm), and autosampler using an Ascentis Express C₁₈ analytical column (150 × 4.6 mm², 2.7 μ m particle size): eluent A: MeCN, eluent B: 0.1% formic acid, flow rate 1.0 mL/min, gradient method: 5% MeCN (0–5 min), 5–100% MeCN (5–15 min). Electrospray ionization mass spectra were obtained using a MSQ mass detector (Thermo Scientific). Thin layer chromatography (TLC) was conducted using silica gel plates (Merck KGaA, Darmstadt, Germany) with a fluorescence indicator (F₂₅₄) or Macherey-Nagel (Macherey-Nagel GmbH, Düren, Germany) precoated plastic sheets with fluorescent indicator UV254 (Polygram SIL G/UV254). Visualization of the spots was effected by irradiation with an UV lamp (254 and 366 nm). A miniGITA

radioTLC scanner (Raytest, Straubenhardt, Germany) was used for the detection of radioTLC spots. Radioactivity measurements were performed with an Atomlab 300 dose calibrator (Biodex medical systems Inc.) and activity is reported in Becquerel (Bq, s⁻¹).

Radiochemistry. All reagents, solvents, and reference compound **1** were purchased from Merck Millipore or Sigma-Aldrich in pharmaceutical grade. Difluorovinyl precursors for **1** (2-(((5-((2,2-difluorovinyl)oxy)-3-methylpyridin-2-yl)-methyl)sulfinyl)-1*H*-benzo[*d*]imidazole) (**3a**) and **2** (2-(((4-((2,2-difluorovinyl)oxy)-3-methylpyridin-2-yl)-methyl)-sulfinyl)-1-methyl-1*H*-benzo[*d*]imidazole) (**3b**) were prepared as described previously. [¹⁸F]Fluoride ([¹⁸F]F⁻) was produced via the ¹⁸O(p,n)¹⁸F nuclear reaction using an IBA Cyclone 18/9 cyclotron.

General Procedure for Synthesis of Compounds 10a–v. 2-Mercaptobenzoxa- and -thiazoles, **9a–e** (1.1 equiv), were treated with a solution of NaOH (3 equiv) in H₂O (10 mL) for 10 min at room temperature (rt). Respective pyridine building blocks, **8a–f** (1.0 equiv), were dissolved separately in H₂O (2 mL) and added slowly to the reaction mixture. Precipitate formation was observed immediately on addition, and reaction contents were allowed to stir for 1 h at rt. The reaction mixture was extracted with dichloromethane (3 × 20 mL) and the organic layers were combined, dried over Na₂SO₄, and concentrated in vacuo to obtain the respective sulfides (**10a–v**).

General Procedure for Synthesis of Compounds 11a–v. Oxidation of sulfide intermediates **10a–v** (1.0 equiv) was achieved using portions of *meta*-chloroperbenzoic acid (*m*-CPBA, 1.1 equiv) in CHCl₃ (8–10 mL) at 0 °C for 30 min. The reaction was quenched with NaHCO₃ (10 mL) and extracted with dichloromethane (DCM) (3 × 10 mL). The organic extracts were combined, washed with brine (20 mL), and dried over Na₂SO₄ to obtain the crude product. The product was purified by column chromatography on silica gel with MeOH–DCM, 1:9, to isolate the respective sulfoxides (**11a–v**).

6-Ethoxy-2-(((3-methyl-4-(2,2,2-trifluoroethoxy)pyridin-2-yl)methyl)thio)benzothiazol (10a) (403 mg, 97%). ¹H NMR (400 MHz, CDCl₃) δ 8.36 (d, *J* = 5.6 Hz, 1H), 7.77 (d, *J* = 9.0 Hz, 1H), 7.22 (d, *J* = 2.5 Hz, 1H), 7.01 (dd, *J* = 9.0, 2.5 Hz, 1H), 6.65 (d, *J* = 5.6 Hz, 1H), 4.78 (s, 2H), 4.40 (q, *J* = 7.8 Hz, 2H), 4.07 (q, *J* = 7.0 Hz, 2H), 2.35 (s, 3H), 1.41 (t, *J* = 7.0 Hz, 3H); ¹³C NMR (100 MHz, CDCl₃) δ 163.1, 161.8, 156.6, 155.9, 148.3, 147.8, 137.0, 122.2, 121.7, 115.4, 105.7, 105.0, 65.5 (q, ²*J*_{CF} = 36.7 Hz), 64.3, 38.2, 14.9, 10.9; ¹⁹F NMR (377 MHz, CDCl₃) δ -73.85 (s, 3F).

6-Ethoxy-2-(((3-methyl-4-(2,2,2-trifluoroethoxy)pyridin-2-yl)methyl)sulfinyl)benzothiazole (11a). (136 mg, 36%) ¹H NMR (400 MHz, CDCl₃) δ 8.33 (d, *J* = 5.6 Hz, 1H), 7.92 (d, *J* = 9.0 Hz, 1H), 7.39 (d, *J* = 2.5 Hz, 1H), 7.14 (dd, *J* = 9.0, 2.5 Hz, 1H), 6.67 (d, *J* = 5.6 Hz, 1H), 4.68 (s, 2H), 4.40 (q, *J* = 7.8 Hz, 2H), 4.12 (q, *J* = 7.0 Hz, 2H), 2.25 (s, 3H), 1.48 (t, *J* = 7.0 Hz, 3H); ¹³C NMR (100 MHz, CDCl₃) δ 173.2, 161.9, 157.9, 150.7, 148.6, 148.2, 137.8, 124.7, 123.6, 117.4, 106.0, 104.8, 65.5 (q, ²*J*_{CF} = 36.7 Hz), 64.3, 63.1, 14.9, 11.2; ¹⁹F NMR (377 MHz, CDCl₃) δ -73.79 (s, 3F); IR (KBr) ν (in cm⁻¹) 3028 (sp² C–H stretching), 2935 (sp³ C–H stretching), 1604 (C=N stretching), 1580, 1475 (C=C stretching), 1447, 1395, 1256, 1212, 1110 (S=O stretching), 1053, 991 (C–O stretching), 938, 855, 800, 716, 658, 569; high-resolution mass spectrometry (HR-MS) (ESI) *m/z* calcd for

$C_{18}H_{17}F_3N_2O_3S_2$, 430.0633; found, 431.0719 (M + H)⁺; HPLC >98%.

2-(((3-Methyl-4-(2,2,2-trifluoroethoxy)pyridin-2-yl)methyl)thio)benzothiazole (**10b**) (351 mg, 95%). ¹H NMR (400 MHz, CDCl₃) δ 8.32 (d, J = 5.7 Hz, 1H), 8.02 (d, J = 8.0 Hz, 1H), 7.88 (d, J = 8.1 Hz, 1H), 7.47 (dtd, J = 15.5, 7.2, 1.2 Hz, 1H), 7.37 (dtd, J = 15.3, 7.2, 1.3 Hz, 1H), 7.11 (d, J = 5.6 Hz, 1H), 4.91 (q, J = 7.8 Hz, 2H), 4.83 (s, 2H), 2.27 (s, 3H); ¹³C NMR (100 MHz, CDCl₃) δ 167.8, 162.3, 152.6, 150.1, 147.9, 135.7, 126.7, 125.5, 123.1, 122.6, 121.1, 105.3, 65.6 (q, ²J_{CF} = 36.7 Hz), 38.1, 11.2; ¹⁹F NMR (377 MHz, CDCl₃) δ -73.83 (s, 3F).

2-(((3-Methyl-4-(2,2,2-trifluoroethoxy)pyridin-2-yl)methyl)sulfinyl)benzothiazole (**11b**) (88 mg, 26%). ¹H NMR (400 MHz, CDCl₃) δ 8.33 (d, J = 5.6 Hz, 1H), 8.07 (d, J = 8.1 Hz, 1H), 8.01 (d, J = 8.1 Hz, 1H), 7.57 (dtd, J = 15.5, 7.2, 1.2 Hz, 1H), 7.50 (dtd, J = 15.3, 7.2, 1.3 Hz, 1H), 6.68 (d, J = 5.6 Hz, 1H), 4.75–4.66 (m, 2H), 4.40 (q, J = 7.8 Hz, 2H), 2.26 (s, 3H); ¹³C NMR (100 MHz, CDCl₃) δ 177.2, 161.9, 153.8, 150.6, 148.6, 136.2, 127.0, 126.3, 124.2, 123.6, 122.4, 106.1, 65.5 (q, ²J_{CF} = 36.7 Hz), 63.0, 11.2; ¹⁹F NMR (377 MHz, CDCl₃) δ -73.78 (s, 3F); IR (KBr) ν (in cm⁻¹) 3059 (sp² C–H stretching), 2932 (sp³ C–H stretching), 1583 (C=N stretching), 1474 (C=C stretching), 1432, 1393, 1261, 1078 (S=O stretching), 1050, 981 (C–O stretching), 866, 796, 764, 730, 680, 597; HR-MS (ESI) *m/z* calcd for $C_{16}H_{13}F_3N_2O_2S_2$, 386.0371; found, 387.0458 (M + H)⁺; HPLC >98%.

2-(((3-Methyl-4-(2,2,2-trifluoroethoxy)pyridin-2-yl)methyl)thio)benzoxazole (**10c**) (241 mg, 90%). ¹H NMR (400 MHz, CDCl₃) δ 8.40 (d, J = 5.6 Hz, 1H), 7.62 (d, J = 8.0 Hz, 1H), 7.45 (d, J = 8.0 Hz, 1H), 7.27 (ddd, J = 15.2, 7.4, 1.2 Hz, 2H), 6.69 (d, J = 5.6 Hz, 1H), 4.81 (s, 2H), 4.41 (q, J = 7.8 Hz, 2H), 2.37 (s, 3H); ¹³C NMR (100 MHz, CDCl₃) δ 168.6, 164.9, 155.0, 152.1, 148.1, 142.0, 133.2, 130.2, 124.4, 118.6, 110.1, 105.9, 66.6 (q, ²J_{CF} = 36.6 Hz), 36.7, 10.9; ¹⁹F NMR (377 MHz, CDCl₃) δ -73.83 (s, 3F).

2-(((3-Methyl-4-(2,2,2-trifluoroethoxy)pyridin-2-yl)methyl)sulfinyl)benzoxazole (**11c**) (54 mg, 23%). ¹H NMR (400 MHz, CDCl₃) δ 8.22 (d, J = 5.6 Hz, 1H), 7.82 (d, J = 8.0 Hz, 1H), 7.65 (d, J = 8.0 Hz, 1H), 7.45 (ddd, J = 15.2, 7.4, 1.2 Hz, 2H), 6.64 (d, J = 5.6 Hz, 1H), 4.87 (s, 2H), 4.38 (q, J = 7.8 Hz, 2H), 2.31 (s, 3H); ¹³C NMR (100 MHz, CDCl₃) δ 164.6, 161.9, 151.8, 150.4, 148.6, 140.6, 127.1, 125.6, 123.6, 121.4, 111.6, 106.1, 66.5 (q, ²J_{CF} = 36.6 Hz), 59.7, 11.2; ¹⁹F NMR (377 MHz, CDCl₃) δ -73.79 (s, 3F); IR (KBr) ν (in cm⁻¹) 3014 (sp² C–H stretching), 2930 (sp³ C–H stretching), 1580 (C=N stretching), 1479 (C=C stretching), 1306, 1261, 1168, 1103 (S=O stretching), 1047, 938 (C–O stretching), 878, 833, 759, 677, 608, 583; HR-MS (ESI) *m/z* calcd for $C_{16}H_{13}F_3N_2O_3S$, 370.0599; found, 371.0687 (M + H)⁺; HPLC >98%.

6-Ethoxy-2-(((4-methoxy-3,5-dimethylpyridin-2-yl)methyl)thio)benzo[d]thiazole (**10d**) (305 mg, 85%). ¹H NMR (400 MHz, CDCl₃) δ 8.23 (s, 1H), 7.76 (d, J = 9.0 Hz, 1H), 7.23 (d, J = 2.5 Hz, 1H), 7.01 (dd, J = 9.0, 2.5 Hz, 1H), 4.62 (s, 2H), 4.11 (q, J = 7.0 Hz, 2H), 3.68 (s, 3H), 2.35 (s, 3H), 2.16 (s, 3H), 1.40 (t, J = 7.0 Hz, 3H); ¹³C NMR (100 MHz, CDCl₃) δ 167.7, 164.3, 156.5, 154.3, 148.1, 147.6, 137.0, 126.1, 124.9, 122.2, 119.1, 104.3, 64.5, 62.9, 36.2, 14.8, 13.6, 10.9.

6-Ethoxy-2-(((4-methoxy-3,5-dimethylpyridin-2-yl)methyl)sulfinyl)benzothiazole (**11d**) (102 mg, 34%). ¹H NMR (400 MHz, CDCl₃) δ 8.21 (s, 1H), 7.91 (d, J = 9.0 Hz, 1H), 7.39 (d, J = 2.5 Hz, 1H), 7.13 (dd, J = 9.0, 2.5 Hz, 1H), 4.63 (s, 2H), 4.11 (q, J = 7.0 Hz, 2H), 3.72 (s, 3H), 2.24 (s, 3H), 2.22 (s, 3H), 1.47 (t, J = 7.0 Hz, 3H); ¹³C NMR (100 MHz, CDCl₃) δ 173.4, 164.3, 157.9, 150.0, 148.8, 148.2, 137.8, 127.2, 126.3, 124.7, 117.3, 104.8, 64.3, 63.3, 60.1, 14.9, 13.5, 11.8; IR (KBr) ν (in cm⁻¹) 3017 (sp² C–H stretching), 2904 (sp³ C–H stretching), 1598 (C=N stretching), 1468 (C=C stretching), 1443, 1397, 1250, 1222, 1079 (S=O stretching), 1042, 983 (C–O stretching), 928, 822, 782, 687, 611, 555; HR-MS (ESI) *m/z* calcd for $C_{18}H_{20}N_2O_3S_2$, 376.0915; found, 377.1006 (M + H)⁺; HPLC >98%.

2-(((4-Methoxy-3,5-dimethylpyridin-2-yl)methyl)thio)benzothiazole (**10e**) (308 mg, 97%). ¹H NMR (400 MHz, CDCl₃) δ 8.22 (s, 1H), 7.89 (d, J = 8.1 Hz, 1H), 7.75 (d, J = 8.0 Hz, 1H), 7.41 (dtd, J = 15.5, 7.2, 1.1 Hz, 1H), 7.29 (dtd, J = 15.4, 7.2, 1.1 Hz, 1H), 4.79 (s, 2H), 3.77 (s, 3H), 2.37 (s, 3H), 2.25 (s, 3H); ¹³C NMR (101 MHz, CDCl₃) δ 166.9, 164.3, 153.7, 153.3, 149.5, 135.6, 126.1, 125.8, 125.4, 124.3, 121.6, 121.1, 60.1, 38.1, 13.4, 11.5.

2-(((4-Methoxy-3,5-dimethylpyridin-2-yl)methyl)sulfinyl)benzothiazole (**11e**) (92 mg, 31%). ¹H NMR (400 MHz, CDCl₃) δ 8.21 (s, 1H), 8.06 (d, J = 8.1 Hz, 1H), 8.00 (d, J = 8.1 Hz, 1H), 7.56 (dtd, J = 15.5, 7.2, 1.1 Hz, 1H), 7.49 (dtd, J = 15.4, 7.2, 1.1 Hz, 1H), 4.70–4.61 (m, 2H), 3.73 (s, 3H), 2.25 (s, 3H), 2.23 (s, 3H); ¹³C NMR (101 MHz, CDCl₃) δ 177.4, 164.3, 153.8, 150.0, 148.8, 136.2, 127.2, 127.0, 126.4, 126.3, 124.2, 122.4, 63.3, 60.1, 13.5, 11.8; IR (KBr) ν (in cm⁻¹) 3047 (sp² C–H stretching), 2940 (sp³ C–H stretching), 1567 (C=N stretching), 1465 (C=C stretching), 1426, 1402, 1272, 1086 (S=O stretching), 1043, 996 (C–O stretching), 873, 791, 759, 726, 669, 588; HR-MS (ESI) *m/z* calcd for $C_{16}H_{16}N_2O_2S_2$, 332.0653; found, 333.0741 (M + H)⁺; HPLC >98%.

2-(((4-Methoxy-3,5-dimethylpyridin-2-yl)methyl)thio)benzoxazole (**10f**) (207 mg, 92%). ¹H NMR (400 MHz, CDCl₃) δ 8.22 (s, 1H), 7.62 (d, J = 7.7 Hz, 1H), 7.45 (d, J = 7.8 Hz, 1H), 7.26 (dddd, J = 15.3, 7.3, 1.0 Hz, 2H), 4.75 (s, 2H), 3.77 (s, 3H), 2.37 (s, 3H), 2.25 (s, 3H); ¹³C NMR (101 MHz, CDCl₃) δ 165.3, 164.2, 153.1, 152.0, 149.5, 142.1, 125.9, 125.2, 124.3, 124.0, 118.5, 110.0, 60.1, 37.3, 13.4, 11.5.

2-(((4-Methoxy-3,5-dimethylpyridin-2-yl)methyl)sulfinyl)benzoxazole (**11f**) (42 mg, 21%). ¹H NMR (400 MHz, CDCl₃) δ 8.05 (s, 1H), 7.58 (d, J = 7.7 Hz, 1H), 7.41 (d, J = 7.8 Hz, 1H), 7.26 (dddd, J = 15.3, 7.3, 1.0 Hz, 2H), 4.86 (s, 2H), 3.74 (s, 3H), 2.52 (s, 3H), 2.22 (s, 3H); ¹³C NMR (100 MHz, CDCl₃) δ 166.6, 155.8, 152.3, 145.8, 141.9, 138.2, 128.7, 128.5, 124.3, 123.9, 118.3, 110.1, 60.6, 29.9, 13.5, 12.6; IR (KBr) ν (in cm⁻¹) 3021 (sp² C–H stretching), 2923 (sp³ C–H stretching), 1573 (C=N stretching), 1472 (C=C stretching), 1315, 1249, 1170, 1110 (S=O stretching), 1043, 972 (C–O stretching), 862, 815, 748, 663, 601, 576; HR-MS (ESI) *m/z* calcd for $C_{16}H_{16}N_2O_3S$, 316.0882; found, 317.0968 (M + H)⁺; HPLC >98%.

6-Ethoxy-2-(((4-(2-fluoroethoxy)-3-methylpyridin-2-yl)methyl)thio)benzodthiazole (**10g**) (174 mg, 92%). ¹H NMR (400 MHz, CDCl₃) δ 8.30 (d, J = 5.6 Hz, 1H), 7.76 (d, J = 9.0 Hz, 1H), 7.21 (d, J = 2.4 Hz, 1H), 6.99 (dd, J = 9.0, 2.5 Hz, 1H), 6.66 (d, J = 5.6 Hz, 1H), 4.88–4.83 (m, 1H), 4.76 (s, 2H), 4.72–4.68 (m, 1H), 4.31–4.27 (m, 1H), 4.22–4.17 (m, 1H), 4.05 (q, J = 7.0 Hz, 2H), 2.32 (s, 3H), 1.43 (t, J = 7.0 Hz,

3H); ^{13}C NMR (100 MHz, CDCl_3) δ 167.1, 161.8, 156.1, 147.9, 147.2, 146.7, 137.1, 125.1, 124.7, 118.2, 105.8, 104.2, 82.2 (d, $^1J_{\text{CF}} = 172.3$ Hz), 67.4 (d, $^2J_{\text{CF}} = 20.7$ Hz), 63.8, 37.5, 14.6, 11.1.

6-Ethoxy-2-(((4-(2-fluoroethoxy)-3-methylpyridin-2-yl)methyl)sulfinyl)benzothiazole (11g) (43 mg, 31%). ^1H NMR (400 MHz, CDCl_3) δ 8.29 (d, $J = 5.6$ Hz, 1H), 7.92 (d, $J = 9.0$ Hz, 1H), 7.39 (d, $J = 2.4$ Hz, 1H), 7.13 (dd, $J = 9.0, 2.5$ Hz, 1H), 6.69 (d, $J = 5.6$ Hz, 1H), 4.84 (t, $J = 4.1$ Hz, 3H), 4.73 (t, $J = 4.0$ Hz, 3H), 4.67 (s, 2H), 4.31–4.28 (m, 1H), 4.24–4.21 (m, 1H), 4.12 (q, $J = 7.0$ Hz, 2H), 2.24 (s, 3H), 1.47 (t, $J = 7.0$ Hz, 3H); ^{13}C NMR (100 MHz, CDCl_3) δ 173.4, 163.1, 157.9, 150.0, 148.5, 148.2, 137.9, 124.7, 123.3, 117.3, 106.1, 104.8, 82.5 (d, $^1J_{\text{CF}} = 172.3$ Hz), 67.4 (d, $^2J_{\text{CF}} = 20.7$ Hz), 64.3, 63.3, 14.9, 11.3; IR (KBr) ν (in cm^{-1}) 2987 (sp^2 C–H stretching), 2917 (sp^3 C–H stretching), 1599 (C=N stretching), 1472, 1445 (C=C stretching), 1296, 1253, 1221, 1085 (S=O stretching), 1050, 940 (C–O stretching), 883, 818, 725, 681, 606, 558; HR-MS (ESI) m/z calcd for $\text{C}_{18}\text{H}_{19}\text{FN}_2\text{O}_3\text{S}_2$, 394.0821; found, 395.0892 (M + H) $^+$; HPLC >98%.

2-(((4-(2-Fluoroethoxy)-3-methylpyridin-2-yl)methyl)thio)benzothiazole (10h) (147 mg, 88%). ^1H NMR (400 MHz, CDCl_3) δ 8.32 (d, $J = 5.7$ Hz, 1H), 7.89 (d, $J = 8.2$ Hz, 1H), 7.75 (d, $J = 8.1$ Hz, 1H), 7.41 (dtd, $J = 15.5, 7.1, 1.1$ Hz, 1H), 7.29 (dtd, $J = 15.3, 7.2, 1.1$ Hz, 1H), 6.68 (d, $J = 5.7$ Hz, 1H), 4.86–4.83 (m, 1H), 4.82 (s, 2H), 4.74–4.71 (m, 1H), 4.30–4.27 (m, 1H), 4.23–4.20 (m, 1H), 2.34 (s, 3H); ^{13}C NMR (100 MHz, CDCl_3) δ 166.9, 161.3, 155.4, 150.6, 147.6, 135.9, 126.1, 125.8, 124.6, 123.1, 122.1, 106.6, 81.5 (d, $^1J_{\text{CF}} = 172$ Hz), 67.3 (d, $^2J_{\text{CF}} = 20.7$ Hz), 38.5, 10.8.

2-(2-(((4-(2-Fluoroethoxy)-3-methylpyridin-2-yl)methyl)sulfinyl)benzothiazole (11h) (37 mg, 32%). ^1H NMR (400 MHz, CDCl_3) δ 8.30 (d, $J = 5.7$ Hz, 1H), 8.07 (d, $J = 8.2$ Hz, 1H), 8.00 (d, $J = 8.1$ Hz, 1H), 7.56 (dtd, $J = 15.5, 7.1, 1.1$ Hz, 1H), 7.49 (dtd, $J = 15.3, 7.2, 1.1$ Hz, 1H), 6.70 (d, $J = 5.7$ Hz, 1H), 4.85 (t, $J = 4.1$ Hz, 3H), 4.73 (t, $J = 4.0$ Hz, 3H), 4.74–4.65 (m, 2H), 4.32–4.28 (m, 1H), 4.25–4.21 (m, 1H), 2.25 (s, 3H); ^{13}C NMR (100 MHz, CDCl_3) δ 177.5, 163.1, 153.9, 149.9, 148.5, 136.3, 127.0, 126.3, 124.2, 123.3, 122.4, 106.1, 81.5 (d, $^1J_{\text{CF}} = 172$ Hz), 67.4 (d, $^2J_{\text{CF}} = 20.7$ Hz), 63.3, 11.3; IR (KBr) ν (in cm^{-1}) 3011 (sp^2 C–H stretching), 2937 (sp^3 C–H stretching), 1580 (C=N stretching), 1475, 1423 (C=C stretching), 1299, 1233, 1103 (S=O stretching), 1047, 948 (C–O stretching), 885, 829, 739, 690, 586, 547; HR-MS (ESI) m/z calcd for $\text{C}_{16}\text{H}_{15}\text{FN}_2\text{O}_2\text{S}_2$, 350.0559; found, 351.0630 (M + H) $^+$; HPLC >98%.

2-(((4-(2-Fluoroethoxy)-3-methylpyridin-2-yl)methyl)thio)benzoxazole (10i) (146 mg, 92%). ^1H NMR (400 MHz, CDCl_3) δ 8.32 (d, $J = 7.2$ Hz, 1H), 7.39 (d, $J = 7.7$ Hz, 1H), 7.23 (d, $J = 7.6$ Hz, 1H), 7.11 (dtd, $J = 7.6, 1.2$ Hz, 2H), 6.78 (d, $J = 7.1$ Hz, 1H), 4.86 (s, 2H), 4.84–4.80 (m, 1H), 4.72–4.68 (m, 1H), 4.30–4.27 (m, 1H), 4.23–4.20 (m, 1H), 2.56 (s, 3H); ^{13}C NMR (100 MHz, CDCl_3) δ 168.9, 164.9, 158.6, 154.4, 149.6, 142.3, 139.2, 125.2, 124.2, 123.3, 119.7, 111.3, 108.6, 81.2 (d, $^1J_{\text{CF}} = 172$ Hz), 68.3 (d, $^2J_{\text{CF}} = 20.4$ Hz), 57.2, 11.1.

2-(((4-(2-Fluoroethoxy)-3-methylpyridin-2-yl)methyl)sulfinyl)benzoxazole (11i) (37 mg, 27%). ^1H NMR (400 MHz, CDCl_3) δ 8.16 (d, $J = 7.2$ Hz, 1H), 7.58 (d, $J = 7.7$ Hz, 1H), 7.42 (d, $J = 7.6$ Hz, 1H), 7.25 (dd, $J = 7.6, 1.2$ Hz, 2H), 6.73 (d, $J = 7.1$ Hz, 1H), 4.91 (s, 2H), 4.86–4.81 (m, 1H), 4.74–4.69 (m, 1H), 4.31–4.26 (m, 1H), 4.24–4.20 (m, 1H), 2.52 (s, 3H); ^{13}C NMR (100 MHz, CDCl_3) δ 166.4, 155.0,

152.3, 147.9, 141.9, 137.1, 124.7, 124.3, 123.9, 118.4, 110.1, 107.3, 81.3 (d, $^1J_{\text{CF}} = 172.8$ Hz), 68.2 (d, $^2J_{\text{CF}} = 20.4$ Hz), 37.8, 12.3; IR (KBr) ν (in cm^{-1}) 3021 (sp^2 C–H stretching), 2913 (sp^3 C–H stretching), 1587 (C=N stretching), 1468, 1431 (C=C stretching), 1289, 1226, 1098 (S=O stretching), 1034, 946 (C–O stretching), 878, 811, 738, 692, 611, 571; HR-MS (ESI) m/z calcd for $\text{C}_{16}\text{H}_{15}\text{FN}_2\text{O}_3\text{S}$, 334.0787; found, 335.0859 (M + H) $^+$; HPLC >98%.

2-(((3-Methyl-4-(2,2,2-trifluoroethoxy)pyridin-2-yl)methyl)thio)-5-(1H-pyrrol-1-yl)-1H-benzimidazole (10j) (178 mg, 85%). ^1H NMR (400 MHz, CDCl_3) δ 12.37 (br s, 1H), 8.32 (d, $J = 5.6$ Hz, 1H), 8.07–7.50 (m, 2H), 7.39 (dd, $J = 8.7, 2.1$ Hz, 1H), 7.09 (t, $J = 2.1$ Hz, 2H), 6.61 (d, $J = 5.6$ Hz, 1H), 6.38 (t, $J = 2.2$ Hz, 2H), 4.89–4.74 (m, 2H), 4.30 (qd, $J = 7.8, 5.2$ Hz, 2H), 2.20 (s, 3H); ^{13}C NMR (100 MHz, CDCl_3) δ 163.0, 157.2, 147.3, 136.8, 121.5, 120.3, 115.9, 110.1, 106.3, 79.2, 65.5 (q, $^2J_{\text{CF}} = 36.3$ Hz), 37.6, 10.8; ^{19}F NMR (377 MHz, CDCl_3) δ -73.78 (s, 3F).

2-(((3-Methyl-4-(2,2,2-trifluoroethoxy)pyridin-2-yl)methyl)sulfinyl)-5-(1H-pyrrol-1-yl)-1H-benzimidazole (11j) (54 mg, 33%). ^1H NMR (400 MHz, CDCl_3) δ 12.47 (br s, 1H), 8.31 (d, $J = 5.6$ Hz, 1H), 7.85–7.52 (m, 2H), 7.38 (dd, $J = 8.7, 2.1$ Hz, 1H), 7.09 (t, $J = 2.1$ Hz, 2H), 6.60 (d, $J = 5.6$ Hz, 1H), 6.38 (t, $J = 2.2$ Hz, 2H), 4.81 (q, $J = 13.9$ Hz, 2H), 4.29 (p, $J = 8.0$ Hz, 2H), 2.18 (s, 3H); ^{13}C NMR (100 MHz, CDCl_3) δ 161.9, 150.4, 148.5, 123.4, 120.1, 110.5, 106.2, 77.1, 65.4 (q, $^2J_{\text{CF}} = 36.3$ Hz), 60.8, 11.10; ^{19}F NMR (377 MHz, CDCl_3) δ -73.77 (s, 3F); IR (KBr) ν (in cm^{-1}) 3310 (N–H stretching), 2961 (sp^2 C–H stretching), 2810 (sp^3 C–H stretching), 1630, 1580 (C=N stretching), 1513, 1485 (C=C stretching), 1411, 1317, 1258, 1166, 1110 (S=O stretching), 1046, 969 (C–O stretching), 892, 854, 808, 730, 663, 604, 576; HR-MS (ESI) m/z calcd for $\text{C}_{20}\text{H}_{17}\text{F}_3\text{N}_4\text{O}_2\text{S}$, 434.1024; found, 457.0913 (M + Na) $^+$; HPLC >98%.

1-Methyl-2-(((3-methyl-4-(2,2,2-trifluoroethoxy)pyridin-2-yl)methyl)sulfinyl)-5-(1H-pyrrol-1-yl)-1H-benzimidazole (11k) (47 mg, 23%). ^1H NMR (400 MHz, CDCl_3) δ 8.23 (d, $J = 5.6$ Hz, 1H), 7.83 (d, $J = 8.7$ Hz, 1H), 7.41 (dd, $J = 8.7, 2.1$ Hz, 1H), 7.36 (d, $J = 2.0$ Hz), 7.13 (t, $J = 2.2$ Hz, 2H), 6.63 (d, $J = 5.7$ Hz, 1H), 6.39 (t, $J = 2.2$ Hz, 2H), 5.07–4.94 (m, 2H), 4.38 (q, $J = 7.8$ Hz, 2H), 4.03 (s, 3H), 2.32 (s, 3H); ^{13}C NMR (100 MHz, CDCl_3) δ 161.8, 153.0, 151.5, 148.3, 140.3, 138.4, 137.1, 124.3, 123.3, 122.1, 120.1, 117.8, 110.8, 105.9, 102.0, 66.5 (q, $^2J_{\text{CF}} = 36.6$ Hz), 59.3, 31.0, 11.1; ^{19}F NMR (377 MHz, CDCl_3) δ -73.76 (s, 3F); IR (KBr) ν (in cm^{-1}) 3457 (N–H stretching), 3111 (sp^2 C–H stretching), 2953 (sp^3 C–H stretching), 1618, 1584 (C=N stretching), 1497, 1464 (C=C stretching), 1367, 1308, 1269, 1157, 1114 (S=O stretching), 1051, 979 (C–O stretching), 879, 813, 741, 664, 639, 611, 578; HR-MS (ESI) m/z calcd for $\text{C}_{21}\text{H}_{19}\text{F}_3\text{N}_4\text{O}_2\text{S}$, 448.1181; found, 471.1109 (M + Na) $^+$; HPLC >98%.

1-Methyl-2-(((3-methyl-4-(2,2,2-trifluoroethoxy)pyridin-2-yl)methyl)sulfinyl)-5-(1H-pyrrol-1-yl)-1H-benzimidazole (11l) (28 mg, 11%). ^1H NMR (400 MHz, CDCl_3) δ 8.22 (d, $J = 5.7$ Hz, 1H), 7.80 (d, $J = 1.8$ Hz, 1H), 7.49–7.43 (m, 2H), 7.11 (t, $J = 2.2$ Hz, 2H), 6.63 (d, $J = 5.6$ Hz, 1H), 6.37 (t, $J = 2.2$ Hz, 2H), 5.07–4.95 (m, 2H), 4.38 (q, $J = 7.8$ Hz, 2H), 4.05 (s, 3H), 2.32 (s, 3H); ^{13}C NMR (100 MHz, CDCl_3) δ 161.8, 153.6, 151.4, 148.2, 142.7, 137.4, 134.8, 123.3, 120.1, 119.1, 112.9, 110.7, 110.5, 105.9, 65.4 (q, $^2J_{\text{CF}} = 36.2$ Hz), 59.3, 31.0, 11.1; ^{19}F NMR (377 MHz, CDCl_3) δ -73.75 (s, 3F); IR (KBr) ν (in cm^{-1}) 3460 (N–H stretching), 3108 (sp^2 C–H stretching), 2947 (sp^3 C–H stretching), 1627, 1578

(C=N stretching), 1503, 1475 (C=C stretching), 1373, 1310, 1264, 1163, 1110 (S=O stretching), 1043, 976 (C–O stretching), 885, 818, 734, 660, 633, 614, 573; HR-MS (ESI) m/z calcd for $C_{21}H_{19}F_3N_4O_2S$, 448.1181; found, 471.1109 (M + Na)⁺; HPLC >96%.

2-(((4-Methoxy-3,5-dimethylpyridin-2-yl)methyl)thio)-5-(1H-pyrrol-1-yl)-1H-benzimidazole (**10k**) (523 mg, 96%). ¹H NMR (400 MHz, CDCl₃) δ 12.37 (br s, 1H), δ 8.13 (s, 1H), 7.52 (d, $J = 8.8$ Hz, 2H), 7.32 (dd, $J = 8.6, 2.1$ Hz, 1H), 7.13 (t, $J = 2.2$ Hz, 2H), 6.27 (t, $J = 2.2$ Hz, 2H), 4.60 (s, 2H), 3.77 (s, 3H), 2.31 (s, 3H), 2.24 (s, 3H); ¹³C NMR (100 MHz, CDCl₃) δ 166.3, 155.3, 149.8, 138.0, 127.7, 127.2, 120.7, 111.0, 60.6, 37.5, 13.4, 11.3.

2-(((4-Methoxy-3,5-dimethylpyridin-2-yl)methyl)sulfinyl)-5-(1H-pyrrol-1-yl)-1H-benzod[*h*]imidazole (**11m**) (263 mg, 51%). ¹H NMR (400 MHz, CDCl₃) δ 12.57 (br s, 1H), 8.18 (s, 1H), 7.88–7.36 (m, 2H), 7.37 (dd, $J = 8.7, 2.1$ Hz, 1H), 7.09 (t, $J = 2.2$ Hz, 2H), 6.37 (t, $J = 2.1$ Hz, 2H), 4.82–4.73 (m, 2H), 3.62 (s, 3H), 2.18 (d, $J = 4.3$ Hz, 6H); ¹³C NMR (100 MHz, CDCl₃) δ 164.5, 149.8, 148.6, 127.0, 126.7, 120.1, 110.5, 60.8, 60.0, 13.4, 11.6; IR (KBr) ν (in cm⁻¹) 3357 (N–H stretching), 3098 (sp² C–H stretching), 2982 (sp³ C–H stretching), 1632, 1587 (C=N stretching), 1517, 1480 (C=C stretching), 1423, 1359, 1271, 1212, 1078 (S=O stretching), 997, 969 (C–O stretching), 889, 848, 801, 720, 615, 607, 581; HR-MS (ESI) m/z calcd for $C_{20}H_{20}N_4O_2S$, 380.1307; found, 403.1199 (M + Na)⁺; HPLC >98%.

1-Methyl-2-(((3-methyl-4-(2,2,2-trifluoroethoxy)pyridin-2-yl)methyl)sulfinyl)-5-(1H-pyrrol-1-yl)-1H-benzod[*h*]imidazole (**11n**) (43 mg, 24%). ¹H NMR (400 MHz, CDCl₃) δ 8.09 (s, 1H), 7.83 (d, $J = 8.7$ Hz, 1H), 7.41 (dd, $J = 8.7, 2.1$ Hz, 1H), 7.35 (d, $J = 2.0$ Hz, 1H), 7.13 (t, $J = 2.2$ Hz, 2H), 6.38 (t, $J = 2.1$ Hz, 2H), 5.02–4.88 (m, 2H), 3.99 (s, 3H), 3.70 (s, 3H), 2.29 (s, 3H), 2.20 (s, 3H); ¹³C NMR (100 MHz, CDCl₃) δ 164.4, 153.3, 149.7, 149.5, 140.3, 138.3, 137.1, 126.8, 126.2, 122.0, 120.1, 117.8, 110.8, 102.0, 60.1, 59.6, 30.9, 13.4, 11.7; IR (KBr) ν (in cm⁻¹) 3461 (N–H stretching), 2098 (sp² C–H stretching), 2934 (sp³ C–H stretching), 1631, 1563 (C=N stretching), 1512, 1467 (C=C stretching), 1408, 1381, 1307, 1263, 1097 (S=O stretching), 1062, 1003 (C–O stretching), 889, 824, 771, 726, 684, 609, 580; HR-MS (ESI) m/z calcd for $C_{21}H_{22}N_4O_2S$, 394.1463; found, 395.1535 (M + H)⁺; HPLC >98%.

1-Methyl-2-(((3-methyl-4-(2,2,2-trifluoroethoxy)pyridin-2-yl)methyl)sulfinyl)-5-(1H-pyrrol-1-yl)-1H-benzod[*h*]imidazole (**11o**) (23 mg, 15%). ¹H NMR (400 MHz, CDCl₃) δ 8.09 (s, 1H), 7.80 (d, $J = 1.7$ Hz, 1H), 7.48–7.41 (m, 2H), 7.11 (t, $J = 2.2$ Hz, 2H), 6.37 (t, $J = 2.2$ Hz, 2H), 5.03–4.88 (m, 2H), 4.00 (s, 3H), 3.70 (s, 3H), 2.29 (s, 3H), 2.21 (s, 3H); ¹³C NMR (100 MHz, CDCl₃) δ 164.4, 153.9, 149.7, 149.5, 142.8, 137.4, 134.7, 126.8, 126.2, 120.1, 119.0, 112.9, 110.6, 110.5, 60.1, 59.5, 31.0, 13.4, 11.7; IR (KBr) ν (in cm⁻¹) 3467 (N–H stretching), 3105 (sp² C–H stretching), 2940 (sp³ C–H stretching), 1626, 1570 (C=N stretching), 1507, 1472 (C=C stretching), 1413, 1370, 1303, 1257, 1101 (S=O stretching), 1068, 997 (C–O stretching), 892, 829, 776, 730, 681, 615, 576; HR-MS (ESI) m/z calcd for $C_{21}H_{22}N_4O_2S$, 394.1463; found, 417.1355 (M + Na)⁺; HPLC >98%.

2-(((4-(2-Fluoroethoxy)-3-methylpyridin-2-yl)methyl)thio)-5-(1H-pyrrol-1-yl)-1H-benzimidazole (**10l**) (285 mg, 75%). ¹H NMR (400 MHz, CDCl₃) δ 13.15 (br s, 1H), 8.39 (d, $J = 5.7$ Hz, 1H), 7.60–7.48 (m, 2H), 7.24 (dd, $J = 8.7, 2.1$ Hz, 1H), 7.10 (t, $J = 2.2$ Hz, 2H), 6.77 (d, $J = 5.7$ Hz, 1H),

6.35 (t, $J = 2.2$ Hz, 2H), 4.90–4.85 (m, 1H), 4.79–4.72 (m, 1H), 4.40 (s, 2H), 4.36–4.31 (m, 1H), 4.29–4.25 (m, 1H), 2.32 (s, 3H); ¹³C NMR (100 MHz, CDCl₃) δ 163.9, 157.0, 147.3, 136.2, 121.6, 120.3, 116.1, 109.9, 106.2, 82.4 (q, $^1J_{CF} = 172$ Hz), 67.6 (q, $^2J_{CF} = 36.3$ Hz), 34.8, 10.9.

2-(((4-(2-Fluoroethoxy)-3-methylpyridin-2-yl)methyl)sulfinyl)-5-(1H-pyrrol-1-yl)-1H-benzod[*h*]imidazole (**11p**) (124 mg, 45%). ¹H NMR (400 MHz, CDCl₃) δ 12.43 (br s, 1H), 8.28 (d, $J = 5.6$ Hz, 1H), 7.75–7.43 (m, 2H), 7.37 (dd, $J = 8.7, 2.2$ Hz, 1H), 7.09 (t, $J = 2.0$ Hz, 2H), 6.65 (d, $J = 5.6$ Hz, 1H), 6.37 (t, $J = 2.0$ Hz, 2H), 4.86–4.76 (m, 2H), 4.76 (t, $J = 4.2$ Hz, 1H), 4.68 (t, $J = 4.2$ Hz, 1H), 4.17 (dddd, $J = 23.0, 15.6, 11.5, 7.8, 4.1$ Hz, 2H), 2.19 (s, 3H); ¹³C NMR (100 MHz, CDCl₃) δ 163.3, 149.6, 148.4, 123.3, 120.1, 110.5, 106.3, 81.4 (d, $^1J_{CF} = 172$ Hz), 67.4 (d, $^2J_{CF} = 20$ Hz), 60.8, 11.2; IR (KBr) ν (in cm⁻¹) 3343 (N–H stretching), 3055 (sp² C–H stretching), 2965 (sp³ C–H stretching), 1638, 1580 (C=N stretching), 1514, 1483 (C=C stretching), 1444, 1306, 1267, 1159, 1103 (S=O stretching), 993, 953 (C–O stretching), 897, 851, 798, 718, 637, 590, 565; HR-MS (ESI) m/z calcd for $C_{20}H_{19}FN_4O_2S$, 398.1213; found, 421.1104 (M + Na)⁺; HPLC >98%.

2-(((4-(2-Fluoroethoxy)-3-methylpyridin-2-yl)methyl)sulfinyl)-1-methyl-5-(1H-pyrrol-1-yl)-1H-benzod[*h*]imidazole (**11q**) (33 mg, 17%). ¹H NMR (400 MHz, CDCl₃) δ 8.18 (d, $J = 5.6$ Hz, 1H), 7.83 (d, $J = 8.7$ Hz, 1H), 7.41 (dd, $J = 8.7, 2.1$ Hz, 1H), 7.35 (d, $J = 2.1$ Hz, 1H), 7.13 (t, $J = 2.2$ Hz, 2H), 6.64 (d, $J = 5.6$ Hz, 1H), 6.38 (t, $J = 2.2$ Hz, 2H), 5.05–4.92 (m, 2H), 4.83 (t, $J = 4.1$ Hz, 1H), 4.71 (t, $J = 4.1$ Hz, 1H), 4.28–4.26 (m, 1H), 4.21–4.19 (m, 1H), 4.01 (s, 3H), 2.29 (s, 3H); ¹³C NMR (100 MHz, CDCl₃) δ 163.1, 153.3, 150.7, 148.2, 140.3, 138.3, 137.1, 123.0, 122.0, 120.1, 117.7, 110.8, 106.0, 102.0, 81.5 (d, $^1J_{CF} = 172$ Hz), 67.4 (d, $^2J_{CF} = 20$ Hz), 59.5, 30.9, 11.2; IR (KBr) ν (in cm⁻¹) 3461 (N–H stretching), 3107 (sp² C–H stretching), 2944 (sp³ C–H stretching), 1630, 1567 (C=N stretching), 1502, 1466 (C=C stretching), 1374, 1298, 1243, 1106 (S=O stretching), 1065, 989 (C–O stretching), 896, 825, 781, 724, 679, 613, 580; HR-MS (ESI) m/z calcd for $C_{21}H_{21}FN_4O_2S$, 412.1369; found, 435.1261 (M + Na)⁺; HPLC >98%.

2-(((4-(2-Fluoroethoxy)-3-methylpyridin-2-yl)methyl)sulfinyl)-1-methyl-5-(1H-pyrrol-1-yl)-1H-benzod[*h*]imidazole (**11r**) (24 mg, 14%). ¹H NMR (400 MHz, CDCl₃) δ 8.17 (d, $J = 5.6$ Hz, 1H), 7.80 (d, $J = 2.0$ Hz, 1H), 7.48–7.42 (m, 2H), 7.11 (t, $J = 2.2$ Hz, 2H), 6.64 (d, $J = 5.6$ Hz, 1H), 6.37 (t, $J = 2.3$ Hz, 2H), 5.06–4.92 (m, 2H), 4.83 (t, $J = 4.1$ Hz, 1H), 4.71 (t, $J = 4.1$ Hz, 1H), 4.28–4.25 (m, 1H), 4.21–4.19 (m, 1H), 4.02 (s, 3H), 2.29 (s, 3H); ¹³C NMR (100 MHz, CDCl₃) δ 163.1, 153.8, 150.7, 148.2, 142.8, 137.4, 134.8, 123.0, 120.1, 119.0, 112.9, 110.6, 110.4, 106.0, 81.4 (d, $^1J_{CF} = 172$ Hz), 67.4 (d, $^2J_{CF} = 20$ Hz), 59.5, 31.0, 11.2; IR (KBr) ν (in cm⁻¹) 3471 (N–H stretching), 3113 (sp² C–H stretching), 2951 (sp³ C–H stretching), 1621, 1572 (C=N stretching), 1499, 1468 (C=C stretching), 1381, 1307, 1259, 1161, 1106 (S=O stretching), 1055, 968 (C–O stretching), 879, 822, 778, 719, 657, 611, 568; HR-MS (ESI) m/z calcd for $C_{21}H_{21}FN_4O_2S$, 412.1369; found, 435.1261 (M + Na)⁺; HPLC >98%.

2-(((4-(2-Fluoroethoxy)-3-methylpyridin-2-yl)methyl)sulfinyl)-1H-benzimidazole (**11s**) (30 mg, 37%). ¹H NMR (400 MHz, CDCl₃) δ 11.96 (br s, 1H), 8.31 (d, $J = 5.7$ Hz, 1H), 7.90–7.38 (m, 2H), 7.35–7.27 (m, 2H), 6.69 (d, $J = 5.7$ Hz, 1H), 4.87–4.70 (m, 2H), 4.82–4.78 (m, 1H), 4.71–4.67 (m, 1H), 4.28–4.23 (m, 1H), 4.20–4.16 (m, 1H), 2.19 (s,

3H); ^{13}C NMR (101 MHz, CDCl_3) δ 163.2, 153.4, 149.9, 148.4, 123.3, 106.2, 82.4 (d, $^1J_{\text{CF}} = 173.6$ Hz), 77.5, 77.3, 77.1, 76.8, 67.4 (d, $^2J_{\text{CF}} = 20.4$ Hz), 60.9, 11.2; IR (KBr) ν (in cm^{-1}) 3323 (N–H stretching), 3057 (sp^2 C–H stretching), 2951 (sp^3 C–H stretching), 1754, 1586 (C=N stretching), 1444, 1354 (C=C stretching), 1279, 1243, 1174, 1103 (S=O stretching), 978 (C–O stretching), 901, 858, 799, 743, 675, 582, 541; HR-MS (ESI) m/z calcd for $\text{C}_{16}\text{H}_{16}\text{FN}_3\text{O}_2\text{S}$, 333.0947; found, 356.0989 (M + Na) $^+$; HPLC >98%.

2-(((4-(2-Fluoroethoxy)-3-methylpyridin-2-yl)methyl)sulfinyl)-1-methyl-1H-benzimidazole (**11t**) (28 mg, 33%). ^1H NMR (400 MHz, CDCl_3) δ 8.19 (d, $J = 5.6$ Hz, 1H), 7.82 (dt, $J = 7.9, 1.0$ Hz, 1H), 7.44–7.38 (m, 2H), 7.38–7.30 (m, 1H), 6.64 (d, $J = 5.6$ Hz, 1H), 5.04–4.92 (m, 2H), 4.85–4.80 (m, 1H), 4.73–4.68 (m, 1H), 4.29–4.23 (m, 1H), 4.22–4.17 (m, 1H), 4.02 (s, 3H), 2.28 (s, 3H); ^{13}C NMR (101 MHz, CDCl_3) δ 163.1, 152.5, 150.8, 148.2, 142.3, 136.6, 124.7, 123.4, 123.0, 121.2, 109.9, 106.0, 81.4 (d, $^1J_{\text{C-F}} = 173.1$ Hz), 67.4 (d, $^2J_{\text{C-CF}} = 20.6$ Hz), 59.5, 30.8, 11.2; IR (KBr) ν (in cm^{-1}) 3043 (sp^2 C–H stretching), 2947 (sp^3 C–H stretching), 1738, 1577 (C=N stretching), 1432, 1347 (C=C stretching), 1288, 1233, 1168, 1109 (S=O stretching), 985 (C–O stretching), 893, 851, 788, 731, 680, 577, 544; HR-MS (ESI) m/z calcd for $\text{C}_{17}\text{H}_{18}\text{FN}_3\text{O}_2\text{S}$, 347.1104; found, 370.1196 (M + Na) $^+$; HPLC >98%.

2-(((6-Fluoro-4-methoxy-3,5-dimethylpyridin-2-yl)methyl)sulfinyl)-1-methyl-1H-benzimidazole (**11u**) (219 mg, 86%). ^1H NMR (CDCl_3 , 500 MHz) δ 7.81 (d, 1H, $J = 8.1$ Hz), 7.45–7.37 (m, 2H), 7.34 (ddd, $J = 8.2, 6.7, 1.7$ Hz, 1H), 4.88 (s, 2H), 4.04 (s, 3H), 3.71 (s, 3H), 2.25 (bs, 3H), 2.13 (bs, 3H); ^{13}C NMR (CDCl_3 , 126 MHz) δ 167.4 (d, $J = 7.9$ Hz), 160.6 (d, $J = 236.1$ Hz), 152.0, 145.1 (d, $J = 16.5$ Hz), 142.0, 136.3, 125.1 (d, $J = 5.4$ Hz), 124.5, 123.2, 120.9, 112.1, (d, $J = 32.5$ Hz), 109.85, 60.2, 58.6, 30.6, 11.4, 8.26; ^{19}F NMR (CDCl_3 , 470 MHz) δ –73.13 (s); HR-MS (ESI+) m/z calcd for $\text{C}_{17}\text{H}_{18}\text{FN}_3\text{O}_2\text{S}$, 347.1104; found, 348.1096 (M + H) $^+$; HPLC >98%.

2-(((6-Fluoro-3,4-dimethoxy-3,5-dimethylpyridin-2-yl)methyl)sulfinyl)-1-methyl-1H-benzimidazole (**11v**) (429 mg, 91%). ^1H NMR (CDCl_3 , 500 MHz) δ 7.83–7.90 (m, 1H), 7.46–7.37 (m, 2H), 7.34 (ddd, $J = 8.4, 6.9, 1.6$ Hz, 1H), 6.35 (d, $J = 1.3$ Hz, 1H), 4.95 (d, $J = 13$ Hz, 1H), 4.76 (d, $J = 13.0$ Hz, 1H), 4.09 (s, 3H), 3.91 (s, 3H), 3.88 (s, 3H); ^{13}C NMR (CDCl_3 , 126 MHz) δ 162.4 (d, $J = 11.8$ Hz), 159.0 (d, $J = 235.3$ Hz), 151.4, 143.7 (d, $J = 4.9$ Hz), 142.0, 140.8 (d, $J = 17.6$ Hz), 136.6, 124.5, 123.25, 120.9, 109.8, 93.1 (d, $J = 44.9$ Hz), 61.7, 56.2, 55.9, 30.7; ^{19}F NMR (CDCl_3 , 470 MHz) δ –67.87 (s); HR-MS (ESI+) m/z calcd for $\text{C}_{16}\text{H}_{16}\text{FN}_3\text{O}_3\text{S}$, 349.0896; found, 350.0912 (M + H) $^+$; HPLC >98%.

■ ASSOCIATED CONTENT

Supporting Information

The Supporting Information is available free of charge on the ACS Publications website at DOI: 10.1021/acsomega.8b00975.

Experimental procedures and results and analytical data
(PDF)

■ AUTHOR INFORMATION

Corresponding Author

*E-mail: patrick.riss@kjemi.uio.no.

ORCID

Patrick J. Riss: 0000-0002-3887-7065

Notes

The authors declare no competing financial interest.

■ ACKNOWLEDGMENTS

This study was funded by the faculty of Mathematics and Natural Sciences (SFI-leader P.J.R.), University of Oslo, and the Department of Chemistry, University of Oslo (startup grant to P.J.R.), the Norwegian Research Council (grant no. ES231553 awarded to P.J.R.), NMS AS (research support to P.J.R.), CORFO Innova Chile (grant no. 14IEAT-28666 awarded to H.A.), and PositronPharma SA. W.R. would like to thank the Kjemisk Institutt, UiO for a Ph.D. fellowship. We are grateful to Federico Carrión and Otto Pritsch, Institute Pasteur of Montevideo, for performing dynamic light scattering assays.

■ REFERENCES

- (1) Alzheimer's Association. Alzheimer's disease facts and figures. *Alzheimer's Dementia* **2013**, *9*, 208–245.
- (2) Feldman, H. H.; Woodward, M. The staging and assessment of moderate to severe Alzheimer disease. *Neurology* **2005**, *65*, S10–S17.
- (3) Bossy-Wetzel, E.; Schwarzenbacher, R.; Lipton, S. A. Molecular pathways to neurodegeneration. *Nat. Med.* **2004**, *10*, S2–S9.
- (4) Braak, H.; Braak, E. Neuropathological staging of Alzheimer-related changes. *Acta Neuropathol.* **1991**, *82*, 239–249.
- (5) Lee, V. M.; Goedert, M.; Trojanowski, J. Q. Neurodegenerative tauopathies. *Annu. Rev. Neurosci.* **2001**, *24*, 1121–1159.
- (6) Komori, T. Tau-positive dial Inclusions in Progressive Supranuclear Palsy, Corticobasal Degeneration and Pick's Disease. *Brain Pathol.* **1999**, *9*, 663–679.
- (7) Delacourte, A. Tauopathies: recent insights into old diseases. *Folia Neuropathol.* **2005**, *43*, 244–257.
- (8) Ross, C. A.; Poirier, M. A. Protein aggregation and neurodegenerative disease. *Nat. Med.* **2004**, *10*, S10–S17.
- (9) Cedazo-Minguez, A.; Winblad, B. Biomarkers for Alzheimer's disease and other forms of dementia: clinical needs, limitations and future aspects. *Exp. Gerontol.* **2010**, *45*, 5–14.
- (10) Guzmán-Martínez, L.; Fariás, G. A.; Maccioni, R. B. Emerging non-invasive biomarkers for early detection of Alzheimer's disease. *Arch. Med. Res.* **2012**, *43*, 663–666.
- (11) Mathis, C. A.; Klunk, W. E. Imaging tau deposits in vivo: progress in viewing more of the proteopathy picture. *Neuron* **2013**, *79*, 1035–1037.
- (12) Small, G. W.; et al. In vivo brain imaging of tangle burden in humans. *J. Mol. Neurosci.* **2002**, *19*, 321–328.
- (13) Villemagne, V. L.; et al. The challenges of tau imaging. *Future Neurol.* **2012**, *7*, 409–421.
- (14) Villemagne, V. L.; Okamura, N. In vivo tau imaging: obstacles and progress. *Alzheimer's Dementia* **2014**, *10*, S254–S264.
- (15) Vermeiren, C.; et al. T807, a reported selective tau tracer, binds with nanomolar affinity to monoamine oxidase-A. *Alzheimer's Dementia* **2015**, *11*, P283.
- (16) Goedert, M.; Spillantini, M. G. Pathogenesis of the tauopathies. *J. Mol. Neurosci.* **2011**, *45*, 425–431.
- (17) Schafer, K. N.; Kim, S.; Matzavinos, A.; Kuret, J. Selectivity requirements for diagnostic imaging of neurofibrillary lesions in Alzheimer's disease: A simulation study. *Neuroimage* **2012**, *60*, 1724–1733.
- (18) Hardy, J.; Allsop, D. Amyloid deposition as the central event in the aetiology of Alzheimer's disease. *Trends Pharmacol. Sci.* **1991**, *12*, 383–388.
- (19) Pike, K. E.; et al. β -amyloid imaging and memory in nondemented individuals: evidence for preclinical Alzheimer's disease. *Brain* **2007**, *130*, 2837–2844.

- (20) Okamura, N.; et al. Quinoline and benzimidazole derivatives: candidate probes for in vivo imaging of tau pathology in Alzheimer's disease. *J. Neurosci.* **2005**, *25*, 10857–10862.
- (21) (a) Riss, P. J.; Aigbirhio, F. I. A simple, rapid procedure for nucleophilic radiosynthesis of aliphatic [¹⁸F]trifluoromethyl groups. *Chem. Commun.* **2011**, *47*, 11873–11875. (b) Riss, P. J.; Ferrari, V.; Brichard, L.; Burke, P.; Smith, R.; Aigbirhio, F. I. Direct, nucleophilic radiosynthesis of [¹⁸F]trifluoroalkyl tosylates: improved labelling procedures. *Org. Biomol. Chem.* **2012**, *10*, 6980–6986.
- (22) Rojo, L. E.; Alzate-Morales, J.; Saavedra, I. N.; Davies, P.; Maccioni, R. B. Selective interaction of lansoprazole and astemizole with tau polymers: potential new clinical use in diagnosis of Alzheimer's disease. *J. Alzheimers Dis.* **2010**, *19*, 573–589.
- (23) Riss, P. J.; et al. Radiosynthesis and characterization of astemizole derivatives as lead compounds toward PET imaging of τ -pathology. *MedChemComm* **2013**, *4*, 852–855.
- (24) Fawaz, M. V.; et al. High affinity radiopharmaceuticals based upon lansoprazole for PET imaging of aggregated tau in Alzheimer's disease and progressive supranuclear palsy: synthesis, preclinical evaluation, and lead selection. *ACS Chem. Neurosci.* **2014**, *5*, 718–730.
- (25) Shao, X.; et al. Evaluation of [¹¹C]N-methyl lansoprazole as a radiopharmaceutical for PET imaging of tau neurofibrillary tangles. *ACS Med. Chem. Lett.* **2012**, *3*, 936–941.
- (26) Hitchcock, S. A.; Pennington, L. D. Structure–brain exposure relationships. *J. Med. Chem.* **2006**, *49*, 7559–7583.
- (27) Ertl, P.; Rohde, B.; Selzer, P. Fast calculation of molecular polar surface area as a sum of fragment-based contributions and its application to the prediction of drug transport properties. *J. Med. Chem.* **2000**, *43*, 3714–3717.
- (28) Meisenheimer, J. Ueber reactionen aromatischer nitrokörper. *Justus Liebigs Ann. Chem.* **1902**, *323*, 205–246.
- (29) Waser, M.; et al. Development of a Scalable and Safe Process for the Production of 4-Chloro-2,3-dimethylpyridine-N-oxide as a Key Intermediate in the Syntheses of Proton Pump Inhibitors. *Org. Process Res. Dev.* **2010**, *14*, 562–567.
- (30) Koenig, T. W.; Wiczorek, J. S. Reactions of trichloroacetyl chloride with 2-picoline N-oxide and pyridylcarbinols. *J. Org. Chem.* **1968**, *33*, 1530–1532.
- (31) Ichihara, Y.; et al. Rational design and synthesis of 4-substituted 2-pyridin-2-ylamides with inhibitory effects on SH2 domain-containing inositol 5-phosphatase 2 (SHIP2). *Eur. J. Med. Chem.* **2013**, *62*, 649–660.
- (32) Rédl, S.; Klecén, O.; Havlíček, J. Synthetic studies connected with the preparation of h⁺/k⁺-ATPase inhibitors rabeprazole and lansoprazole. *J. Heterocycl. Chem.* **2006**, *43*, 1447–1453.
- (33) Reddy, G. M.; et al. Identification and characterization of potential impurities of rabeprazole sodium. *J. Pharm. Biomed. Anal.* **2007**, *43*, 1262–1269.
- (34) Fier, P. S.; Hartwig, J. F. Selective CH fluorination of pyridines and diazines inspired by a classic amination reaction. *Science* **2013**, *342*, 956–960.
- (35) Schöll, M.; et al. PET imaging of tau deposition in the aging human brain. *Neuron* **2016**, *89*, 971–982.
- (36) *OECD Guidelines for Testing of Chemicals, No.117*; OECD: Paris, 1992.

Paper
III

Cu(I)-mediated ^{18}F -trifluoromethylation of arenes: Rapid synthesis of ^{18}F -labeled trifluoromethyl arenes†

T. Rühl,^a W. Rafique,^a V. T. Lien^b and P. J. Riss^{*ab}

Cite this: *Chem. Commun.*, 2014, 50, 6056

Received 4th March 2014,
Accepted 15th April 2014

DOI: 10.1039/c4cc01641f

www.rsc.org/chemcomm

This report is concerned with an efficient, Cu^I-mediated method for the radiosynthesis of [^{18}F]trifluoromethyl arenes, abundant motifs in small molecule drug candidates and potential radiotracers for positron emission tomography. Three ^{18}F -labelled radiotracer candidates were synthesised from [^{18}F]fluoride ions as proof of principle. The new protocol is widely applicable for the synthesis of novel radiotracers in high radiochemical yields.

Molecular imaging with positron emission tomography (PET) allows for non-invasive, quantitative studies of radiotracer distribution in living subjects. In consequence of its maturation, PET is being increasingly used in routine clinical diagnosis, commercial drug development, and in biomedical research. Novel radiotracers for imaging a variety of biological targets are continually needed to fully exploit the potential of PET.¹ ^{18}F is the most frequently employed PET nuclide, due to the extensive use of 2-[^{18}F]fluoro-2-deoxy-D-glucose ([^{18}F]FDG) for clinical diagnosis.^{2,3} The relevance of ^{18}F is based on its expedient half-life (109.7 min) rendering it suitable for multi-step reactions, transport of radiotracers over moderate distances, convenient handling of the tracer in imaging studies and high-yield cyclotron production of no-carrier-added (n.c.a) [^{18}F]fluoride ions. The ability to form stable C–F bonds promotes the straight introduction of F atoms into most small organic molecules.

Despite the strong demand for novel radiotracers for a variety of disease related biological mechanisms, radiotracer development is a complex process. Researchers and clinicians often struggle to obtain a desired radiotracer within a reasonable time frame because discovery of suitable molecular structures that can be labelled by established procedures often require time-consuming iterative cycles of candidate synthesis and biological evaluation.

Due to its properties, a wide portfolio of synthetic drug molecules and derivatives contain the metabolically stable CF_3 group, and consequently an operationally simple and direct

arene-trifluoromethylation methodology has become a key focus in current organic chemistry.⁴ Radiolabelling these CF_3 groups is attractive to reposition known drug molecules for PET.⁵

We, hence, sought an efficient method for producing [^{18}F]trifluoromethyl arenes starting from [^{18}F]fluoride ions within our radiotracer development program. Radiosynthesis of the ^{18}F -labelled aryl trifluoromethane scaffold has been reported, however, mostly through the use of rare and unavailable electrophilic fluorinating agents or harsh conditions.⁵ A more recent breakthrough employed Cu^{I} in combination with aryl iodides.^{5a} We have explored a new route inspired by a recent report on [^{18}F]fluoroform by Vugts *et al.*⁶

For successful outcomes, reactions involving [^{18}F]fluoroform require diligent control of the gaseous intermediate, including low temperature distillation and trapping of the product at $-80\text{ }^\circ\text{C}$ in a secondary reaction vessel. These conditions and technical requirements are limiting factors with respect to the automated synthesis of high activity batches using automated synthesiser systems. Few commercially available systems provide more than one reactor and generally disfavour low temperature processes. We surmised that widespread adoption of trifluoromethylation reactions would strongly benefit from a straightforward nucleophilic one-pot method generally applicable to latest generation synthetic hardware. Such a methodology would, furthermore, feature direct installation of nucleophilic [^{18}F]fluoride ions into candidate radiotracers to avoid loss of radioactivity, conserve specific radioactivity and achieve rapid and operationally simple radiosynthesis.⁶ To achieve this we focused our efforts on the *in situ* formation of a suitable ^{18}F -trifluoromethylating reagent from an appropriate precursor and its direct conversion into the title compounds in the same reaction vessel (Scheme 1).

Difluoroiodomethane (CHF_2I) was selected as the starting material to provide a convenient source of $\text{Cu}[^{18}\text{F}]\text{CF}_3$. Our choice of $\text{Cu}[^{18}\text{F}]\text{CF}_3$ was encouraged by the work of Grushin *et al.*,^{7a,b} who provided comprehensive insights into the formation and use of CuCF_3 for trifluoromethylation reactions using fluoroform, which we attempted to implement at first, albeit without success.†

To our dismay, the published reaction conditions translated poorly into radiochemistry.^{7a}† This is most likely due to the crucial presence of phase transfer catalysts in the radiofluorination reaction

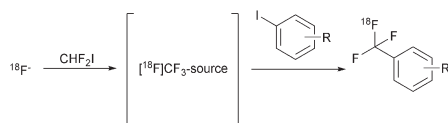
^a Kjemisk Institutt, Universitetet i Oslo, Sem Sælvaes vei 26, 0371, Oslo, Norway.
E-mail: Patrick.Riss@kjemi.uio.no

^b Norsk Medisinsk Syklotronsenter AS, Postboks 4950 Nydalen, 0424, Oslo, Norway

† Electronic supplementary information (ESI) available: Experimental details and analytical data. See DOI: 10.1039/c4cc01641f



Communication

Scheme 1 Strategy for the radiosynthesis of $[^{18}\text{F}]$ trifluoromethyl arenes.

mixture to activate the $[^{18}\text{F}]$ fluoride ion. Such reagents are known to increase the basicity and reactivity when combined with strong, anionic bases like KOtBu in dipolar aprotic solvents.^{7d-f} Although such strong bases were deemed crucial to deprotonate fluoroform ($\text{p}K_{\text{a}} = 27$ in DMSO) in previous reports,⁷ only rapid discoloration along with low yields was observed in our radiochemical experiments. Grushin and co-workers described that the use of KOtBu in excess would even permit omission of a supporting ligand and added triethylamine HF-complex to stabilise the $\text{Cu}-\text{CF}_3$ reagent. Addition of non-radioactive fluoride ions to the labelling reaction is prohibitive in the context of the tracer principle, a prerequisite for PET imaging. A second issue may be the fact that CuF is only stable as a complex in solution and otherwise disproportionates to Cu^0 and CuF_2 . Since the development of a one-pot method would require both species, n.c.a. $[^{18}\text{F}]$ fluoride ions and Cu^+ , to coexist, this mechanism may deprive the reaction mixture of ^{18}F , which is only present in very low concentrations (μM). Hence, obtaining the short-lived $[^{18}\text{F}]\text{CF}_3$ -source *in situ* prior to trifluoromethylation in the same reaction vessel is rather challenging and, unfortunately, the Grushin method did not furnish the desired labelled products in useful radiochemical yields. Given this apparent incompatibility of reagents a methodological optimisation of various parameters became inevitable.

This prompted us to test our working hypothesis. We surmised that KOtBu may not be required since the formation of difluorocarbene *via* α -elimination of HI from CHF_2I in the presence of 4,7,13,16,21,24-hexaoxa-1,10-diazabicyclo[8.8.8]hexacosan (crypt-222), K_2CO_3 , and $^{18}\text{F}^-$ facilitates the formation of $\text{Cu}-[^{18}\text{F}]\text{CF}_3$. In addition we considered that a supporting ligand may be beneficial to address the sensitivity of the reaction to Cu -disproportionation and potentially stabilise a Cu -difluorocarbene complex.^{7g} Consequently, we chose the screening for the most efficient Cu -ligand system in combination with the most frequently used source of reactive ^{18}F -fluoride; crypt-222, K_2CO_3 , and $^{18}\text{F}^-$ as the starting point for our investigations, as we now report here.

We initially aimed to discover a simple Cu -ligand system capable of mediating the trifluoromethylation reaction without impeding the nucleophilic radiofluorination with the $[^{18}\text{F}]$ fluoride ion. In a model reaction, we chose to use CHF_2I , CuI , and a ligand in a 1:1:1 molar ratio (see Table 1) and a model substrate, iodoarene 4-iodo benzonitrile **1a** ($\sim 40 \mu\text{mol}$) in DMF (0.3 mL). In preliminary experiments (not shown) we found that a temperature of 145°C was necessary to achieve rapid conversion. Attempts to substitute the low boiling starting material CHF_2I (b.p. 22°C) by a higher boiling difluoromethyl sulfonate, in order to permit better control of the reaction stoichiometry and for easy handling of the reagent, were not successful. Neither difluoromethyl tosylate nor difluoromethyl triflate were found to react to give the desired product under a variety of conditions. Consequently, we resorted to using CHF_2I for all further experiments. Despite this minor inconvenience, an activity balance of the reaction did not reveal any loss

Table 1 Effect of the base/ligand on the RCY of $[^{18}\text{F}]\text{1b}$. The concentration of the ligand in the reaction mixture was 200 mM

Entry	Ligand ^a	RCY ^b (%) [^{18}F] 1b
1	None	0
2	<i>t</i> BuOK	2
3	Triphenylphosphine	1
4	Pyridine	2
5	DMAP	9
6	2,2'-Bipyridine	8
7	Phenanthroline	5
8	IPr-CuBF ₄	2
9	TMEDA	19
10	DBU	3
11	NEt ₃	28
12	DIPEA	42

^a Abbreviations: DBU = 1,8-diazabicyclo[5.4.0]undecene; IPr-CuBF₄ = bis(1,3-(2,6-diisopropylphenyl)imidazol-2-ylidene)copper(i) tetrafluoroborate; DMAP = 4-(dimethylamino)pyridine; TMEDA = *N,N,N',N'*-tetramethyl ethylenediamine; NEt₃ = triethylamine; DIPEA = *N,N*-diisopropyl-*N*-ethylamine. ^b Decay-corrected radiochemical yield in % of dispensed ^{18}F determined by radioHPLC or radioTLC.

of the gaseous radioactive material. In control experiments upon omitting either ligand, or CHF_2I no ^{18}F -labelled product was obtained (Table 1, entries 1 and 2), likewise, the use of triphenylphosphine gave only traces of the product (Table 1, entry 3). Surprisingly, none of the screened pyridine derivatives gave significant yields of $[^{18}\text{F}]\text{1b}$ (Table 1, entries 4–7). When the commercially available Cu -NHC complex bis(1,3-bis(2,6-diisopropylphenyl)imidazol-2-ylidene)copper tetrafluoroborate was used, $[^{18}\text{F}]\text{1b}$ was formed in about 2% yield (Table 1, entry 8). At this point we deduced that a slightly more basic ligand would be required in dipolar aprotic media and turned our attention to aliphatic, tertiary amines. This hypothesis was rewarded with the first double-figured yield when tetramethylethylenediamine (TMEDA), a ligand that had proved its value previously, was used.⁸ Under these conditions (Table 1, entry 9) $[^{18}\text{F}]\text{1b}$ was obtained in 19% radiochemical yield after 10 min at 145°C . Encouraged by these positive findings we briefly considered DBU (3%, Table 1, entry 10) which turned out to be inferior to TMEDA. Further improved, albeit not yet satisfactory, yield (28%, Table 1, entry 11) was achieved through the use of NEt₃ in combination with **1a**. Further screening of ligand-catalyst combinations (Table 1, entry 12) revealed *N,N*-diisopropyl-*N*-ethylamine (DIPEA) to be very effective with regard to the formation of $[^{18}\text{F}]\text{1b}$; without further optimisation a radiochemical yield of 42% was achieved. We hence refrained from further ligand screening and focussed further efforts on the CuI -DIPEA system. Although the majority of $[^{18}\text{F}]$ fluoride ions had been consumed within 10 minutes of the reaction time, a considerable amount of residual $[^{18}\text{F}]$ fluoride ions left in the reaction mixture indicated further potential for improvement. In order to boost the conversion of $[^{18}\text{F}]$ fluoride, which we surmised would lead to further improvements in RCY, we considered that alternative sources of naked $[^{18}\text{F}]$ fluoride ions might prove to be beneficial. Sources of the $[^{18}\text{F}]$ fluoride ion were obtained by trapping $[^{18}\text{F}]$ fluoride ions on a strong anion exchange resin followed by elution of the trapped radioactive material using an appropriate base in aqueous acetonitrile ($\text{MeCN}-\text{H}_2\text{O}$, 9:1). Through this protocol, reactive $[^{18}\text{F}]$ fluoride ion complexes are obtained that have found widespread application in PET chemistry.



Table 2 Effects of the fluoride ion source on the RCY of [¹⁸F]1b^a

Entry	Base	Ligand	[¹⁸ F]1b ^a (%)
1	K ₂ CO ₃ /crypt-222	DIPEA	42
		TMEDA	19
2	K ₂ CO ₃ /18-crown-6	DIPEA	49
3	TBAOH	DIPEA	2
		TMEDA	18
4	TEAHCO ₃	DIPEA	56
5	Cs ₂ CO ₃	DIPEA	83
		TMEDA	38
		DBU	27
6	KHCO ₃ /crypt-222	DIPEA	83
		TMEDA	48
		DBU	47

^a Abbreviations: TBAOH = tetrabutylammonium hydroxide; TEAHCO₃ = tetraethylammonium bicarbonate.

In the context of our one-pot approach we conducted control experiments with DBU and TMEDA alongside DIPEA to avoid overlooking synergies in between the ¹⁸F-complex, ligand and Cu^I. However, under the screened conditions, DIPEA was generally found to be superior to TMEDA and DBU. Substitution of the cryptand crypt-222 (Table 2, entry 1) by the corresponding crown ether 18-crown-6 (Table 2, entry 2) led to a slightly improved radiochemical yield of about 49%. Whereas the use of tetrabutylammonium hydroxide (TBAOH) to form tetrabutylammonium fluoride (TBA[¹⁸F]F) (Table 2, entry 3) did not have any effect, the use of tetraethylammonium carbonate (TEAHCO₃) to essentially obtain tetraethylammonium fluoride (TEA[¹⁸F]F) (Table 2, entry 4) had a remarkable impact (56%). The use of Cs₂CO₃ as a base, led to a significant increase in the radiochemical yield in the formation of [¹⁸F]1b (up to 83%, Table 2, entry 5). In the end, these conditions were equivalent to the combination of KHCO₃, crypt-222 and DIPEA which resulted in up to 83% RCY after 10 min at 145 °C (Table 2, entry 6).

Notably, screening of various combinations of inorganic bases and phase transfer catalysts used to activate the [¹⁸F]fluoride ion in the next step indeed facilitated a duplication of the radiochemical yield even when a milder base was used, highlighting the strong influence of these reagents under our conditions. These conditions were used in all further experiments. In order to further optimise the reaction outcome, we focussed our attention on the contribution of the reaction time. Increasing the reaction time beyond 10 minutes did not improve the yield, instead it became apparent, that the bulk of the [¹⁸F]fluoride ions had already been consumed within 10 minutes of the reaction time under our optimised conditions and the yield did not improve, but only degraded further from this point.

Table 3 Effects of the reaction time and solvent on the RCY of [¹⁸F]1b

Entry	Solvent	Time (minutes)	RCY (%)
1	DMF	10	83
2	DMSO	10	0
3	MeCN	10	78
4	THF	10	8
5	DMF	20	82

Table 4 Effects of the copper source on the RCY of [¹⁸F]1b

Entry	Catalyst ^a	RCY ^b (%)
1	CuI	83
2	None	0
3	CuCl	40
4	CuBr	89
5	CuCN	60
6	CuOAc	10
7	CuF·PPh ₃	0 ^b
8	CuOTf·(MeCN) ₄	5 ^b
9	CuOTf·benzene	0 ^b
10	CuOTf·toluene	0 ^b
11	CuOTf·(MeCN) ₄	93

^a Abbreviations: CuOTf·(MeCN)₄ = tetrakisacetonitrile copper(i) triflate; CuOTf·benzene = copper(i) trifluoromethane sulfonate benzene complex; CuOTf·toluene = copper(i) trifluoromethane sulfonate toluene complex; CuF·PPh₃ = fluorotris(triphenylphosphine)copper(i). ^b DIPEA was omitted.

Substitution of DMF with DMSO or THF was detrimental (Table 3, entries 2 and 4), both of these solvents were ineffective. However, substitution of DMF with MeCN provided a viable alternative and similar yields were obtained. The main disadvantage of using MeCN under these conditions is the fairly pronounced pressure build-up in the reactor, which may result in difficulties during automation. Moreover, a loss of activity was observed using acetonitrile as the solvent.

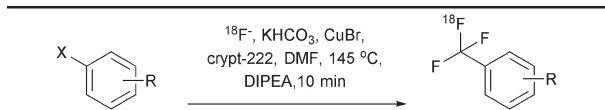
Variation of the copper catalyst source. We tested whether CuI was the preferred source of the copper catalyst by changing the copper salt in the promising reaction example that used DIPEA–CuI (Table 4, entry 1). The reaction did not occur when CuI was omitted (Table 4, entry 2). Equimolar replacement of CuI with CuCl, CuOAc, CuCN, or fluorotris(triphenylphosphine) Cu^I led to diminished radiochemical yields (Table 4, entries 3–7). Also arene complexes of CuOTf (Table 4, entries 8–10) were not effective in the absence of DIPEA or gave only traces of the ¹⁸F-labelled product (Table 4, entry 8). Tetrakis acetonitrile CuOTf and CuBr provided the highest yields (Table 3, entry 4). In our case CuBr was established as the preferred copper source.

General conditions, as optimised above, were used to investigate the substrate scope of the ¹⁸F-trifluoromethylation. A variety of commercially available aryl halides were screened (Table 5). In essence, aryl iodides were confirmed to be the most appropriate halides for our purpose (Table 5, entry 1), a steep decline in radiochemical yield occurred upon switching to the corresponding bromide **3a** or chloride **4a** (Table 5, entries 3 and 4). Most assayed functional groups were found to be compatible with the reaction conditions. Potentially sensitive substrates such as 4-cyano or 4-methoxycarbonylbenzenes, which may be sensitive to exposure to carbanionic forms of trifluoromethylating reagents, gave the desired radioactive products in high to excellent yields. Even **12a** containing a protic hydroxyl group was tolerated to some extent. The protic carboxamide **10a** gave low yield and two unidentified by-products were observed. Electron deficient substrates globally resulted in slightly higher radiochemical yields compared to electron-rich arenes.

Translation of the method: Radiotracer synthesis. Having confirmed that we were able to prepare a variety of [¹⁸F]trifluoromethyl arenes

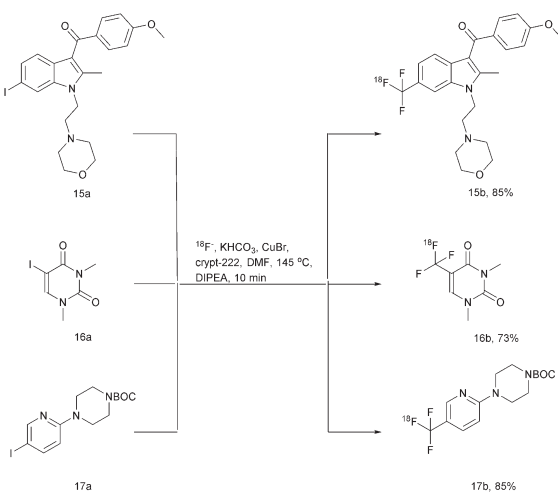


Communication

Table 5 Substrate scope of the ^{18}F -trifluoromethylation reaction


Substrate	R	X	Product	RCY ^{a,b} (%)
1a	4-Cyano	I	[^{18}F]1b	93 ± 3
2a	4- <i>t</i> -Butyl	I	[^{18}F]2b	69 ± 8
3a	4- <i>t</i> -Butyl	Br	[^{18}F]2b	1
4a	4- <i>t</i> -Butyl	Cl	[^{18}F]2b	1
5a	4-Methoxycarbonyl	I	[^{18}F]5b	86 ± 7
6a	4-Nitro	I	[^{18}F]6b	89 ± 4
7a	4-Pyridinyl	I	[^{18}F]7b	58 ± 17
8a	3-Methoxycarbonyl	I	[^{18}F]8b	86 ± 8
9a	4-Phenyl	I	[^{18}F]9b	84 ± 2
10a	4-Carboxamido	I	[^{18}F]10b	44 ± 14
11a	4-Benzoyloxy	I	[^{18}F]11b	85 ± 6
12a	4-Hydroxy	I	[^{18}F]12b	12 ± 1
13a	3,5-Dimethyl	I	[^{18}F]13b	63 ± 6
14a	2,6-Dimethyl	I	[^{18}F]14b	75 ± 6

^a Screening conditions: 100 MBq scale, CuBr (58 μmol), CHF₂I (169 μmol), KHCO₃ (13 μM), crypt-222 (35 μmol), aryl halide (41 μmol), DIPEA (59 μmol), 145 °C, 10 min, DMF (300 μL). ^b RCY values are mean ± S.D.

Scheme 2 Direct radiosynthesis of [^{18}F]trifluoromethyl arenes.

efficiently within only 10 min, we investigated the feasibility of synthesising prospective radiotracer candidates bearing molecular structures common for small molecule drugs (Scheme 2).

Treatment of precursor **15a** with ^{18}F under our standard conditions afforded the potential subtype selective cannabinoid receptor agonist [^{18}F]**15b** in 85% RCY. Likewise, we investigated the direct radiosynthesis of trifluorothymine **16b** from the corresponding iodide precursor **16a** in order to provide this compound for our ongoing cancer imaging efforts in rodent models of peripheral tumours.⁹ [^{18}F]**16b** was obtained in a radiochemical yield of 73%. In an extension of our concept the BOC-protected piperazine **17a** was converted into the ^{18}F -trifluoromethylated BOC-protected piperazine **17b** in 85%

yield and deprotected with TFA in a second step to obtain the prospective 5-HT receptor radiotracer **17c**.

In this report, we have shown that Cu^I mediated ^{18}F -trifluoromethylation reactions are highly efficient in the presence of a simple combination of DIPEA, CuBr and iodoarenes. We extended this methodology to three examples of a single-pot synthesis of candidate radioligands for PET imaging (Scheme 2). The resulting [^{18}F]trifluoromethyl arenes were obtained in sufficient yields by using an operationally convenient protocol, suitable for straightforward automation. This direct and rapid conversion of iodoarenes is tolerant to diverse functional groups and consequently provides convenient access to a variety of drug molecules containing the CF₃-group. Given the high prevalence of the CF₃-group and its prominent role in drug development, paired with the availability of ^{18}F at most PET centres, we expect this novel methodology to be widely adapted for the development of PET radiotracers in particular from known and well characterised drug molecules.

Notes and references

- L. Cai, S. Lu and V. W. Pike, *Eur. J. Org. Chem.*, 2008, 2853–2873.
- (a) P. W. Miller, N. J. Long, R. Vilar and A. D. Gee, *Angew. Chem., Int. Ed.*, 2008, 47, 8998–9033; (b) P. J. H. Scott, *Angew. Chem., Int. Ed.*, 2009, 48, 6001–6004.
- G. J. Meyer, S. L. Waters, H. H. Coenen, A. Luxen, B. Mazière and B. Långström, *Eur. J. Nucl. Med.*, 1995, 22, 1420–1432.
- (a) D. A. Nagib and D. W. C. MacMillan, *Nature*, 2011, 480, 224–228; (b) A. Deb, S. Manna, A. Modak, T. Patra, S. Maity and D. Maiti, *Angew. Chem., Int. Ed.*, 2013, 52, 9747–9750; (c) S. Mizuta, K. M. Engle, S. Verhoog, O. Galicia-Lopez, M. O'Duill, M. Medebielle, K. Wheelhouse, G. Rassias, A. Thompson and V. Gouverneur, *Org. Lett.*, 2013, 15, 1250–1253; (d) T. Furuya, A. S. Kamlet and T. Ritter, *Nature*, 2011, 473, 470–477; (e) S. Mizuta, S. Verhoog, K. M. Engle, T. Khotavivattana, M. O'Duill, K. Wheelhouse, G. Rassias, M. Medebielle and V. Gouverneur, *J. Am. Chem. Soc.*, 2013, 135, 2505–2508.
- (a) M. Huiban, M. Tredwell, S. Mizuta, Z. Wan, X. Zhang, T. L. Collier, V. Gouverneur and J. Passchier, *Nat. Chem.*, 2013, 5, 941–944; (b) L. Zhu, K. Ploessl and H. F. Kung, *Science*, 2013, 342, 429–430; (c) S. Mizuta, I. Stenhagen, M. O'Duill, J. Wolstenhulme, A. Kirjavainen, S. Forsback, M. Tredwell, G. Sandford, P. Moore, M. Huiban, S. Luthra, J. Passchier, O. Solin and V. Gouverneur, *Org. Lett.*, 2013, 15, 2648–2651; (d) M. Tredwell and V. Gouverneur, *Angew. Chem., Int. Ed.*, 2012, 51, 11426–11437; (e) P. J. Riss, V. Ferrari, L. Brichard, P. Burke, R. Smith and F. I. Aigbirhio, *Org. Biomol. Chem.*, 2012, 10, 6980–6986; (f) P. J. Riss and F. I. Aigbirhio, *Chem. Commun.*, 2011, 47, 11873–11875; (g) M. R. Kilbourn, M. R. Pavia and V. E. Gregor, *Int. J. Radiat. Appl. Instrum., Part A*, 1990, 41, 823–828; (h) O. Josse, D. Labar, B. Georges, V. Grégoire and J. Marchand-Brynaert, *Bioorg. Med. Chem.*, 2001, 9, 665–675; (i) W. R. Dolbier Jr, A.-R. Li, C. J. Koch, C.-Y. Shiue and A. V. Kachur, *Appl. Radiat. Isot.*, 2001, 54, 73–80.
- D. van der Born, J. D. M. Herscheid, R. V. A. Orru and D. J. Vugts, *Chem. Commun.*, 2013, 49, 4018–4020.
- (a) A. Lishchynskiy, M. A. Novikov, E. Martin, E. C. Escudero-Adán, P. Novák and V. V. Grushin, *J. Org. Chem.*, 2013, 78, 11126–11146; (b) O. A. Tomashenko and V. V. Grushin, *Chem. Rev.*, 2011, 111, 4475; (c) E. A. Symons and M. J. Clermont, *J. Am. Chem. Soc.*, 1981, 103, 3127–3130; (d) M. Halpern, *Phase-Transfer Catalysis, Ullmann's Encyclopedia of Industrial Chemistry*, Wiley-VCH, Weinheim, 2002; (e) E. V. Dehmlow and S. S. Dehmlow, *Phase Transfer Catalysis*, VCH, Weinheim, 3rd edn, 1993; (f) C. M. Starks, C. L. Liotta and M. E. Halpern, *Phase-Transfer Catalysis*, Chapman & Hall, New York, 1994; (g) W. Kirmse, *Carbene Chemistry*, Academic Press, Inc. LTD, New York-London, 2nd edn, 1971, vol. 1.
- P. J. Riss, S. Lu, S. Telu, F. I. Aigbirhio and V. W. Pike, *Angew. Chem., Int. Ed.*, 2012, 51, 2698–2702.
- K. Virdee, P. Cumming, D. Caprioli, B. Jupp, A. Rominger, F. I. Aigbirhio, T. D. Fryer, P. J. Riss and J. W. Dalley, *Neurosci. Biobehav. Rev.*, 2012, 36, 1188–1216.



Paper
IV

Paper

V

Paper

VI

Paper

VII

